A high-resolution coupled physical-biogeochemical model of the northeastern US continental shelf: MOM6-COBALT-NEUS25v1.0

Dalton Kei Sasaki[1], Cristina Schultz[1], and Enrique Curchitser[2]

[1]Northeastern University, Boston MA, USA

[2]Department of Environmental Sciences, Rutgers University, New Brunswick NJ, USA

Correspondence: Dalton Kei Sasaki (d.sasaki@northeastern.edu/dalton.sasaki@gmail.com)

Abstract. Coastal communities along the northeastern U.S. depend on marine resources that have been increasingly affected by ocean warming, marine heatwaves and associated ecosystem shifts over recent decades. High-resolution regional ocean-biogeochemical modeling using the Modular Ocean Model 6 (MOM6) enables studies of fisheries production, marine carbon dioxide removal and sediment biogeochemistry. The northeastern US (NEUS) continental shelf is one of the most widely sampled and measured ocean areas, providing a favorable testbed for regional model development. In this context, we present an assessment of MOM6 coupled with the Carbon, Ocean Biogeochemistry and Lower Trophics (COBALT) model in the NEUS at 1/25° resolution (MOM6-COBALT-NEUS25 version 1.0). The model is validated against a suite of observation databases, satellite products, ocean reanalysis and climatologies for the period between 1993 and 2019 considering different skill metrics. A reasonable representation of the Gulf Stream separation led to realistic simulation of parameters on the continental shelf based on the evaluation of seasonal structure, long-term time series, and spatial variability patterns. For temperature, and salinity, the main biases in the model are located in the Mid-Atlantic Bight, where the vertical and bottom structure show mixed-quality results that are dependent on season and depth, while surface fields and the vertical structure results in the Gulf of Maine are comparable with global ocean reanalysis and other regional model results. The inclusion of tides allowed the regional patches of cold sea surface temperature to develop, a feature generally absent in global ocean reanalysis. Simulated biogeochemical parameters for surface chlorophyll, nutrients and integrated mesozooplankton showed the expected seasonal structure with peaks occurring in spring and fall. Discrepancies between the performance of the model in representing physical and biogeochemical parameters indicate that improved boundary conditions of biogeochemistry parameters may be necessary to a further enhance representation of seasonal and interannual variability of biogeochemistry in this domain. Despite these challenges, this version of the model reproduces the major physical and biogeochemical patterns of the NEUS, providing a robust foundation for various future applications.

1 Introduction

The need to provide decision-makers with information required to prepare and adapt to changing ocean and climate has increased due to the adverse effects felt by society and ecosystems worldwide, including the Gulf of Maine in the northeastern coast of United States (NEUS). The Northwest Atlantic experiences interconnected regional effects related to changes where shifts in the variability and structure of the Gulf Stream (Andres, 2016) have impacted the water mass structure in the continental slope of the Northeastern US (NEUS) (Gonçalves Neto et al., 2021), altering the distribution of water masses in the Gulf of Maine (Townsend et al., 2010; Balch et al., 2022). These changes have also been linked to ocean acidification (Siedlecki et al., 2021), increased mortality/reduced recruitment of marine species of economical relevance (Pershing et al., 2015), and hypoxia (Scully et al., 2022). Some of the initiatives to reduce CO_2 concentrations in the atmosphere involve marine carbon removal with kelp farms that may be economically relevant (Coleman et al., 2022). These interconnected impacts highlight the need for improved understanding and prediction capabilities of the ocean. Despite decades of research and investment making the NEUS one of the most extensively monitored regions in the world, significant observational gaps remain. These gaps limit our ability to understand feedbacks and forecast regional impacts derived from climate and antropic activities.

The high costs associated with comprehensive observation of the ocean prevent full-spectrum measurements of physical and biogeochemical parameters across all relevant scales of variability. General circulation ocean models based on well-established physical laws of the water dynamics, provide valuable insights when properly calibrated and validated against observational information (e.g. Fox-Kemper et al., 2019). Similarly, biogeochemical models incorporate simplified representation of ecological network (usually plankton dynamics) and their relationship with ocean physics and chemistry, enabling understanding of parameters related to upper trophic levels, ocean acidification and blue carbon removal (Fennel et al., 2022). Coupled ocean dynamics and biogeochemistry models allow the representation of lateral advection of tracers related to nutrients, phytoplankton, zooplankton, which is relevant in the connectivity between water masses of the Gulf of Maine and the Slope Sea (Townsend et al., 2023, 2010).

While coupled ocean dynamics and biogeochemical models exist, relevant challenges remain. For instance, the diverse range of spatial and temporal scales involved (O[10^{-3} m] to O[10^{6} m], O[10^{0} s] to O[10^{3} years]) (Stommel, 1963) in the ocean cannot be explicitly resolved by computers. Models resolve ocean dynamics by employing numerical grids that cannot describe subgrid-scale processes, which must be parameterized vertically and horizontally (Fox-Kemper et al., 2008; Gent and Mcwilliams, 1990; Large et al., 1994). This is relevant for the Gulf Stream and its separation point at Cape Hatteras, where it moves away from the shelf break and produces a pocket in the ocean along the continental slope between Mid-Atlantic Bight and Nova Scotia – the Slope Sea. When the separation is not well represented, the Gulf Stream impinges on or separates from the continental slope in incorrect locations (Chassignet and Xu, 2017) leading to bias in the representation of the Slope Sea environment, which is relevant in the representation of physical-biogeochemical parameters in the continental shelf and slope (Gonçalves Neto et al., 2021). Properly resolving the separation requires a spatial resolution of at least $1/10^{o}$, with good representation typically achieved at $1/50^{o}$ (Chassignet and Xu, 2017).

Biogeochemical dynamics in the ocean is represented as systems of partial differential equations that represent the food web dynamics of plankton in terms of both new and regenerated production, and are usually a function of nitrogen. Most biogeochmical models extend the concept of the nutrient-phytoplankton-zooplankton-detritus by including additional state variables, that may include more nutrients, or phytoplankton and zooplankton functional groups (Fennel et al., 2022).These models have been formulated and coupled with general circulation models in a number of regional, including the NEUS domain, global, and Earth System models (Lehmann et al., 2009; Stock et al., 2014; Zang et al., 2021).

Earth System Models are usually designed to resolve centennial time scales, which constrains its components' numerical grids into resolutions that are unable to resolve several regional features in the oceans (e.g. Dunne et al., 2012; Lovato et al., 2022), such as the Gulf Stream and the continental shelf of NEUS. Therefore, regional simulations are complementary tools that allow better representation of regional and local features by employing grids with higher resolution in restricted domains. Global ocean models, climatologies, and Earth System Models, however, can provide boundary conditions for regional models (Stock et al., 2014; Jean-Michel et al., 2021; Marchesiello et al., 2001; Ross et al., 2023).

The Modular Ocean Model version 6 (MOM6) is a suitable option to represent continental shelf and slope dynamics, as it has been used as a global model in ESM systems (Dunne et al., 2012) and is also equipped with regional capabilities (e.g. Ross et al., 2023). Four key advantages of MOM6 are relevant for NEUS: First, its finite volume discretization of the pressure gradient force is independent of coordinates and effectively handles thermobaric instabilities and complex topography that can occur in models that use sigma-coordinate or isopycnal vertical schemes (Adcroft et al., 2008). This is important in domains where significant steepness is present, such as the continental slope. Second, the vertical scheme removes the CFL restriction on vertical advection, making the model unconditionally stable for very thin layers (Griffies et al., 2020) and allowing efficient integration of the model. Third, it includes several different physical closures for both horizontal and vertical parameterizations (Reichl and Hallberg, 2018; Jackson et al., 2008; Large et al., 1994; Gent and Mcwilliams, 1990; Fox-Kemper et al., 2008; Bodner et al., 2023) making it a flexible model that can be used both from coarse (1°) to fine resolutions (<0.1°). Fourth, MOM6 can be coupled with the Carbon, Ocean Biogeochemistry and Lower Trophics (COBALT) model (Stock et al., 2014, 2020), allowing biogeochemistry to be represented in regional ocean models.

Here, we present the implementation and evaluation of a 1/25° regional ocean and biogeochemistry model, MOM6-COBALT-NEUS25 designed to support a future implementation of a benthic model (Rakshit et al., submitted) and assess marine carbon dioxide removal studies in this region. The resolution balances representation of mesoscale features in the Slope Sea/Gulf Stream domains (Hallberg, 2013) with the computational cost of COBALT coupling. Other coupled ocean-biogeochemistry high-resolution regional models ($\leq 0.1^\circ$) have been used in previous studies to assess Earth System Models in the northwest North Atlantic Shelf (Lehmann et al., 2009; Laurent et al., 2021) by employing less complex biogeochemical models that did not necessarily represent phosphorus, iron, oxygen, carbon, silicon, and alkalinity dynamics (Stock et al., 2014; Tian et al., 2015).

While this work focuses on the continental shelf, we also provide a brief assessment of the Gulf Stream. This paper is organized as follows: Section 2 describes key features in the area of study; Section 3 details the physical and biogeochemical model configuration along with the datasets used in preprocessing and validation stages; Section 4 (Results) is subdivided

into four main subsections: first, we evaluate circulation patterns, focusing on the Gulf Stream, Mid-Atlantic Bight, Georges Bank, and Gulf of Maine. Second, we assess temperature and salinity considering seasonal fields, vertical structure, time series, and subseasonal to interannual variability. Third, we examine sea surface height using tide gauges to evaluate model results. Finally, we evaluate biogeochemistry considering seasonal nitrate, chlorophyll, and zooplankton spatial distributions. In Section 5 we discuss the results across different subsections, and also the model's strengths and limitations in the context of existing literature; Section 6 offers our concluding remarks and recommendations for future research.

2 Area of Study

The area of study extends from Cape Hatteras to Nova Scotia (Figure 1). The following paragraphs present different features related to the continental shelf water masses, dynamics and biogeochemistry of the continental shelf regions - the Gulf of Maine (including Georges Bank) and Mid-Atlantic Bight - as well as relevant Gulf Stream characteristics.

In the North Atlantic, the Gulf Stream is a subtropical western boundary current that flows along the U.S Coast before separating from the continental margin offshore of Cape Hatteras in North Carolina. This current redistributes heat and saline water poleward, balancing the equatorward transport away from the western boundaries. Detailed depth-stratified estimates indicate transport above 1000m of 57.3 Sv at Cape Hatteras increasing to 75.6 Sv in the area southeast of Cape Cod (MA), while transport below 1000 m has estimates of 54.5 Sv and 69.9 Sv, respectively (Heiderich and Todd, 2020). Approximately 1000 km downstream from Cape Hatteras, the Gulf Stream begins to destabilize and meander, with its path envelope widening fivefold (Andres, 2016).

The Gulf Stream position has been related to warming of the Northeastern US continental shelf and has influenced the penetration of Labrador water onto North America's continental margin. The Gulf Stream acts as a valve controlling Labrador Current intrusion, with the mechanism related to the impingement of the Gulf Stream at the Tail of the Grand Banks that influences the Sea Surface Height (SSH). When the Gulf Stream position is closer to the Tail of the Grand Banks, mean SSH increased by 10.8 cm between 2009-2018, when compared with 1993-2008 (Gonçalves Neto et al., 2021). The westward flow of the Labrador Current into the Slope Sea can contribute significantly to the T-S variability on the Gulf of Maine shelf (Petrie and Drinkwater, 1993) through inflow of slope water in the Northeast Channel. Properties of this intruding slope water at the Northeast Channel are related with the Gulf Stream position and the warm-core rings it sheds (Du et al., 2021, 2022). One hypothesis is that these warm-core rings are able to bring modified Gulf Stream Water, which has lower content of nutrients than the slope waters (Townsend et al., 2023).

The Gulf of Maine is a semi-enclosed shelf sea along the NEUS coast almost fully separated from the Atlantic Ocean by Brown Banks and Georges Banks. It is connected with the North Atlantic via the deeper Northeast Channel with about 230 m depth, and the shallower 70-m deep Southwest Channel. The Gulf of Maine has a complex topography with average depth of 150 m and with three major basins, the Wilkinson Basin in the west, Jordan Basin south of Maine and west of Nova Scotia, and Georges Basin, which is connected to the Northeast Channel (Brooks, 1992). Different water mass classification exist in the Gulf of Maine, but here we select the following: The Scotian Shelf Water, with characteristic temperature and salinity

of 2°C and 32.0, respectively; the Warm Slope Water (12°C , 35.4), and the Labrador Slope Water (6°C , 34.6). While this classification has been used to identify changes in water masses composition in the Gulf of Maine (Townsend et al., 2010, 2023), it is important to note that the properties of these water masses may vary interannually (Mountain, 2012). Inside Gulf of Maine, the intruding subsurface slope water from Northeast Channel to Jordan Basin is warmer in winter than in summer, contrasting with the surface seasonality of surface waters. These slope waters interact with fresher water from Nova Scotia, strengthening near-surface stratification and suppressing deep convection during winter time (Du et al., 2021).

The cyclonic current system in the Gulf of Maine is characterized by seasonal intensification. During this process, waters originating from the Scotian Shelf and continental slope flow approximately parallel to the coastline and bathymetry, while leaving the area by flowing around Cape Cod or through circulation around Georges Bank that connects the Gulf of Maine to the Slope Sea. This circulation spins up from April to June, strengthens from June to December, then spins down from December to February, when erosion of the stratification deepens the cyclonic circulation, which starts to lose energy due to interaction with bottom friction (Xue et al., 2000). Combined model and observation efforts suggest that convective overturning during winter at Wilkinson Basin is relevant in the deepening of the mixed layer. It can deepen the mixed layer to a depth of about 120 m, while wind stress alone in similar conditions mixes it only to about 80 m. In this case, lateral advection may increase local stability, counteracting pure vertical mixing (Mupparapu and Brown, 2002). The cyclonic circulation presents many features, such as the counterclockwise gyres around Jordan and Wilkinson basins, and the cyclonic circulation connecting Georges Basin and the Northeast Channel (Brooks, 1985). Off the Maine coast, the cyclonic circulation consists of two segments: the Eastern Maine Coastal Current (EMCC) originates from outflows near the Bay of Fundy, with subtidal currents ranging from 0.15 to 0.30 m s^{-1}. In spring and summer, it veers offshore around Penobscot Bay, while during the same season, the Western Maine Coastal Current (WMCC) extends from Penobscot Bay into Massachusetts Bay. EMCC's currents range between 0.05 to 0.15 m s^{-1}, even though they can leak into the WMCC near Penobscot Bay (ME). Also, during winter, the deep EMCC may decouple from the surface and veer offshore into the cyclonic circulation over Jordan basin (Pettigrew et al., 2005). The WMCC has a strong seasonal signal associated with freshwater inputs in the western Gulf of Maine, although its dynamics is predominantly barotropic (Geyer et al., 2004). During fall and winter, currents are generally weaker and the EMCC has a more continuous flow into the WMCC at the surface. The connectivity peaks twice over the year, first more strongly in winter and then in late spring/early summer (Li et al., 2022).

The Gulf of Maine is influenced by tides, with nearly resonant semi-diurnal tidal responses, a large semidiurnal M_2 tidal current, and tidal range of over 8 m in the Bay of Fundy (Garrett, 1972). In Georges Bank, M_2 tides are relevant to its mean clockwise circulation through tidal rectification (Loder, 1980) and keep the well-mixed waters at areas shallower than 60 m throughout the year (Townsend and Pettigrew, 1996). Over the New England Shelf, a zone of minimum sea level occurs due to encountering tidal waves coming from east of Cape Cod and south of Nantucket Island, a transition region between the tidal environments of the less energetic MAB and tidally amplified Gulf of Maine (Chen et al., 2011; He and Wilkin, 2006). Two relevant regions with internal tidal energy flux in the Gulf of Maine are the northeastern flank of Georges Bank, and the Northeast channel, where internal tide M_2 flux has been identified as 0.15 GW, and 1.06 GW, respectively (Chen et al., 2011).

Tides have been related to strengthening of the summer circulation in the Gulf of Maine around Georges Bank, Browns Bank by enhancing the coastal current through tidal rectification and mixing (Xue et al., 2000).

Primary productivity in the Gulf of Maine is supported by nitrogen fluxes from multiple sources, including slope waters, rivers, atmospheric deposition, and water column nitrification (Townsend, 1998). Surface chlorophyll concentrations exhibit distinct spatial and temporal patterns, with consistently higher values maintained throughout the year over shallow banks and nearshore, while the lowest concentrations occur in deeper basins and along the shelf-break (Thomas et al., 2003). The region follows the seasonal cycle, with low winter concentrations (<1 mg m^{-3}), an annual maximum during the spring bloom (>2 mg m^{-3}), reduced summer concentrations when vertical stratification is maximal, and a secondary fall bloom beginning in September-November (O'Reilly and Zetlin, 1998; Thomas et al., 2003). During summer stratification, a subsurface chlorophyll maxima develop with concentrations reaching 50 to 75% of spring bloom levels (O'Reilly and Zetlin, 1998).

The Mid-Atlantic Bight waters are commonly divided into two water masses: shelf water and slope water, which are bounded by the shelfbreak front (Linder and Gawarkiewicz, 1998). The shelf water in MAB is the result of mixing of waters in the Gulf of Maine associated with low salinity water from the Scotian Shelf and the Slope Water that enters the Gulf of Maine through the Northeast Channel (Mountain, 2003, 2012). Oxygen-isotope tracers revealed a connection between shelf water in the Mid-Atlantic Bight and waters originating along the southern shelf of Greenland (Chapman and Beardsley, 1989), with this circulation being driven primarily by the wind stress and secondarily by buoyancy fluxes (Chen and Yang, 2024). At MAB, the equatorward advection associated with surface heat and freshwater exchanges and mixing with saltier slope waters modify the properties of the shelf water (Lentz, 2010). On the surface, interannual variability of salinity is driven largely by river discharge and precipitation (Manning, 1991), with large interannual variations being advected into MAB from the Gulf of Maine (Mountain, 2003). The shelf water in MAB exhibits a cold (<10°C) near-bottom water mass that persists over the mid-shelf and outer shelf, from spring to fall. It is a winter remnant feature located between the seasonal thermocline and warmer slope water, with gradual warming from spring to summer at a rate of about 1°C $month^{-1}$ (len).

In MAB's tidal currents, the M_2 constituent is the dominant signal representing on average 51.63 % of the total tide signal, with maximum of 10 cm s^{-1} on the mid-shelf, local maxima near the mouths of estuaries, and a phase that sweeps from north to south. Seasonal stratification and internal waves are associated with localized seasonal and interannual tidal amplitude variations in Nantucket Shoals (Brunner and Lwiza, 2020). Internal waves have been found to be influenced by the Gulf Stream and the shelfbreak front. The shelfbreak front can decrease by about 10 % the generation of topographic internal tides, while the Gulf Stream can prevent internal tides from radiating into the North Atlantic depending on the angle of incidence (Kelly and Lermusiaux, 2016).

Chlorophyll concentration in Mid-Atlantic Bight has two major periods of enhanced activity over the year, corresponding to fall-winter and spring periods (Xu et al., 2011). Nearshore areas close to estuaries are regions where chlorophyll is high throughout the year, similarly to the Gulf of Maine (O'Reilly and Zetlin, 1998), with outflow plumes of Chesapeake and Delaware Bay areas having higher annual rates of net primary productivity than the mid-shelf area to the north of Chesapeake and areas influenced by the Gulf Stream (Filippino et al., 2011). Seasonal vertical stratification has an important role in the

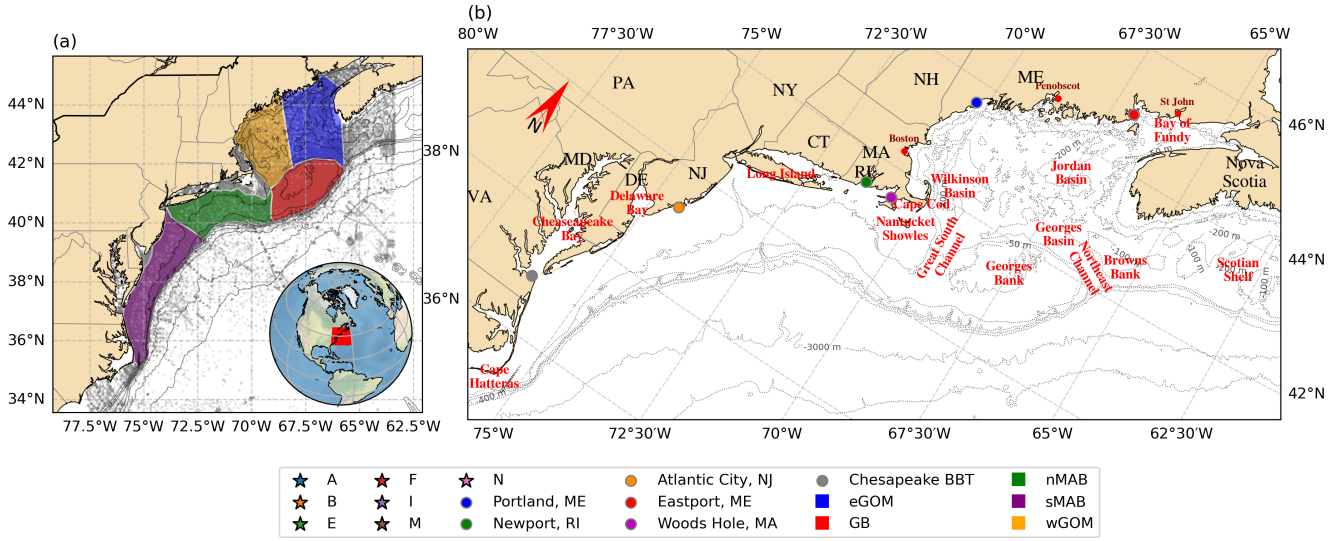

Figure 1. Model domain, Bathymetry, Observations (~~left panel~~a), and locations references (~~right panel~~b): Stars represent NERACOOS moorings, circles indicate CO-OPS tide gauges, and grey dots show high-resolution CTD data from the World Ocean Database. Colored shapes mark the locations of eastern Gulf of Maine (eGOM), western Gulf of Maine (wGOM), Georges Bank (GB), northern Mid-Atlantic Bight (nMAB), and southern Mid-Atlantic Bight (sMAB).

vertical mixing on the continental shelf and on the control of nitrogen availability, with the near shelf front transiting from well mixed during the winter to stratified in summer (Lentz, 2003; Rasmussen et al., 2005).

3 Methods

3.1 Model Configuration

195 The results in this work were produced by coupling the Geophysical Fluid Dynamics Laboratory's (GFDL) MOM6 and COBALT biogeochemical model (Adcroft et al., 2019; Stock et al., 2014, 2020). The configurations of MOM6 and COBALT largely followed configurations and datasets (initial conditions, boundary conditions and surface forcing) used in Ross et al. (2023) (R23, hereinafter). This hindcast simulation represents the period from 1993 to 2019. The datasets and differences in parameterization choices from R23 and other model configurations are briefly described below.

200 The model employs a z* coordinate with 75 layers following R23 with near-surface layer thickness of 2 m that increases progressively to a maximum of 250 m at 6500 m. The time steps are defined as 600 s for the baroclinic component, ~~1200~~ 1800 s for coupling, thermodynamics, and biogeochemistry, while the time-varying barotropic time step is constrained to 90 % of the CFL-limited maximum stable step. A Flather (1976) radiation boundary condition was used for barotropic velocity and subtidal, and tidal sea level, while the baroclinic flow was configured using Orlanski (1976) radiation scheme and nudging following

(Marchesiello et al., 2001) from The Copernicus Marine Global Ocean Reanalysis (Glorys). Lateral boundary conditions nudging had time scales of 5 days for inflow and 360 for outflow considering the baroclinic component. Lateral boundaries were associated with nudging close to the borders of the domain in order to constrain the separation of the Gulf Stream at Cape Hatteras. This is a strategy similar to the one adopted by (Azevedo Correia De Souza et al., 2023). A maximum damping rate of 7 days is applied at the borders for temperature and salinity , reaching timescales of several thousand days in the domain center to minimize interior constraints.

The topography was linearly interpolated from the General Bathymetric Chart of the Oceans (GEBCO) (GEBCO Bathymetric Compilation Group 2023, 2023) and didn't require smoothing. A horizontal Arakawa C grid with 430x396 tracer points and a nominal resolution of approximately 1/25° is interpolated from a subset of a 1/12° grid of the North Atlantic (Chassignet and Xu, 2017), with typical zonal and meridional distances between grid points of approximately 4 km at mid-latitudes. The grid is defined from South Carolina to Nova Scotia and includes the Mid-Atlantic Bight, Gulf of Maine, and Bay of Fundy (Figure 1).

Starting from R23, a calibration phase testing several combinations of parameterizations and parameters determined the final model configuration. The tests combined vertical mixing schemes including KPP (Large et al., 1994), ePBL (Hallberg, 2013), shear stress parameterization (Jackson et al., 2008), mixed-layer eddy parameterization (Fox-Kemper et al., 2008; Fox-Kemper and Ferrari and different advection-Coriolis schemes (Arakawa and Lamb, 1981; Sadourny, 1975). Table 1 summarizes the main configurations of ~~MOM6-NEUS25. Differences in parameter values with R23 were necessary due to the higher resolution of the model. The Arakawa and Lamb advective scheme better constrained~~ MOM6-COBALT-NEUS25. The Arakawa and Lamb's (1981) coriolis-advective scheme better confined tracer fields to continental shelf bathymetry than ~~Sadourny 75~~ Sadourny (1975) scheme (not shown). Sadourny's (1975) energy-conserving scheme tends to spuriously accumulate enstrophy at smaller scales which could be problematic for high resolution models. When coupled with the horizontal viscosity scheme (maximum between biharmonic and Smagorinsky) under the R23 configuration, ~~Arakawa's~~ Arakawa and Lamb's (1981) advective scheme rapidly eroded the ocean mesoscale structure. ~~Increasing~~ In this context, increasing the Smagorinsky viscosity corrected ~~this~~ the erosion, perhaps by better constraining horizontal viscosity relative to vertical viscosity, which affected the inverse energy cascade, though the exact mechanism remains unclear. The model employs a hybrid boundary layer mixing scheme based on the maximum between ePBL and KPP diffusivities~~, creating a hybrid mixing approach~~. R23 mentioned improved description of bottom temperature when employing the mixed-layer parameterization Fox-Kemper et al. (2008), however this was not found in our calibration phase.

A summary of the datasets and respective variables used to produce the initial conditions, boundary conditions and surface forcing fields for MOM6 and COBALT are presented in Table A1. MOM6 was initialized directly from interpolated initial conditions from Glorys in 1993 following R23, and COBALT initialized from the interpolated information from a global MOM6+COBALT simulation (Stock et al., 2014), World Ocean Atlas (Garcia et al., 2024b, a), and a fit using Esper (Carter et al., 2021). Riverine forcing is also present in the coupled model. Since our domain of NEUS25 is relatively restricted and is continuously forced by boundary conditions, the spin-up requires less than one month to start presenting reliable information at 1/25th resolution.

Table 1. Model Parameters

Parameter	Value	Reference
Vertical coordinate	75-layer z*	~~(Adcroft and Campin, 2004)~~ Adcroft and Campin (2004)
Baroclinic/Thermodynamic time step	300/1800	-
Planetary boundary layer parameterization	max(ePBL,KPP)	~~(Large et al., 1994; Reichl and Hallberg, 2018)~~ Large et al. (1994); Reichl and Hallberg (2018)
Shear driven turbulence	Jackson Parameterization	~~(Jackson et al., 2008)~~ Jackson et al. (2008)
Biharmonic viscosity	Maximum of Smagorinsky and resolution-dependent viscosities	Griffies and Hallberg (2000)
Smagorinsky coefficient	0.1	-
Resolution-dependent viscosity	0.01	~~(Adcroft et al., 2019)~~ Adcroft et al. (2019)
Bottom boundary layer mixing efficiency	~~0~~ 0.0	-
Background kinematic viscosity	1.0×10^{-6} m^2 s^{-1}	-
Background diapycnal diffusivity	1.0×10^{-6} m^2 s^{-1}	-
Sea level and barotropic velocity	Flather scheme	~~(Flather, 1976)~~ Flather (1976)
Baroclinic velocity	Radiation and nudging scheme (3 d inflow, 360 d outflow timescales)	~~(Marchesiello et al., 2001; Orlanski, 1976)~~ Marchesiello et al. (2001); Orlanski (1976)
Coriolis scheme	Arakawa and Lamb scheme (1981)	~~(Arakawa and Lamb, 1981)~~ Arakawa and Lamb (1981)
Nudging (sponge)	Temperature and salinity, interpolation in time and space	-
Opacity scheme	Manizza+05	-

The Copernicus Marine Global Ocean Reanalysis (Glorys) provides eddy-resolving (1/12°) global simulation results from 1993 onward, assimilating observational data (Jean-Michel et al., 2021). The assimilated data consist of 0.25° AVHRR sea surface temperature, altimeter information, in situ temperature and salinity profiles, and sea ice extent over polar oceans (Drévil-

lon et al.). ERA5 is a fifth-generation ECMWF reanalysis of global weather and climate, representing a detailed atmospheric record beginning in 1940. It combines model results with global observations through data assimilation performed every 12 hours (Hersbach et al., 2020). TPXO9 is a global ocean tidal model for barotropic tides that optimally fits the Laplace tidal equations using bathymetry and satellite altimeter data. It provides gridded harmonic constants for semidiurnal (M2, S2, N2, K2), diurnal (K1, O1, P1, Q1), two long-period (Mf, MM), and three nonlinear (M4, MS4, MN4) tidal constituents. The specific constituents adopted in MOM6 are listed in Table A1. River discharge data are obtained from the Global Flood Awareness System (GloFAS), an operational forecasting and monitoring system developed by the European Commission's Copernicus Emergency Management Service. This satellite-based service utilizes Copernicus Sentinel-1 Synthetic Aperture Radar (SAR) data at 0.1 ° resolution (Harrigan et al., 2021).

The World Ocean ~~Atlas23~~ Atlas 23 (Garcia et al., 2024b, a) consists of objectively analyzed, quality controlled fields based on the World Ocean Database, that can be used in creating boundary and/or initial conditions for ocean models. The Esper multiple regression algorithm (Carter et al., 2021) is used to fit the Alkalinity and DIC based on salinity and potential temperature in the boundary conditions from WOA23 considering the monthly climatology product, without the year-varying adjustment applied by R23. The implications are discussed in Section 5. We used the climatology of Stock et al. (2014) to determine multiple variables required by COBALT in both initial and boundary conditions. This is a global ocean-ice-ecosystem model that was able to capture cross-biome features and observation-based planktonic web fluxes estimates. The River Chemistry for the U.S. Coast (RC4USCoast) is a historical dataset containing river chemistry and discharge for 140 monitoring sites of the US Coast, from 1950 to 2022, derived from the Water Quality Database of the US Geological Survey (USGS), and including river discharge from the U.S. Army Corps of Engineers and the USGS's Surface-Water Monthly Statistics for the Nation (Gomez et al., 2022, 2023). For the atmosphere, historical atmospheric CO2 concentrations up to 2014 and its extension under the SSP2-4.5 are used (Meinshausen et al., 2020). Monthly climatologies of GFDL's ESM4.1 earth system model (Dunne et al., 2020) provided the wet and dry deposition of NO_3 and NH_4, and lithogenic dust. Iron was assumed to represent 3.5 % of the dust, while dry deposition of phosphorus assumed a concentration of 563 ppm, where 22 % is available for biology (Baker and Croot, 2010; Herbert et al., 2018) . These approaches followed (Stock et al., 2020) and R23.

Our model initialization starts directly from GLORYS temperature and salinity field in a similar manner to R23. Given the relatively restricted and shallow domain we are working, the biogeochemistry in the domain spin-up takes about 3 months to adjust from the climatological conditions, which is associated with the relatively shallow environment on the continental shelf and the intense horizontal and vertical mixing associated with the presence of the Gulf Stream on the slope. We include the spin-up period of the model in the model evaluation since it is relatively short.

3.2 Observations

MOM6-COBALT-NEUS25 results were evaluated by comparing simulated fields against in-situ observations, satellite-derived products, and climatological datasets. Our strategy targeted physical oceanographic variables (temperature, salinity, sea level), and biogeochemical parameters (chlorophyll, NO_3, zooplankton biomass). The data products used to evaluate the coupled model results are summarized in Table 2. In our evaluation, delta difference maps are used for comparisons between data

Table 2. Data products used to evaluate the coupled model. Spatial and temporal resolution are represented, respectively by Δs and Δt.

Dataset	Variables	Δs	Δt	Depth/Location	Period	Ref
GLORYS12v2	T,S,ssh	1/12°	daily	multiple depths	1993-2019	Jean-Miche
NERACOOS	T,S	~~-~~sparse	<1 ~~hour*~~ hour	multiple depths	~2001-2019	Pettigrew
~~NOAA OISST v2~~ OSTIA	SST	1/~~4~~20°	daily	surface	1993-2019	~~Reynolds et al. (2008~~
NCEI Climatologies	SSS	1/10°	climatology	surface	1955-2017	Seidov et a
~~bias-corrected~~ Bias-corrected model results	T	1/12°	daily	bottom	1993-2019	Du Pontavi
EMOLT	T	~~-~~sparse	<~~1 hour*~~ 1hour	bottom	1993-2019	Manning and
COPEPOD	333μm zoop.	~~-~~sparse	sparse	depth integrated	multidecadal	Rebuck and T
OC-CCI	chlorophyll a	4km	8-day	surface	1993-2019	Sathyendran
CODAP-NA	TA	1°	climatology	multiple depths	2003-2018	Jiang et
NNGv2LDEO	DIC	1°	climatology	multiple depths	1972-2017	Broullón
World Ocean Database	T, S	~~-~~sparse	climatology	multiple depths	multidecadal	Mishor
CO-OPS	water level	~~-~~sparse	< ~~1hour*~~ 1hour	surface	multidecadal	

references and MOM6-COBALT-NEUS25 results. Their color palettes are configured to be comparable with R23 whenever possible. We present a brief overview of the datasets below.

The Northeastern Regional Association of Coastal Ocean Observing Systems (NERACOOS) has deployed oceanographic moorings in the Gulf of Maine since 2001. These buoys provide high-temporal resolution measurements enabling detailed assessment of tracer field variability. Temperature, salinity, and Acoustic Doppler Current Profiler (ADCP) sensors record information at various depths in the water column, with the data being maintained and made available on the NERACOOS website (neracoos.org). The positions of the buoys are shown in Figure1.

Sea surface ~~temperatures are evaluated using the NOAA Optimum interpolation Sea Surface Temperature Analysis version 2 (Reynolds et al., 2008) (OISST) ,~~ temperature (SST) is evaluated using a long-term, reprocessed dataset SST (OSTIA) (Worsfold et al., 2024) with a grid resolution of ~~0.25~~0.05°. This dataset ~~uses Advanced Very High-resolution Radiometer data, from the Pathfinder AVHRR SST, and was built as a climate-oriented dataset with a two-satellite merged constellation, designed to ensure long-term consistency~~is a daily gap-free analysis that uses in-situ and satellite data processed at Met Office (UK). Daily sea level gridded data based on satellite observations from 1993 to the present were produced by Copernicus Climate Change Service (C3S sea level dataset) (Lopez, 2018).

Sea surface salinity evaluation is based on the National Centers for Environmental Information (NCEI) Northwest Atlantic Regional Climatology (Seidov et al., 2018, 2019), which is derived from World Ocean Database and presents a resolution of 0.1°. Despite the existence of satellite data products for salinity, their relatively short time range precludes the assessment at longer timescales and makes it more advantageous to use the regional climatology for evaluation.

Simulated bottom temperature in the northeast U.S. continental shelf from MOM6-COBALT-NEUS25 was evaluated using two distinct datasets. The first consists of a high-resolution long-term bottom temperature product, created based on a bias-

corrected ROMS simulation, and two global ocean reanalysis (Glorys12v1 and PSY4V31) (Du Pontavice et al., 2023), with good performance in reproducing both seasonal and annual variability of reference datasets. It enables the evaluation of the seasonal horizontal distribution of bottom temperature on the continental shelf. The second dataset consists of temperature time series measured by thermistors in lobster traps (Manning and Pelletier, 2009) distributed along the western edge of the Gulf of Maine and along the shelf edge in the northern Mid-Atlantic Bight in water depths ranging from 1-300 m. It complements the spatial analysis by including detailed temporal variability at multiple locations.

World Ocean Database is a quality-controlled dataset including more than 18.6 million oceanographic casts consisting of up to 3.13 billion individual profile measurements. Here we select only high-resolution CTD information with temperature and salinity information (Mishonov, 2024) to evaluate the seasonal vertical structure of temperature and salinity along the continental shelf based on the subregions defined in Figure 1.

Long-term measurements of sea level using tide gauges operated and maintained by Center for Operational Oceanographic Products and Services are used in the validation of the sea surface elevation at the coast .

The following datasets present biogeochemistry data in terms of nutrients, chlorophyll, and zooplankton, useful in the evaluation of seasonal results. A data collection ranging from 1932 to 2011 was organized by Rebuck and Townsend (2014) in the Gulf of Maine including dissolved inorganic nitrogen, silicate and phosphate from several sources, such as the World Ocean Database, and Integrated Science Data management among others. These data are used to calculate seasonal climatologies of NO_3 + NO_2 and PO_4. Chlorophyll was obtained from the Ocean-Colour Climate Change Initiative (OC-CCI), which derives chlorophyll-a from ocean-colour data. It uses the Medium Spectral Resolution Imaging Spectrometer (MERIS) from the European Space Agency, the Sea-viewing Wide-Field-of-view Sensor (SeaWiFS), and Moderate-resolution Imaging Spectroradiometer-Aqua (MODIS-Aqua) from National Oceanic and Atmospheric Administration, with a time series covering the period from late 1997 to end of 2018 at 4 km resolution (Sathyendranath et al., 2019), which closely matches the model's resolution. The Coastal & Oceanic Plankton Ecology, Production & Observation Database (COPEPOD) is a global online database that consolidates 60 years of plankton monitoring. It has been created by the National Marine Fisheries Service with data from several fisheries and research institutes around the world (Moriarty and O'Brien, 2013). This dataset provides the monthly 200 m average biomass estimate of epipelagic mesozooplankton and is compared with the mesozooplankton simulated by MOM6-COBALT-NEUS25.

Carbon chemistry is evaluated through total dissolved inorganic carbon (DIC) and total alkalinity (TA).NNGv2LDEO (Table 2 consists of a feedforward neural network calibrated with the Lamont-Doherty Earth Observatory datasets (Takahashi et al., 2017) , Global Ocean Data Analysis Project version 2.2019 (Olsen et al., 2019), among others. The DIC climatology was produced by passing WOA23 temperature, salinity, and oxygen climatologies — along with phosphate, nitrate, and silicate fields derived from those same variables using a different neural network (Bittig et al., 2018) — through the trained NNGv2LDEO network (Broullón et al., 2020). NNGv2LDEO climatology will be refered hereinafter as 'Broullón climatology'. The Coastal Ocean Data Analysis Product in North America (CODAP-NA) (Jiang et al., 2021, 2022) is a data product focused on coastal ocean acidification, with two decades of discrete measurements of several carbon system parameters, nutrients and oxygen from the North American continental shelves including TA.

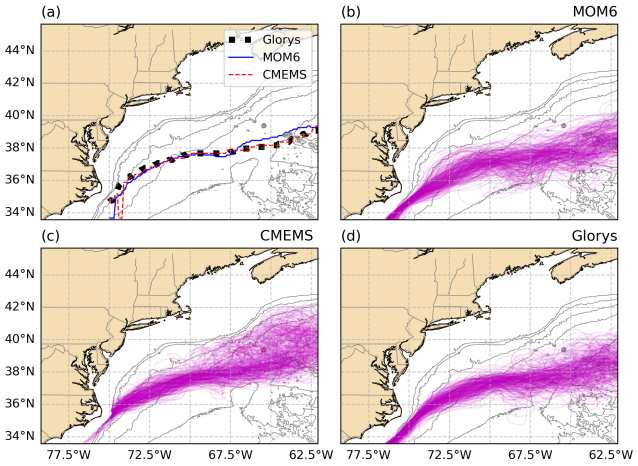

Figure 2. Path comparison of the Gulf Stream ~~path comparison~~ for the period between the years of 1993-1994 across MOM6, ~~results,~~ CMEMS satellite SSH L4 product and Glorys. ~~The position~~ Position of the Gulf Stream based on the maximum standard deviation of SSH ~~is presented in the upper left panel~~(a). In the remaining panels (b to d), magenta lines represent the 0 m contour of monthly SSH anomaly. Gray lines represent isobaths of 1000, 2000, 3000, 4000, and 5000m

4 Results

4.1 Circulation

Average SSH results of ~~MOM6~~ MOM6-COBALT-NEUS25 generally represent the separation of the Gulf Stream at Cape Hatteras, but exhibits a northward bias west of 67.5°W of approximately 0.5° that makes it closer to the shelf, relative to both Glorys SSH and CMEMS satellite ADT L4 product (Figure 2) in the period from 1993 to 2019. Following separation from the continental slope off Cape Hatteras, MOM6's Gulf Stream displays a tendency to meander northward along the Mid-Atlantic Bight shelfbreak, contrasting with the more southerly path demonstrated in both the CMEMS satellite SSH L4 product and Glorys reanalysis. Monthly averages of all three datasets reveal paths of Gulf Stream with pronounced presence of meanders in CMEMS reaching the shelf break south of the Scotian Shelf. These processes, associated with mesoscale activity and warm-core rings, have significant influence on slope water intrusions into the Gulf of Maine (Du et al., 2022). Even though the reduced meandering in MOM6 and Glorys could lead to misrepresentation of tracer fields in the Gulf of Maine and biases in the primary production simulation by COBALT, the model and reanalysis are able to realistically simulate the waters in the Gulf of Maine. Bias-correction of lateral boundary nudging and initial conditions can potentially improve the solution, but they often return mixed results with no clear advantage over using original reanalysis outputs (e.g López et al., 2020; Lehmann et al., 2009).

Seasonal averages of MOM6-COBALT-NEUS25, Glorys and their comparison are shown in Figure 3. On the slope, the average position of the Gulf Stream is represented by the largest horizontal SSH gradients. Our simulation represents the

region on the Slope Sea marked by lower SSH values (<-0.55 m) and the areas south of the Gulf Stream's North Wall where the highest SSH values are present. On the continental shelf, MOM6-COBALT-NEUS25 has isolines of SSH (-0.5 m) pattern that are more complex than Glorys', marking features associated with the Northeastern Channel in the Gulf of Maine and the region influenced by Georges Bank. On the slope domain, the model underestimates positive SSH values, and overestimates negative SSH values (Figure 3i to l).

Currents at the surface and at 75 m show the general structure in the Gulf of Maine described in Section 1 is reproduced, with the representation of features such as the ~~the~~ Shelf Break Jet , WMCC, EMCC, the anticyclonic circulation around Georges Banks, and the cyclonic circulation connecting Georges Basin with the Northeast Channel (Figure 4). The intensification of the cyclonic circulation in the Gulf of Maine associated with seasonal surface heat flux (Xue et al., 2000) occurs in the model, with stronger circulation parallel to the coast line, with a WMCC flowing parallel to NH coast, differently from winter. The analysis reinforces the relevance of topography to the circulation in the Gulf of Maine, with the currents generally following isobaths, as expected at first order from the tendency of the flow to follow the Taylor-Proudman theorem and vorticity constraints. The cyclonic recirculation in Georges, Wilkinson and Jordan Basin occupies the entire water column in all seasons (not shown). The slope waters pathways into the Gulf of Maine are defined by the intensified flow (>0.16 m s^{-1}) at the northern wall of the Northeastern Channel, with part of flow being redirected into the recirculation in Georges Basin and Browns Bank, part of being redirected into the interior of the Gulf of Maine, and part flowing parallel to the coastline.

Hovmöller Diagrams of daily composites for the period between 2009 and 2019 of NERACOOS ADCP moorings show the model reproduces the seasonal structure with mixed performance, based on a bulk correlation displayed in Figure 5 for moorings A, I, M, N (Figure 1). For along-bathymetric currents, larger error metrics (RMSE, MAE, and bias) are present and are likely a consequence of the higher magnitudes of these currents. At ~~M01~~mooring M (Figures 1,5M), the low correlations (<0.1) are associated with the relatively low currents (<6 cm s^{-1}~~$^{-1}$~~), where a relatively poor signal-to-noise ratio occurs. In the Gulf of Maine, the grid resolution does not resolve the first Rossby radius of deformation Radius (Hallberg, 2013), which may contribute to the low correlation in the solution of currents at different moorings.

Even though relevant differences in magnitude of the along-bathymetry currents at ~~N01~~ mooring N (Figures 1,5N) occur, some similarities are still observed. Two seasonal regimes are evident in ~~N01~~ mooring N following the NERACOOS observations. The first occurs in mid-year (approximately days 180-260), while the second occurs during the remainder of the year. The mid-year structure has more intense currents (<10 cm s^{-1}) at the subsurface, with its core at about 100 m. The second, on the other hand, shows surface intensified currents, while currents flow out of the Gulf of Maine below approximately 70 m. During mid-year, the current structure is roughly reproduced by the model, with a relatively deeper penetration of the current with its core at about 50 m and surface along-bathymetry currents near 0 cm s^{-1}. The current intensification in the model does not reach the bottom, similarly to the observations. During other periods, the surface intensification biases reaches about 8 cm s^{-1}, while at depth the model shows currents that approach 0 cm s^{-1}.

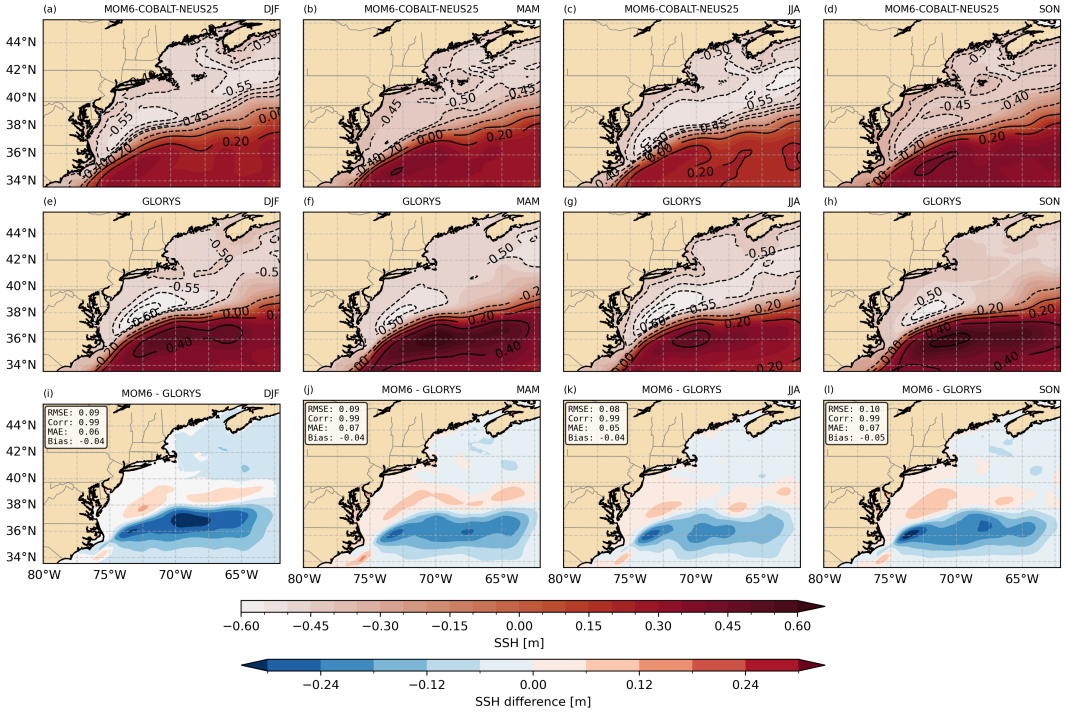

Figure 3. ~~Streamlines~~ Seasonal averages of ~~MOM6 surface currents in winter~~ SSH considering MOM6-COBALT-NEUS25 (~~DJF~~a to d), GLORYS (e to h) and ~~summer~~ their difference, MOM6-COBALT-NEUS25 - GLORYS (~~JJA~~i to l)~~in the Gulf of Maine~~. Black contours and filled contours represent SSH intervals.

4.2 Temperature and Salinity

4.2.1 Seasonal surface fields

Sea surface temperature (SST) patterns provide further metrics to evaluate the Gulf Stream structure and the continental slope and shelf fields. The SST representation in MOM6-COBALT-NEUS25 is evaluated using ~~OISST~~ OSTIA level 4 data product for the entire period of the simulation. Figure 6 shows a seasonal climatological comparison between the SST of MOM6, ~~OISST~~ OSTIA and their difference. Domain-averaged biases are relatively small (<0.2°C) across all seasons, with the surface 20°C isotherm delimiting warmer waters in the domain of the Gulf Stream and Slope Sea, and cooler waters on the continental shelf. A similar Glorys evaluation provides additional context for performance assessment (Figure A1). In general, MOM6 shows some ~~improved~~ similar statistics compared with Glorys, with absolute biases being generally less than ~~0.17~~0.19°C in MOM6 compared to ~~0.35~~0.25°C in Glorys on average. Similarly, MOM6 shows ~~lower~~ similar mean absolute error (MAE) values (~~typically <~~ 0.40°C)~~compared to Glorys~~. Spatial correlation also present similar values(0.99 to 1.0)~~and root mean square error have similar performance in both simulations when compared with OISST~~, while MOM6 has a slight higher RMSE (0.63°C) than Glorys (0.55°C).

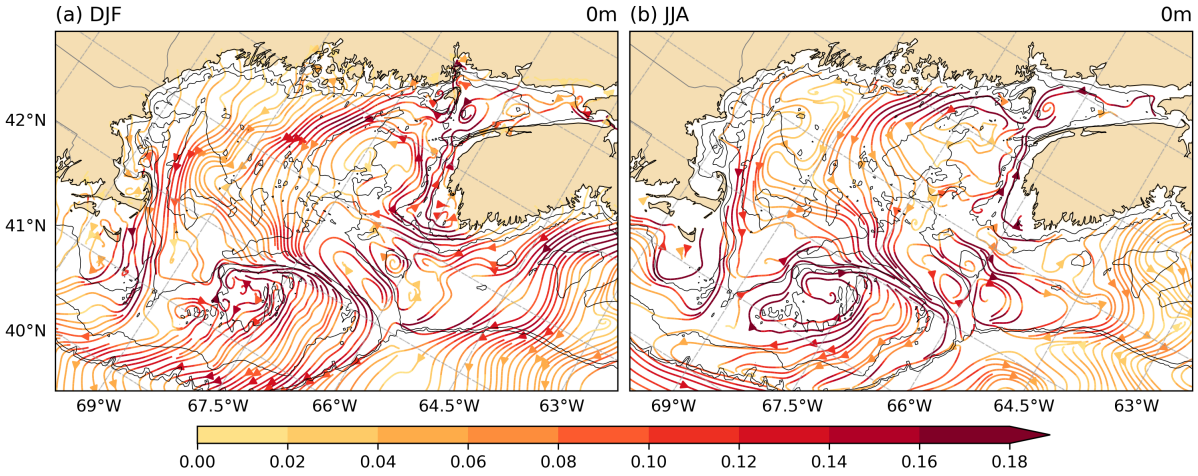

Figure 4. ~~Hovmöller diagram of currents~~ Winter (~~daily compositea~~) ~~measured by NERACOOS ADCP~~ and ~~simulated by MOM6-COBALT-NEUS25~~ summer (~~row labelsb~~) ~~, considering cross-, and along-bathymetry currents. Positive values of along-bathymetry panels are referenced as equatorward flow for moorings A01, and I01, towards the Gulf~~ integral curves of ~~Maine at N01, and in the cyclonic direction at M01. In~~ the ~~cross bathymetric panels~~instantaneous MOM6 surface velocity field, ~~positive values are perpendicular and to the right of the along-bathymetry direction. The evaluation period spans the years between 2009 to 2019 and correlation values represent the correlation between observed and modeled currents~~ computed ~~over all time-depth pairs (flattened time-depth matrix). The position~~ via numerical integration of the ~~moorings is found in Figure 1~~tangent vector field.

MOM6-COBALT-NEUS25 representation of the Gulf Stream separation in Cape Hatteras (Figures 6,2), leads to an improved description of the SST in the Slope Sea and in the Gulf Stream domains relative to NWA12 (Ross et al., 2023, Figure 3). Considering the Gulf Stream and Slope Sea regions, DJF and SON have the warmest positive bias typically ranging between +0.5°C and +1.5°C, followed by MAM and JJA when biases are typically between 0.0°C and 1.0°C (Figure 6). The higher biases in Winter and Fall in MOM6 represent remnants of the Gulf Stream meandering northward of its most typical position after the separation from Cape Hatteras.

In the Gulf of Maine, the seasonal differences between MOM6-COBALT-NEUS25 SST and ~~OISST~~ OSTIA are typically below 0.5°C – these values are comparable with a similar evaluation of the mean SST using eight reanalysis products (Castillo-Trujillo et al., 2023). During JJA and SON, MOM6-COBALT-NEUS25 shows ~~negative biases (<~~biases up to -1°C ~~) in JJA and SON close to the coast of~~ in the Nova Scotia and ~~Maine, which could be related to the resolution limitation of OISST data product (1/4°), as it is unable to resolve local features such as the EMCC, which carries relatively cold waters (Pettigrew et al., 2005). South of Cape Cod,~~ a patch of strong negative biases (<-2°C) ~~is present~~south of Cape Cod, which is also identifiable in R23 evaluation. These seasonal representations are an improvement relative to Glorys (Figure A1) in the coast of Maine, Nova Scotia, and Georges Bank when considering JJA and SON. At these regions Glorys presents local differences that are larger than 3°C likely due to absence of tides representation in the reanalysis.

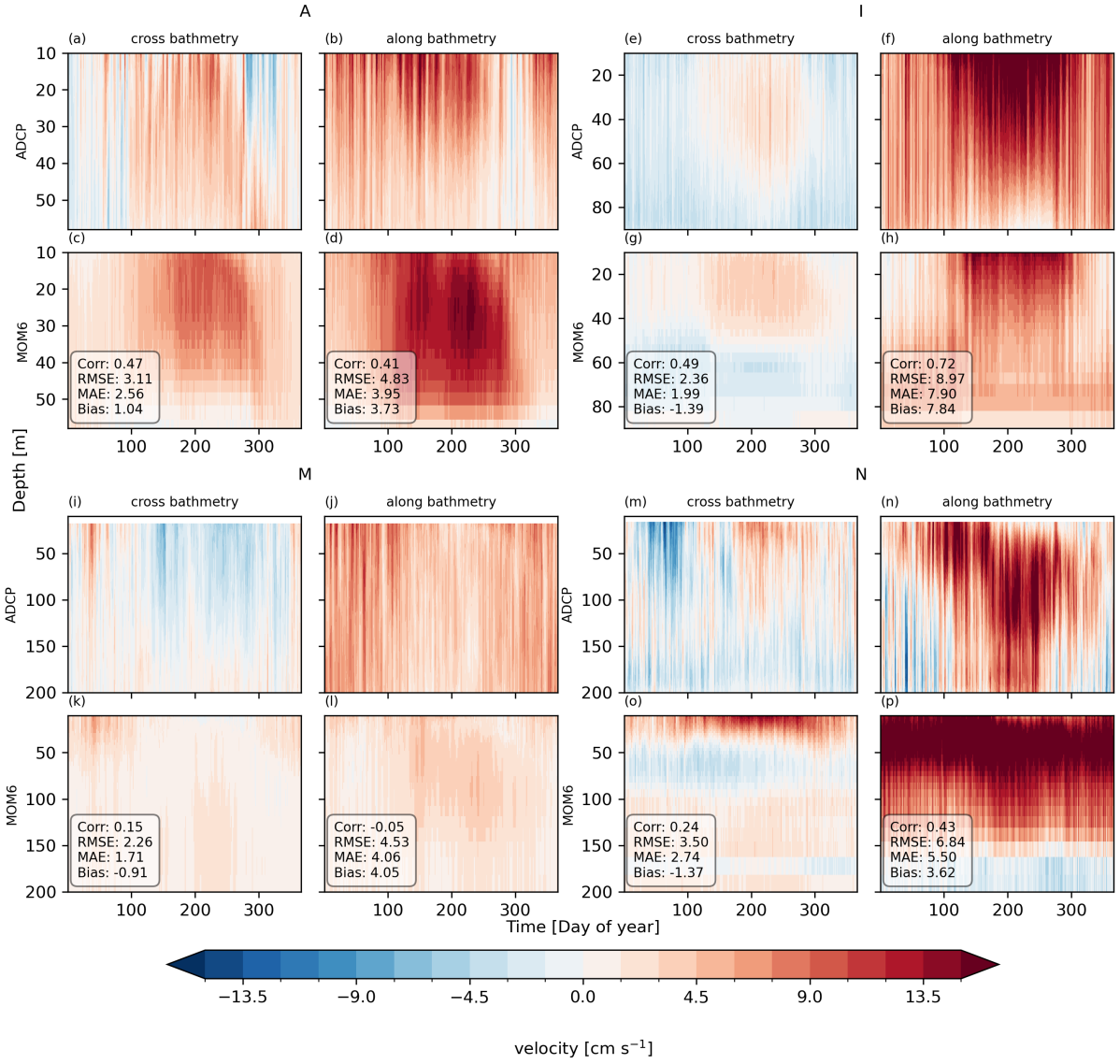

Figure 5. Hovmöller diagram of currents (daily composite) measured by NERACOOS ADCP and simulated by MOM6-COBALT-NEUS25 (row labels), considering cross-, and along-bathymetry currents. Moorings (A, I, M, N) are referenced by the subtitles. Positive values of along-bathymetry panels are referenced as equatorward flow for moorings A, and I, towards the Gulf of Maine at mooring N, and in the cyclonic direction at mooring M. In the cross bathymetric panels, positive values are perpendicular and to the right of the along-bathymetry direction. The evaluation period spans the years between 2009 to 2019 and correlation values represent the correlation between observed and modeled currents computed over all time-depth pairs (flattened time-depth matrix). The position of the moorings is found in Figure 1

The seasonal sea surface salinity (SSS) represented by MOM6 is generally similar to NCEI regional climatology (Figure 7) considering the period from 1993 to 2019, with domain-averaged absolute bias presenting values typically lower than 0.1,

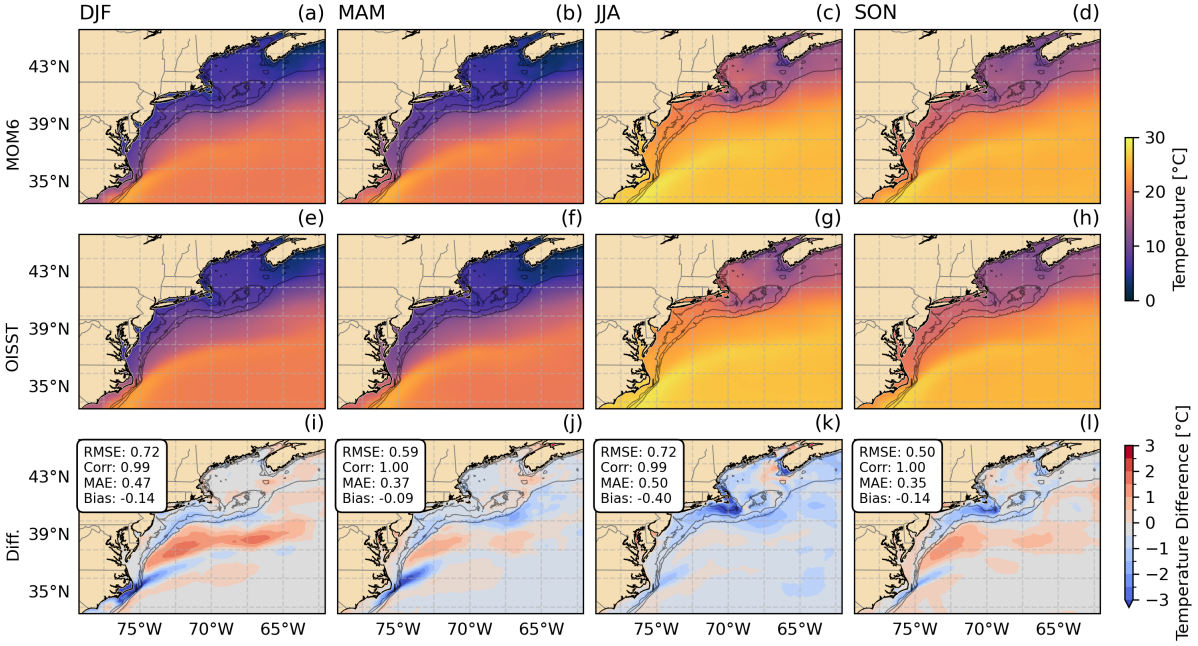

Figure 6. Seasonal averages of sea surface temperature considering MOM6 (~~top panels~~a to d), ~~OISST~~ OSTIA SST (~~middle panels~~e to h) and their differences (~~lower panels~~i to l, MOM6 - ~~OISST~~OSTIA). ~~MOM6 results were upscaled to OISST resolution~~ OSTIA SST was interpolated (~~0.25°~~bilinear) ~~by binning corresponding areas and calculating averages~~into MOM6 horizontal grid. Black contours are the ~~isobath~~ isobaths of 40, 80, and 400 m.

and spatial correlation higher than 0.95~~(Figure 7)~~. The isohaline of 34 roughly marks the limit between the continental shelf and the continental slope, with NCEI climatology showing slight deviations from this pattern in the region of the Mid-Atlantic Bight. ~~Lowest~~ The lowest salinities (<30) occur along the coast in the NCEI climatology, with emphasis on the Scotian Shelf and during the spring (MAM), and summer (JJA), when a fresher strip of water between the coast of Maine and Cape Hatteras is present. In MOM6, this fresher water feature is not represented, appearing as a positive bias, with salinity values up to +1.8 saltier during spring (Figure 7c,k). Along Chesapeake and Delaware bays, MOM6 shows fresher salinity biases that, throughout the year, may exceed -2.0, and continues as a fresh bias tongue over the shelfbreak in DJF, JJA, and SON with values varying approximately between -0.4, and -1.2. In the Gulf of Maine, Georges Bank and areas beyond the 400 m isobath show more moderate salinity biases between ±0.4. In general, MOM6-COBALT-NEUS25 biases on the shelf and slope in the domain between Cape Hatteras and the Scotian Shelf are lower than those in R23, where positive biases (roughly between +0.4 and +1.2) were present. Compared to Glorys, MOM6-COBALT-NEUS25 exhibits similar spatial correlation and bias magnitudes, but slightly elevated RMSE values during spring and summer seasons (Figures 7, A2). MOM6-COBALT-NEUS25 exhibits a salinity drift pattern similar to that of Glorys (Figure A3). The absolute salinity difference between MOM6-COBALT-NEUS25

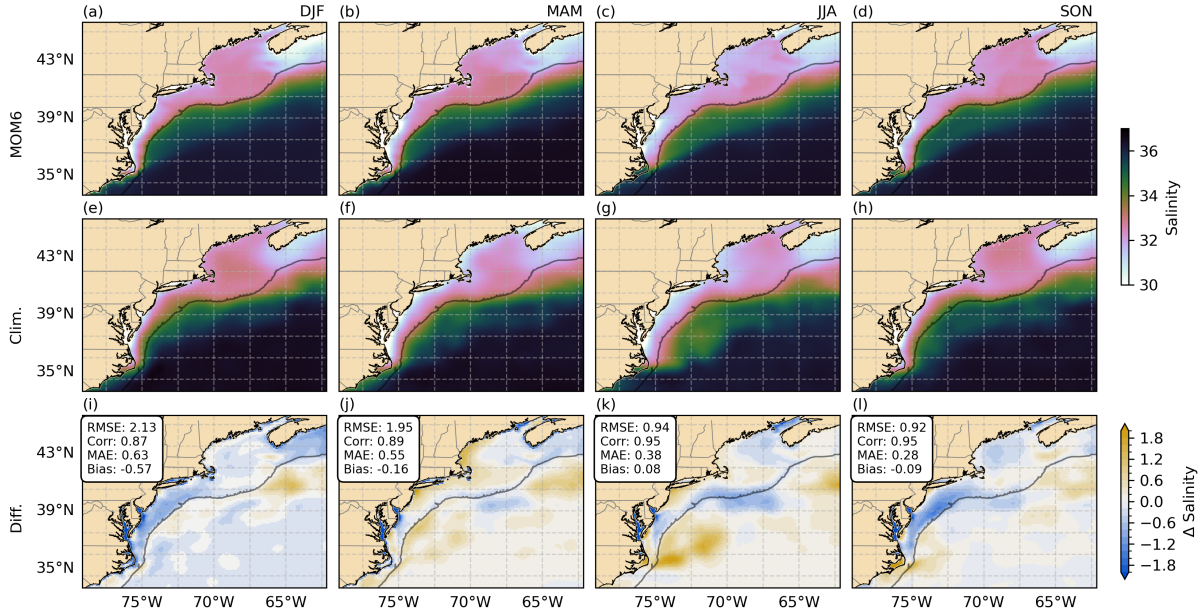

Figure 7. Seasonal averages of sea surface salinity from MOM6 (~~top panels~~a to d) and NCEI regional climatologies (Clim., ~~middle panels~~e to h) and seasonal differences (~~lower panels,~~ MOM6 - Clim., i to l). Black contour indicates the 400m isobath, roughly representing the position of the shelf break. MOM6 results were upscaled to NCEI climatologies resolution (0.1°) by binning corresponding areas and calculating averages.

and Glorys are generally lower than 0.2 in the period between 1993 and 2019 and shows no significant trend over time indicating an evaporative-freshwater flux balance.

4.2.2 Bottom temperature evaluation

Seasonal fields of bottom temperature of MOM6 are comparable to the seasonal averages dataset of Du Pontavice et al. (2023) having absolute averaged-domain biases lower than 1°C, and spatial correlation higher than 0.77 (Figure 8). In the Mid-Atlantic Bight, the seasonal maximum migrates spatially throughout the year: during winter and spring (~~DJF,MAM~~Figure 8a,b,e,f), maximum temperature occurs at the mid-shelf and shelf break (>40m), while in summer and fall (~~JJA,SON~~Figure 8c,d,g,h), they shift to the inner-shelf (<40 m). The Gulf of Maine has a similar seasonal pattern, with higher temperatures (>10°C) associated with locations closer to the coast during summer and fall, whereas near-coastal waters have typically lower temperatures (<8°C) in winter and spring.

Model performance varies seasonally, with MOM6 bottom temperature showing its best performance during fall across all subdomains in terms of spatial correlation (0.94). A warm bias varying from 0.0 to 2.0°C is present in waters shallower than 80 m during spring and summer along the continental shelf of Mid-Atlantic Bight and Georges Banks, which is potentially linked with the overmixing associated with the upper ocean boundary layer scheme (section Methods) and could lead to enhanced

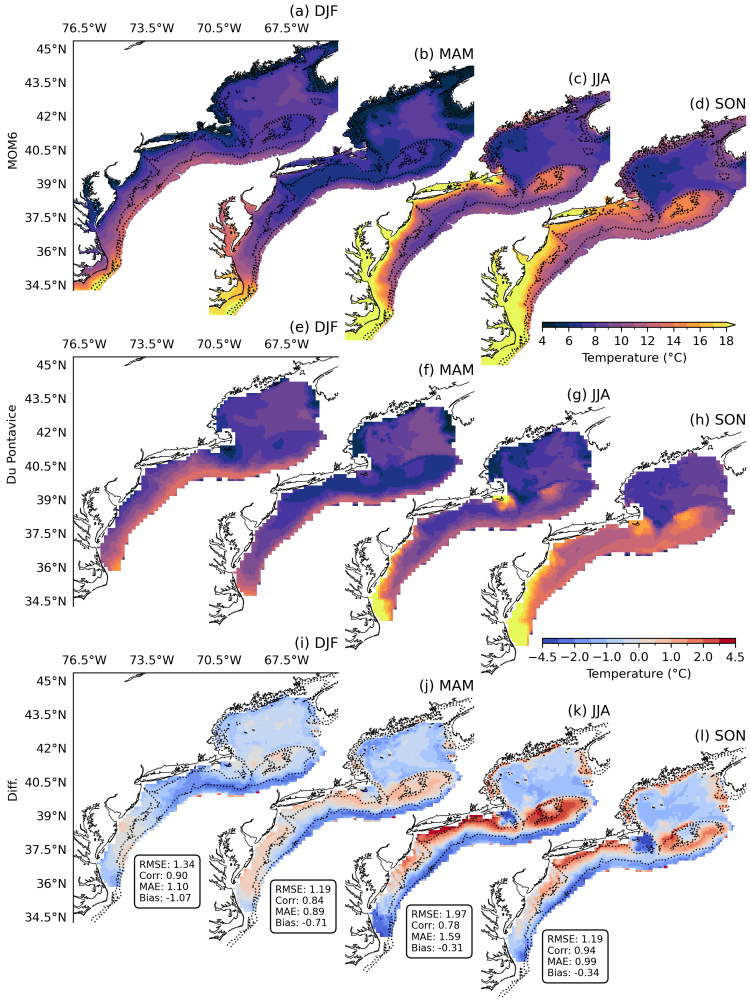

Figure 8. Seasonal averages of bottom temperature in MOM6 (~~upper panels~~a to d), Du Pontavice bottom temperature dataset (~~mid panels~~e to h), and their difference (MOM6 - duPontavice, i to l) considering the period between 1993 to 2019. Dotted lines correspond to the isobaths of 40 and 80 m. MOM6 results were upscaled to Du Pontavice's resolution (1/12°) by binning corresponding areas and calculating averages.

mixing between warmer surface waters and colder bottom waters. On the other hand, the model shows cold biases (<2°C) near the shelf break throughout the year relative to Du Pontavice et al. (2023). In the Gulf of Maine, areas deeper than 40 m exhibit cold biases usually between 0.0 to 1.0°C in winter, summer, and fall, while spring shows bias up to –2°C.

Bottom temperatures from MOM6-COBALT-NEUS25 are evaluated against eMOLT lobster trap thermistors measurements (1993-2014) along with an analysis of Glorys results (Figures 9 and A5). Only datasets containing over one hundred observation days were included in this analysis.

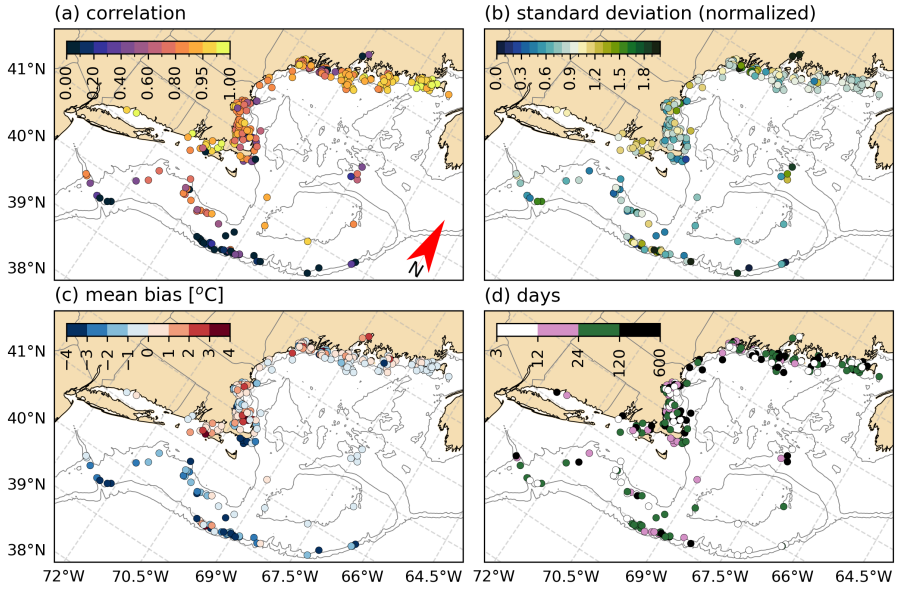

Figure 9. ~~Correlation~~Daily averaged bottom temperature statistics between MOM6 results and eMOLT dataset corresponding to (a) correlation, (b) standard deviation, (c) mean bias and (d) number of days available ~~in eMOLT (logarithmic~~ log scale)~~of daily averaged bottom temperature considering MOM6 results~~. The contours represent depths of 60, 200, and 1000 m.

MOM6 and Glorys have similar performance in simulating bottom temperatures time series (Figure 9), with MOM6 presenting more sites with correlation greater than 0.95 within 0-200 m isobath range. Both model and reanalysis have decreased skill in deep waters (>200 m) along the shelf break, where correlations drop below 0.85, normalized standard deviations fall below 0.7°C, and mean bias exceeds 2.0°C. On the mid- to outer-shelf south of Massachusetts/Rhode Island and close to the 60 m isobath, MOM6 displays a cold bias up to 2-3°C relative to Glorys.

The spatial statistics maps reveal regional performance variations, with MOM6 achieving higher correlation coefficients, normalized standard deviations closer to unity, and lower absolute mean biases along Maine and New Hampshire coastlines. On the other hand, Glorys demonstrates better performance along the eastern Massachusetts coast.

MOM6 implementation has at least two advantages relative to Glorys, which can explain its improved results: first, its finer spatial resolution allows the model a more accurate representation of bathymetric features and coastlines; second, the inclusion of a tidal signal likely provides a better representation of horizontal mixing particularly in macrotidal areas of the Gulf of Maine. In general, MOM6 has better performance in representing the bottom temperatures within the 200 m isobath.

4.2.3 Seasonal vertical structure

Seasonal climatological profiles based on the World Ocean Database (WOD) were built by calculating the horizontal average of temperature and salinity for each depth using the high-resolution CTD dataset within the different subregions listed in Figure 1.

To ensure statistical robustness, only depths containing more than one hundred points were selected in the profile calculations. Data density varies seasonally, with measurements in the surface ranging from 2000-8000 points in all seasons except for winter, when counts decrease to approximately 1000 points (or less).

Figure 10 presents a comparison between the temperature and salinity profiles of MOM6 and WOD, while skill metrics, such as as bias, MAE, and RMSE are graphically presented respectively in Figure A4. Depth-averaged bias, MAE, and RMSE suggest better performance in general of MOM6 in the Gulf of Maine for both temperature and salinity relative to Glorys, while Glorys better represents these fields in Georges Bank and Mid-Atlantic Bight.

The seasonal changes of the thermohaline structure across subregions show temperature represents the dominant control on seasonal stratification, with maximum surface values showing during summer and fall (JJA, SON) and minimum in winter and spring (DJF, MAM) (Figure 10). Seasonal temperature variability influences depths to 150 m in the Gulf of Maine regions (GM: wGOM and eGOM), while affecting the entire water column in the shallower Georges Bank and Mid-Atlantic Bight (GB/MAB: GB, nMAB and sMAB, Figure 1a).

During warm seasons, a horizontal temperature gradient characterizes the shelf. Average surface temperatures are cooler (approximately 12°C) in the northeastern areas of the domain and progressively increase southwestward, where maximum seasonal averages occur (24°C) (Figures 6,10). The northeast-to-southeast temperature gradient persists in colder seasons, when eGOM exhibits temperature of about 5°C , while sMAB shows warmer conditions with temperature near 10°C (Figure 10). These patterns reflect the influence of latitudinal surface heating differences and the effects of different water masses on the continental shelf.

The vertical structure can be organized in two distinct regions corresponding to the GM and GB/MAB. Temperature generally decreases with depth down to 75 m in all regions during summer, but GB/MAB depicts a subsurface temperature minimum between 25-80 m depth, below which temperature increases towards the ~~bottom~~(Figure 10). This minimum in MAB is compatible with the Cold Pool depths and temperatures. MOM6 generally represents the seasonal structure of temperature in DJF/MAM especially in GM, but underestimates subsurface warming, showing discrepancies up to 5°C in GB/MAB. These discrepancies are evaluated in Section 5.

During fall (SON), the vertical stratification weakens through all domains, with the subsurface minimum disappearing in most of GB/MAB (Figure 11). Model-observation disparities remain in this season, with the model exhibiting a cold bias of 3-4°C in deeper areas and underestimating MAB temperatures by approximately 2°C throughout the water column. Winter (DJF) brings the weakest vertical stratification in all domains, with temperatures increasing towards the bottom. Minimal biases are present in GB and reach -5°C in nMAB. MOM6 successfully represents the stratification in wGOM, eGOM, sMAB, but shows a warm bias (1°C) in GB and underestimates the warming at lower levels in nMAB.

Salinity profiles (Figure 10f to j) show seasonal variability restricted to the upper 50 m in GM and GB, while MAB has pronounced variations throughout the water column. In all regions, salinity values increase toward the bottom, reaching maximums between 34–35 in GM, and 33–36 in GB/MAB. MOM6 reproduces the seasonal profiles of salinity in GM and upper GB, with deviations of salinity of 0.5 in the deepest parts of the water column at wGOM . In deep parts of GB salinity pro-

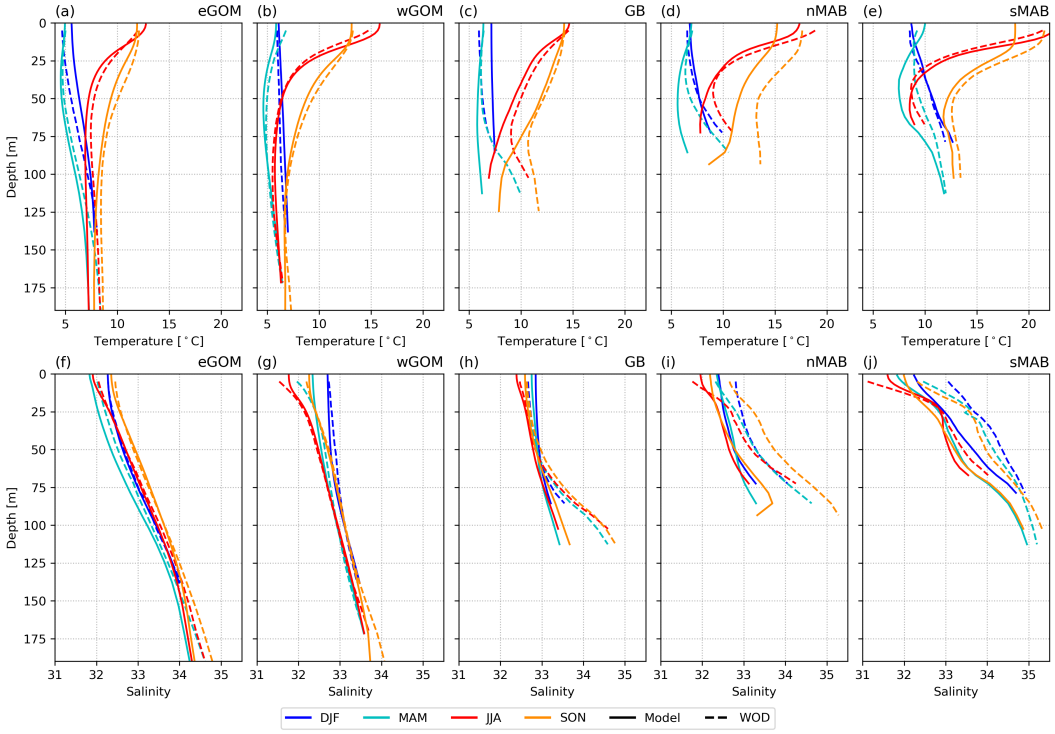

Figure 10. Seasonal profiles of (~~upper panels~~a to e) temperature and (~~bottom panels~~f to j) salinity on the continental shelf. High-resolution CTDs obtained from the World Ocean Database (solid lines) and MOM6 results (dashed lines).

file, MOM6 underestimates the salinity by 2.0. In MAB, MOM6 is able to reproduce the vertical gradients of salinity but is negatively biased by approximately 1.0 throughout the water column.

4.2.4 Time series evaluation - NERACOOS

The evaluation of temperature and salinity time series between MOM6 results and NERACOOS moorings (Figure 1) show MOM6-COBALT-NEUS25 generally has a good skill (>0.95, Willmott, 1981) in representing temperature considering levels shallower than 50 m, with more skill values between 0.75 and 0.9 at depths below 50 m (Figure 11). In terms of salinity, the model representation is still relatively good, despite the skill approximately between 0.6 and 0.95 when compared with temperature. At upper levels (<50 m) in all buoys, the model shows better agreement with observations, with correlations ranging from 0.95-0.99 and normalized standard deviation between 0.8 and 1.2.

Buoys M and N, located in deeper regions (>200 m) in the Gulf of Maine (Figure 1), generally show a drop in the skill to values between 0.74 and 0.92 when representing temperature time series (Figure 11). The correlations between measurements and model results range from 0.8 to 0.95 while normalized standard deviation values are between 0.6 to 0.9 for buoy M considering depths below 100 m. At the same levels, buoy N exhibits correlation and normalized standard deviations ranging

between 0.6 to 0.8 and 0.7 to 1.2, respectively. Lower correlation coefficients of subsurface series of these moorings is expected since the influence of atmospheric fluxes reduces with increasing depth and depends more on the internal variability of the ocean and the inflow through the Northeast Channel.

The salinity evaluation using Taylor Diagram (~~bottom panel of Figure 11~~Figure 11b) shows that surface values are not as well represented in MOM6-COBALT-NEUS25, when compared with its temperature counterparts, as correlation coefficients show values of approximately 0.7 and standard deviation below 0.6 for coastal buoys (buoys A to I). These lower skill metrics are likely due to uncertainties in the continental input of freshwater, that force salinity to values below 30 (Figure A6 to A12). Considering depths of 20 and 50 m at coastal buoys, the model has correlation coefficients and standard deviation that are relatively good (0.7 to 0.9, and 0.6 to 1.1, respectively). At buoys M and N, the best representation of the MOM6-COBALT-NEUS25 is related to the depths between 100 to 250 m, with correlation coefficients of approximately 0.6 and typical standard deviation of about 0.7. At these levels, both moorings show systematic biases of salinity ($\sim$0.6) and temperature ($\sim$1.5°C).

In general, these metrics are similar to a simulation using a non-structured mesh with resolution of approximately 200 m nearshore and typically of 1 km for the period from 2017 to 2018 (Wang et al., 2022), and to results of a similar coupled hydrodynamic and biogeochemistry model (Lehmann et al., 2009), with MOM6-COBALT-NEUS having better skill in representing levels below 100 m at NERACOOS moorings. This improved representation could be related to the longer simulation period from MOM6-COBALT-NEUS25, which captures the interannual frequency range, as opposed to the shorter simulation of Wang et al. (2022). Global reanalyses (CFSR, ECCO, ORAS, SODA, BRAN, Glorys, GOFS3.0, GOFS3.1) often have worse skill in representing NERACOOS surface data when compared with MOM6-COBALT-NEUS25 considering the Taylor Diagram metrics (Castillo-Trujillo et al., 2023, Figure 20).

4.2.5 Interannual evaluation - SST

~~Comparison~~ A comparison between empirical Orthogonal Function (EOF) analysis of SST daily anomalies of MOM6 and ~~OISST~~ OSTIA (Figure 12) demonstrates that MOM6-COBALT-NEUS25 has good skill in representing the dominant modes of variability in both Gulf of Maine and Mid-Atlantic Bight from 1993 to 2019. The first mode accounts for about ~~50~~ 40 % of the explained variance in MOM6 and ~~OISST~~OSTIA, while the second mode represents about 12 % of the explained variance in both cases~~(Figure 12)~~.

The spatial and temporal patterns of both EOFs are similar in the model and observational product. The first mode (Figure 12a,c,e) behaves as a monopole with well-marked regional features, including the lower-amplitude signals south of Cape Cod (MA), Georges Bank, and associated with the eastern Gulf of Maine Coastal Current system, where the EMCC steers into the Gulf of Maine at about 44°N near Penobscot Bay (ME). These lower amplitude systems are ~~more clearly defined in~~ defined in both MOM6-COBALT-NEUS25 ~~compared to OISST~~and OSTIA. The second mode (Figure 12b,d,f) displays a seesaw pattern between the Mid-Atlantic Bight and Gulf of Maine, with MOM6 capturing features associated with the circulation and topography in the Gulf of Maine.

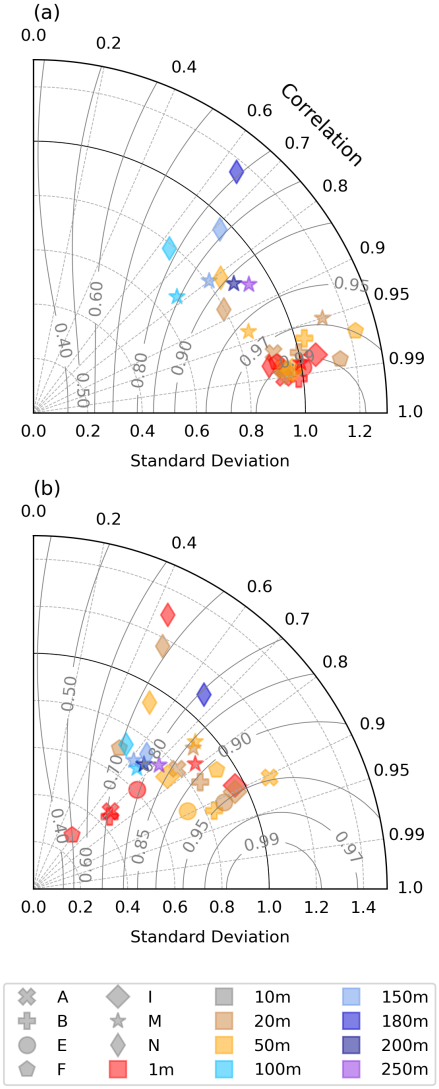

Figure 11. Taylor diagram evaluating MOM6 ~~(upper panel)~~ daily temperature ~~and (lower panel~~a) and salinity (b) performance against NERACOOS measurements. Gray shapes in the legend represent the mooring identification, while colors represent measurement depths. The standard deviation of the model results is normalized by the standard deviation of the observations. Curved contours represent isolines of skill score (Willmott, 1981).

The Principal Components time series (Figure 12e,f) shows a high correlation between model and satellite measurements for the first and second modes (~~0.93 and 0.78~~0.94 and 0.88, respectively). Both modes present relevant variability spanning subseasonal and interannual timescales.

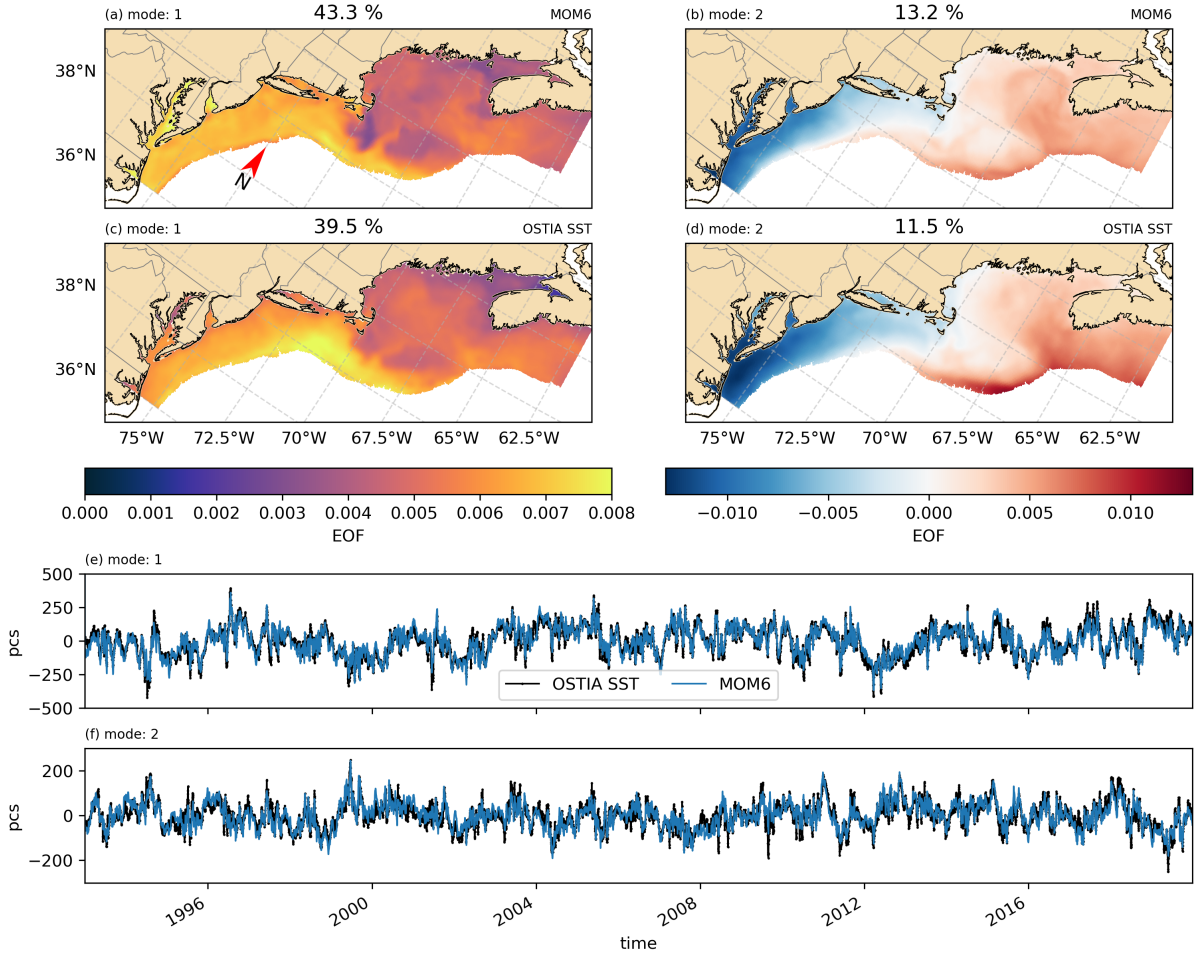

Figure 12. First (~~left panels~~a,c,e) and second (~~right panels~~b,d,f) modes of empirical orthogonal functions and principal component time series considering SST detrended daily anomalies of MOM6 (~~top panels~~a,b) and ~~OISST~~ OSTIA SST (~~bottom panels~~c,d). For the first (second) mode of principal components correlation, normalized standard deviation, mean bias and mean absolute error are ~~0.93~~0.94, ~~0.99~~1.04, ~~-3.57~~0.4487, and ~~35~~ 167.73 (~~0.78~~0.88, ~~0.93~~1.02, ~~-0.38~~-0.08, ~~29~~27.74), respectively. The explained variance of MOM6 (~~OI~~ OSTIA SST) first mode is ~~49.5~~ 43.3 % (~~52.7~~ 39.5 %), while the second mode has ~~12.1~~13.2% (11.5%).

4.2.6 Sea surface height

The sea surface elevation measured by CO-OPS tide gauges were compared with ~~MOM6-COBALT-NEUS~~ MOM6-COBALT-NEUS25 results for the simulated period starting in 1993, at sites where long term measurements were available (~~figure area of study~~Figure 1a). To ensure comparison at the same datum, we removed their respective time average values before performing the evaluation presented below. In order to isolate subtidal variability, tidal signals were fitted using harmonic analysis with the U-tide

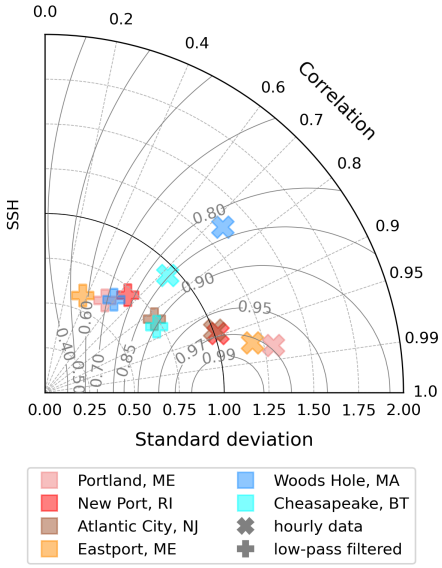

Figure 13. Taylor diagram of hourly SSH ~~information~~ data at tide gauges at multiple coastal areas in the Gulf of Maine and Mid-Atlantic Bight alongside ~~low pass Lanczos filtered information~~ low-pass data with a cutoff period of 24 hours (Lanczos filter). The standard deviation of the model results is normalized by the standard deviation of the observations. Curved contours represent isolines of skill score (Willmott, 1981).

package (Codiga, 2011) and removed from the original time series. The resulting detided signals were filtered using a Lanczos filter with a 24-hour cut-off period.

A Taylor Diagram (Figure 13) summarizes the comparison between observed and modeled sea surface height anomalies, showing generally good agreement. Correlations were $\geq$0.95 at all tide gauges except Woods Hole, where the correlation was approximately 0.7. The normalized standard deviation of the simulated results was approximately 1.0 in the coastal stations of the Mid-Atlantic Bight (Chesapeake Bay, Atlantic City, and New Port), while at Woods Hole, Portland and East Port tide gauges, the normalized standard deviation ranged between 1.05 and 1.35.

Detided signal comparisons show reduced correlation (0.4-0.8) (Figure 13), indicating limited skill of MOM6-COBALT-NEUS25 in representing the subinertial variability and indicating the model skill in coastal sea surface height is driven primarily by the tidal signal. Key factors contributing to reduced skill in representing the subinertial variability include known biases in ERA5 fluxes in coastal areas, where wind forcing tends to be underestimated.

4.3 Biogeochemistry

The seasonal climatology of NO_3 (Figure 14) was built using the dataset described in Rebuck and Townsend (2014) between the surface and 10 m. This was used to calculate an objective analysis, which finds the best fit of data onto a grid based on decorrelation scales of the datapoints and their positions. Here, decorrelation scales were determined by fitting a gaussian

curve into a semi-variogram. Horizontal data density varies between seasons, with DJF months having the fewest observations (998), followed by SON, with 1548, JJA with 1886, and MAM with the highest data counts (3048) (Figure 14). The spatial distribution of points does not allow this interpolation to resolve scales under 25 km. While more sophisticated objective analysis approaches exist for continental shelf environments (e.g., Sasaki et al., 2024), our two-dimensional objective analysis provides adequate estimates and enables direct comparisons with the surface krigging derived monthly climatology presented in Rebuck and Townsend (2014).

The validation of surface NO_3 concentrations focuses on seasonal cycles and spatial patterns given the inherent uncertainties in the observational climatology due to sparse data coverage. MOM6 simulated surface NO_3 concentrations exhibit the expected seasonal cycle – in areas where the Gulf of Maine is deeper than 200 m, from DJF to JJA, NO_3 surface concentration decreases from about 10.0 to 0.0 μmol kg^{-1} , before rising again from JJA to DJF (Figure 14). There are asymmetries between transition seasons, with of spring NO_3 averages (8.0 μmol kg^{-1}) showing higher concentrations than fall (4.0 μ mol kg^{-1}) . Within the 200 m isobath and near Maine and Nova Scotia coasts, MOM6 shows relatively constant NO_3 surface concentration year-round, maintaining approximately 7.0 μmol kg^{-1}. In contrast, the concentrations of NO_3 along the coast of Massachusetts and New Hampshire align more closely with the climatology, suggesting adequate representation of riverine nitrate inputs.

The largest biases in the model results (Figure 14 i to l) occur during MAM and SON. In Georges Bank, MOM6 surface NO_3 presents higher concentrations ($\Delta NO_3 \approx 5.0$ μmol kg^{-1}) than in deep regions in Gulf of Maine (>200 m isobath) during all seasons, except in summer. These patterns are not observed in the climatology, which may suggest enhanced vertical mixing that brings nutrients from deeper layers to the surface at Georges Bank.

While MOM6 and the climatology have similar seasonal magnitudes, the climatology generally shows lower coastal NO_3 values than the model (Figure 14). These climatological values require careful consideration as discrepancies from the observational seasonal averages arise mainly from two aspects that can be evaluated~~from Figure 14~~: first, the heterogeneous data distribution in time and space which may introduce biases; second, the objective analysis prioritizes scales compatible with the decorrelation length, while dampening signals of other scales.

The evaluation of chlorophyll fields (Figure 15) shows the model has generally lower and more uniform concentrations, with values higher than 1 mg m^{-3} present on the continental shelf, particularly close to the shoreline. In the area corresponding to Georges Bank, OC-CCI shows concentrations higher than 2 mg m^{-3}, while MOM6-COBALT-NEUS25 presents values between 1 to 2 mg m^{-3}~~(Figure 15)~~, approximately. These hotspots of higher concentration in the model are present along the coast and Georges Bank, with maximum concentrations of about 2 mg m^{-3} along coastlines from Cape Hatteras up to Delaware, between Rhode Island and Massachusetts and between the coasts of Maine, Bay of Fundy and Nova Scotia. The distribution of chlorophyll in MOM6-COBALT-NEUS25 is very similar to a high resolution model with coupled ROMS and biogeochemistry model at NEUS (Lehmann et al., 2009, Figure 4).

In OC-CCI, two seasonal peaks of chlorophyll are observed in the Gulf of Maine: the first in spring, when concentrations are approximately 1 mg m^{-3}, and during fall, when chlorophyll has values between 1 and 2 mg m^{-3}, while minima occur in winter and summer (Figure 15). Similarly, MOM6-COBALT-NEUS25 chlorophyll peaks in spring and fall, but exhibits maximum seasonal concentrations in MAM (1 mg m^{-3}) instead of SON (0.5 to 1 mg m^{-3}), with minimum values in summer

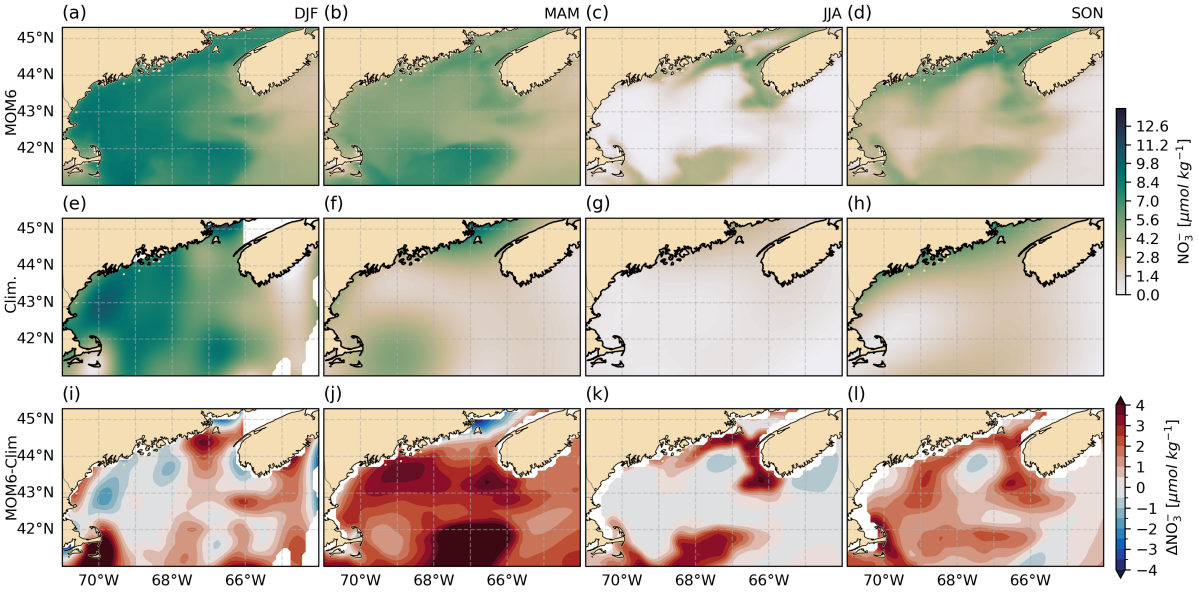

Figure 14. Seasonal surface distribution of nitrate in the Gulf of Maine region considering the climatology of surface concentrations from MOM6 (~~first row~~a to d), a seasonal climatology calculated from Rebuck's dataset (~~second row~~e to h), and their difference (i to l) (MOM6 – Climatology). Columns represent seasons: DJF, MAM, JJA, SON.

(<0.25 mg m^{-3}). Spatial correlations are relatively low, with values typically close to 0.5, except for spring, when correlation is the lowest (0.38), while the remaining metrics are relatively stable across the seasons for RMSE (∼1.3), MAE (∼0.45) and Bias (-0.13, with exception of DJF -0.33).

In the slope, MOM6-COBALT-NEUS25 presents spurious higher chlorophyll concentrations associated with the Gulf Stream (Δ Chlorophyll 0.5 mg m^{-3}, Figure 15 ~~, bottom row)as a result of the coarse resolution from WOA nutrients climatology that provides~~ i to l). The phytoplankton boundary conditions in MOM6 are provided by a long-term climatology of a global COBALT simulation (Stock et al., 2014), which was also used in R23. The difference between R23 and MOM6-COBALT-NEUS25 lies in the turnover times of phytoplankton association with the boundary conditions. ~~WOA resolution of 0.25° does not resolve lateral boundary gradients, which results in chlorophyll biases in the Gulf Stream simulated by MOM6-COBALT-NEUS25~~In our case, differently from R23, the Gulf Stream introduces fast currents (> 2.0m s^{-1} in some cases which does not allow phytoplankton to equilibrate during summer with the seasonality of macronutrients (such as nitrate) inducing the jet-like phytoplankton feature seen throughout the year, which is more apparent in the summer fields. A second aspect that could be an issue is the lower resolution of 1^o ($\sim$ 100 km) in global COBALT, which doesn't resolve the gradients associated with the shelf-slope continuum.

~~Difference between seasonal averages of MOM6-COBALT-NEUS25 and OC-CCI satellite.~~

Seasonal and monthly gridded depth-average measurements of mesozooplankton carbon biomass on the continental shelf available from the COPEPOD database are used in the evaluation of mesozooplankton fields of MOM6-COBALT-NEUS25

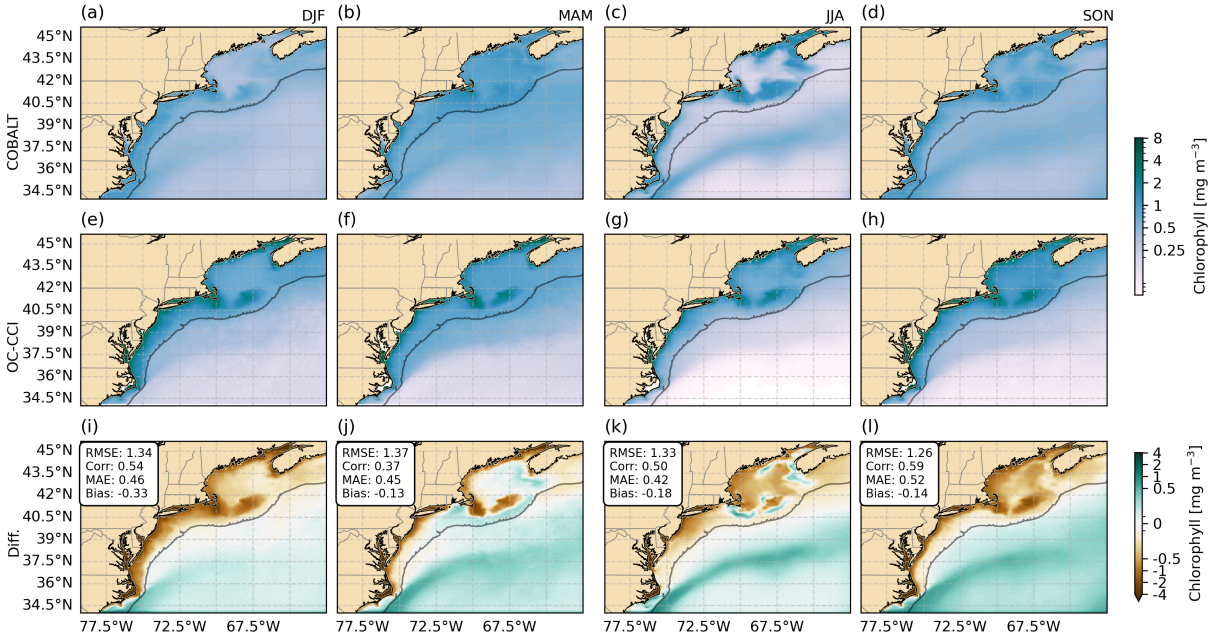

Figure 15. Difference between seasonal averages of surface chlorophyll from MOM6-COBALT-NEUS25 results and OC-CCI satellite data product.

(Figure 16). The monthly boxplots represent the horizontal distribution of monthly and depth-averaged carbon biomass of the upper 200 m. ~~The~~ Because the gridded COPEPOD dataset does not provide ~~the number of samples used in the calculation of each point, which can introduce uncertainty and biases in the evaluation. For this reason, we avoid calculating~~ sample counts per grid point, we avoid formal correlation or skill metrics ~~for the seasonal spatial evaluation but provide quantitative comparisons through boxplot analysis~~ and instead use boxplot analysis for quantitative comparison (Figure 16~~).~~

~~Seasonal and monthly evaluation of MOM6-COBALT-NEUS25 of mesozooplankton carbon biomass show the similarities between model and COPEPOD dataset throughout the seasons~~c). Model and observations agree on the broad seasonal cycle, with average concentration below 10 mgC m^{-3} during the winter (DJF) and fall (SON), ~~and biomass higher than~~ rising to 20 mgC m^{-3} over spring (MAM) and summer (JJA). Monthly averages ~~show biomass of~~ from April to August reach 20 mgC m^{-3} ~~from April to August~~ in the observations, which is higher compared with model values of 15 mgC m^{-3}. The spatial distribution of the model has an interquartile range around the median of about $\pm$5 mgC m^{-3}, contrasting with the observations' range of about $\pm$20 mgC m^{-3} from mid spring (MAM) to early fall (SON).

In the Gulf of Maine, simulated depth-averaged mesozooplankton biomass is underestimated in regions beyond the isobath of 80 m (Figure 16 a, b), with concentrations varying from less than 5 mgC m^{-3} up to 15 mgC m^{-3}, while COPEPOD suggests values generally over 15 mgC m^{-3}. Concentrations in the Mid-Atlantic Bight are approximately 20 mgC m^{-3} in spring and summer (JJA), with lower values between 5 mgC m^{-3} to 20 mgC m^{-3} in winter (DJF) and fall (SON). COPEPOD has similar values, but some hotspots in the observations are absent from the model results. These hotspots occur mainly at Georges

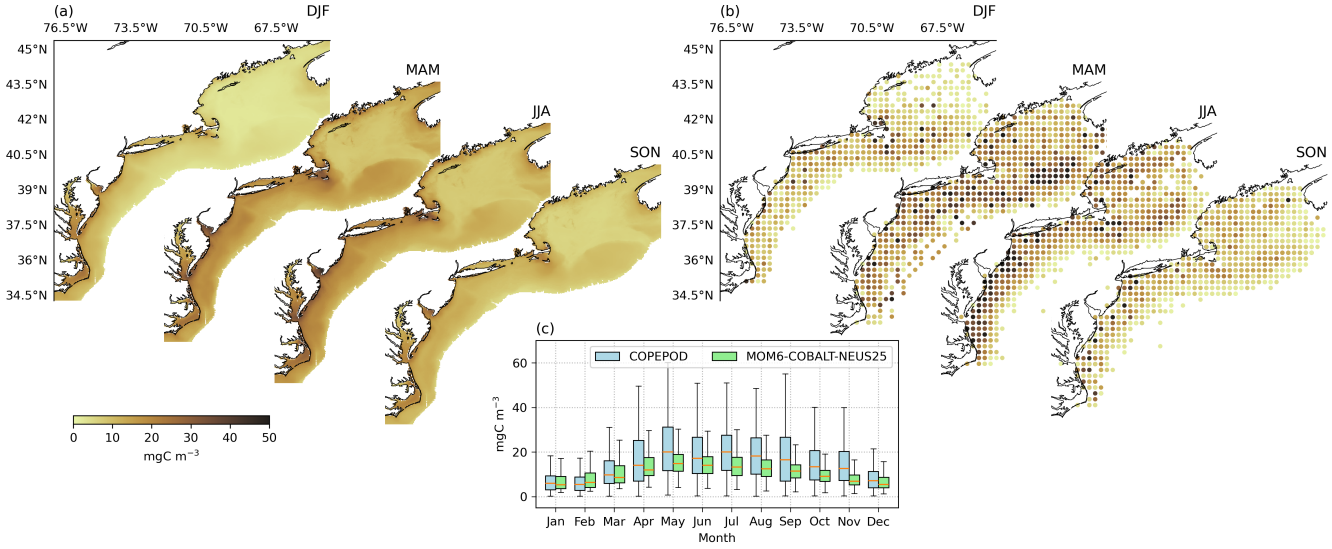

Figure 16. Seasonal averages carbon biomass (depth-averaged over the top 200 m) on the continental shelf (within the 400 m isobath) encompassing the Mid-Atlantic Bight, Georges Bank and Gulf of Maine for (a) MOM6-COBALT-NEUS25 , and (b) COPEPOD dataset. Boxplots represent the distribution of the horizontal fields of monthly and depth-averaged biomass. Seasonal bias are (DJF, MAM, JJA, SON) (1.3, 5.7, 7.2, 10.9) mgC m^{-3}.

Bank in MAM (spring) and coastal areas along Cheasapeake and Delaware Bays during summer (JJA), where the biomass concentrations reach values higher than 40 mgC m^{-3}.

In general, the model captures the seasonal and spatial patterns while underestimating possible regional maxima. The underestimates in the model could be related to the mesozooplankton size that is represented. Our results contrast with R23 evaluation of mesozooplankton~~. In order to make the results comparable, they~~ , who multiplied COPEPOD biomass estimates by a factor of ~~2~~ two due to the different fraction sizes represented in COBALT (200-2000 μm), relative to COPEPOD's biomass adjustment to a 333 μm mesh. Here, we make no such correction, and the observed and modeled values correspond to their respective size fractions rather than following the R23 approach.

~~Seasonal averages carbon biomass (depth-averaged over the top 200 m) on the continental shelf (within the 400 m isobath) encompassing the Mid-Atlantic Bight, Georges Bank and Gulf of Maine for (a) MOM6-COBALT-NEUS25 , and (b) COPEPOD dataset. Boxplots represent the distribution of the horizontal fields of monthly and depth-averaged biomass. Seasonal bias are (DJF, MAM, JJA, SON) (1.3, 5.7, 7.2, 10.9) mgC m^{-3}.~~

The boxplot of monthly climatological anomalies relative to the total period of dissolved inorganic carbon (DIC) in the upper 10 m of the water column for the entire domain are shown in Figure 17. Removing the average DIC is required for the evaluation of the model results, since boundary conditions were derived from the static WOA climatology without a year adjustment in contrast to R23, leading to the magnitude differences in Figure 17 (b, c). In these panels, the relevant information is associated with the horizontal gradients that increase in the offshore direction in both model results and the reference climatology. The

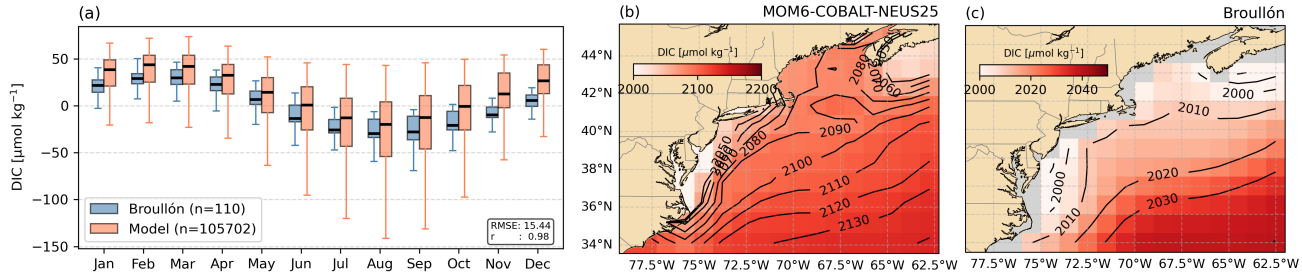

Figure 17. Monthly DIC anomalies in the upper 10 m relative to the long-term monthly mean for MOM6-COBALT-NEUS25 and Broullón (a), where n is the number of horizontal grid points in each dataset. Long-term mean DIC in the upper 10 m over the full period for MOM6-COBALT-NEUS25 (b) and Broullón climatology(c) (background colors). The model results were coarsened to the same resolution as the climatology. Black contours represent the DIC isolines and gray color represent areas where data was not available.

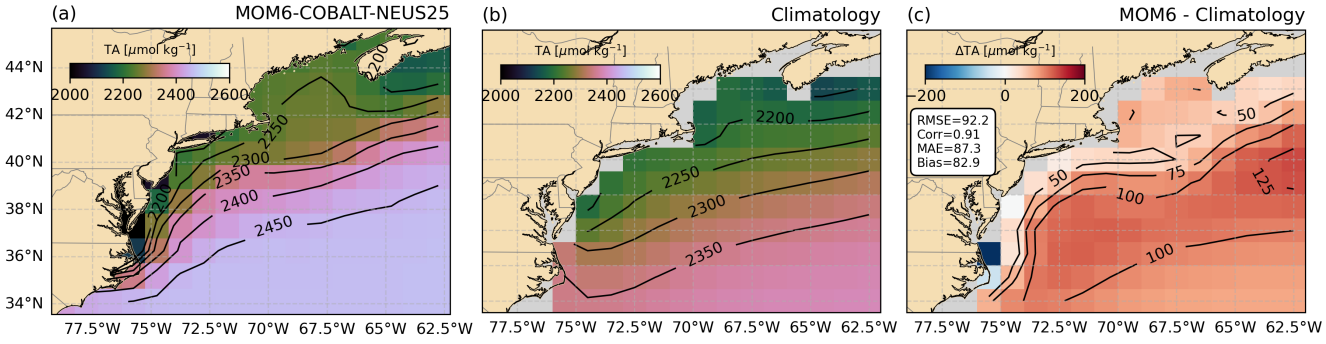

Figure 18. Long term average of total alkalinity (TA) considering MOM6-COBALT-NEUS25 (a), the observation-derived climatology (b), and their difference (c). TA field in the model was binned (and averaged) into the same resolution as the climatology with a resolution of 1°.

larger spread around the median (Figure 17a) in the model reflects the 4km resolution with a number of points of O[10^5], compared with the horizontal resolution of about 100km in Broullón product. The seasonal cycle maps are included in Figure A13.

An evaluation between the long-term average of TA in MOM6-COBALT-NEUS25 and an observation-based climatology (Jiang et al., 2021, 2022) (Figure 18) shows similar spatial structure in both fields (spatial correlation is approximately 0.9) with horizontal gradients of TA increasing in the offshore direction. The model's average bias is approximately 88 μmol kg^{-1} in TA. The largest biases are associated with the Gulf Stream and Slope Sea domains. The lowest TA values occur in Chesapeake Bay and surrounding continental shelf. The lowest difference value in Figure 18c south of Chesapeake Bay is a consequence of the high resolution of MOM6-COBALT-NEUS25, which partially represents coastal inlets. These inlets are associated with freshwater inflow, which introduces low TA values in the surrounding continental shelf.

5 Discussion

MOM6-COBALT-NEUS25 demonstrates strong skill in reproducing SST variability across the continental shelf at both seasonal and interannual timescales (Figures 6, 12). This performance indicates the model appropriately represents the region's dominant SST drivers, which are primarily surface heat fluxes (Li and He, 2014). The consistency between our model EOF patterns and those from ~~OISST~~satellite information, particularly their resemblance to the seasonal EOF structure documented by (Li and He, 2014), suggests the model captures the fundamental physical processes controlling temperature variability in this region, with heat flux forcing and vertical mixing dominating over advective processes at these temporal scales.

While early measurements and analysis (1979-1987; Mountain et al., 1996) indicated heat fluxes were relevant at interannual scales, the eastern Gulf of Maine SST was dominated by advective changes. Different factors could contribute to this apparent difference relative to our model results. First, observational coverage has evolved substantially since the 1980s and presently benefits from comprehensive satellite coverage. Second, physical changes in the Gulf of Maine (Townsend et al., 2010) could have had substantial impacts on circulation, leading to more uniform SST variability across the Gulf of Maine

~~In addition to these larger-scale patterns, negative SST differences in~~

In the Coast of Maine, Nova Scotia and Georges Banks, positive biases present in Glorys (Figure A1) are generally absent from MOM6-COBALT-NEUS25~~relative to OISST at Nantucket Shoals and Georges Bank are absent in GLORYS results (Figures 6, A1)~~. Glorys reanalysis does not resolve tides, which is relevant for strong nonlinear currents in Nantucket Shoals and Georges Bank (Chen et al., 2011). The observed differences in SST likely reflect physical processes rather than model biases, as tides enhance vertical mixing and generate residual currents in shallow regions with steep bathymetric gradients in the region (Chen et al., 1995; Xue et al., 2000), which mix colder deeper water with the upper layers of the ocean. Furthermore, satellite SST products often misrepresent or exclude data from regions with strong tidal mixing and coastal upwelling, as these signals are frequently flagged as poor quality (Pereira et al., 2020; Murphy et al., 2021). ~~The biases in SST associated with the relatively low resolution of OISST produces fields estimates that do not represent these shallower colder waters on the continental shelf.~~ Further analysis is required to validate the SST in these tidally active region, but the model strong overall SST skill suggests it captures the net regional heat budget appropriate for present conditions.

Representing the Gulf Stream separation enabled MOM6-COBALT-NEUS25 to capture the shelf-slope environment~~with relatively low bias~~, as shown by ~~temperature and salinity~~ timeseries of NERACOOS moorings in the Gulf of Maine. A possible explanation for cold and fresh biases below 100 m in Northeast Channel and Jordan Basin, in moorings M and N, may be linked with the model tendency to damp the Gulf Stream meanders, which reduces warm core ring formation. Warm rings introduce Warm Slope Water into Jordan Basin through the Northeast Channel (Du et al., 2022) and with fewer warm core rings, the colder and fresher Labrador Slope Water becomes more dominant in the deep Gulf of Maine, leading to the simulated cold/fresh bias.

In the Gulf of Maine, the seasonal vertical structure and bottom temperatures showed good agreement with observations, contrasting with Georges Bank and the Mid-Atlantic Bight, where skill is more limited, particularly in levels below 50 m. The model represents the Cold Pool – the bottom-trapped cold water mass (temperature <10°C, salinity <34) that originates in the

Gulf of Maine and persists in the Mid-Atlantic Bight during summer and fall (Fairbanks, 1982; Chen and Curchitser, 2020). In the Mid-Atlantic Bight, bottom temperatures in areas shallower than approximately 40 m show positive biases during JJA and SON, while a persistent cold bias occurs beyond the 80 m isobath. Varying bottom boundary layer efficiency (bbl_effic) parameters indicated that warm bottom biases within the 40 m isobath during summer and fall are insensitive to bbl_effic changes, contrasting with deeper regions where the biases were reduced. ~~Experiments with different parameterizations and mixing coefficients, suggest that the persistence of~~ One possibility is that these shallow biases could be linked with insufficient vertical resolution in the z*-coordinate.

In the Mid-Atlantic Bight, Georges Bank, and Gulf of Maine, SST and surface chlorophyll patterns have an inverse relationship, where cold temperatures are usually linked with higher chlorophyll concentrations (Yoder et al., 2002). This relationship reflects the replenishment of nutrients in the surface through vertical mixing, which is facilitated by less stratified environments. Seasonal SST fields and surface chlorophyll in MOM6-COBALT-NEUS25 are in agreement with observed patterns, with colder temperatures and higher chlorophyll concentrations in the EMCC, Georges Bank, and the region south of Cape Cod. Biases on the continental shelf are difficult to assess, as chlorophyll estimates from satellite measurements present uncertainties related to the ocean color, which does not depend on the concentration of phytoplankton and chlorophyll alone, particularly in coastal regions (Dierssen, 2010).

The salinity in MOM6-COBALT-NEUS25 generally represents the seasonal cycle of SSS relative to the high-resolution NCEI regional climatology (Seidov et al., 2018, 2019), model represent generally the salinity variability measured by the NERACOOS buoys. An evaluation of eight distinct reanalysis (Castillo-Trujillo et al., 2023) show that models with low resolution (0.25°) generally overestimates the salinity climatology over the entire sMAB with bias typicall greater than 1.5, while the Gulf of Maine shows negative biases of approximately -0.6. Higher resolution reanalysis (<0.1°) are generally better in representing salinity with absolute bias usually lower than 0.5. In the NEUS domain, R23's mean surface salinity show biases spread along the shelf from Cape Hatteras to the Gulf of St Lawrence that is attributed to mild issues in The Gulf Stream representation.

A realistic Gulf Stream path in MOM6-COBALT-NEUS25 assessed using SSH standard deviation, is in agreement with satellite observation. Biases in SST and SSS in the Slope Sea are reduced when compared with coarser resolution models (e.g Saba et al., 2016; Ross et al., 2023). Beyond the high resolution, this is possibly also a consequence of the more restricted domain in MOM6-COBALT-NEUS25, where the open boundary conditions and rim nudging have a stronger influence on the mean state, while potentially suppressing internal variability. Considering the Gulf Stream evaluation through SSH standard deviation, it is worth mentioning that the effective resolution of the CMEMS SSH product is about 200km at mid latitudes (Pujol et al., 2016), which does not resolve the first baroclinic radius in the model domain (Hallberg, 2013; Chelton et al., 1998) . The SSH biases in the Slope Sea likely reflect excessive dissipation of turbulent EKE in the current model configuration, or an influence of the nudging close to the boundaries. Despite recent improvements in the representation of SSH in coastal regions in CMEMS SSH (Sánchez-Román et al., 2023), the usage of CO-OPS tide gauges is desirable in the evaluation of tidal variability and subinertial variability in the coastal zone.

In the Gulf of Maine during summer and fall, MOM6-COBALT-NEUS25 underestimates surface chlorophyll concentration. This contrasts with other regional coupled ocean dynamics and biogeochemistry models, such as the Atlantic Canada

Model (ACM; Brennan et al., 2016; Rutherford and Fennel, 2018), which better represent surface chlorophyll in the Gulf of Maine during these seasons (Laurent et al., 2021). MOM6-COBALT-NEUS25 and ACM have different domains, with ACM extending from the Massachusetts coast to Newfoundland and Labrador. These different domains allow ACM more realistic biogeochemical fluxes through the Nova Scotia shelf into the Gulf of Maine compared with MOM6-COBALT-NEUS25. Improving boundary condition estimates with well-constrained machine learning methods such as ESPER (Carter et al., 2021) could potentially address these issues, although formal experiments are required.

The seasonal cycle of surface chlorophyll from OC-CCI and depth-averaged mesozooplankton do not coincide, which is expected as mesozooplankton concentration is coupled not only with surface spring and fall blooms, but also with a widespread chlorophyll subsurface maximum that has 2 to 8 times the concentration of the overlying and underlying waters during summer (O'Reilly and Zetlin, 1998). Since MOM6-COBALT-NEUS25 captures this summer subsurface maximum (not shown), the model successfully reproduces the seasonal and monthly structure of depth-integrated mesozooplankton biomass throughout the year, demonstrating its capability to represent key ecosystem dynamics beyond surface processes.

Our results show that MOM6-COBALT-NEUS25 reproduces the seasonal cycle of DIC broadly consistent with the Broullón climatology (Broullón et al., 2020). The increased resolution and process-oriented design of numerical models allow a better representation of cross-shelf gradients compared with the climatological product. Despite MOM6-COBALT-NEUS25 showing a realistic Gulf Stream path, the mean DIC remains 30–50 μmol kg^{-1} higher, suggesting the offset is primarily driven by the boundary conditions without a interannual adjustment rather than differences in physical circulation. The cross-shelf gradients agree with observational evidence in the Mid-Atlantic Bight (Li et al., 2024), where nearshore surface waters show DIC concentrations below 2000 μmol kg^{-1} and offshore waters near the shelf break reach approximately 2050 μmol kg^{-1}. TA fields in MOM6-COBALT-NEUS25 have spatial patterns similar to what was observed in R23 results and the climatology product (Jiang et al., 2022), with the systematic bias in the Gulf Stream being a common feature in both model results. The sensitivity of the TA field to the OBC relaxation parameters (obc_lfac_in = 0.03, obc_lfac_out = 1.0), inherited from the configuration of R23, was not explored in this study and may contribute to the systematic bias. The biases in both DIC and TA mean state share a common origin in the boundary condition configurations.

6 Conclusions

MOM6-COBALT-NEUS25 is now part of a growing group of ocean-biogeochemistry models for the Northeast U.S. Shelf, offering advantages through its MOM6-COBALT infrastructure that is part of the CMIP framework. This coupling enables the regional detail required for shelf-specific applications including mCDR assessments, benthic modeling, hypoxia prediction, and fisheries evaluation. The model demonstrates particular skill in the Gulf of Maine and upper water column processes across the domain, making it suitable for studies requiring accurate representation of seasonal stratification and tidal mixing.

The model skill in the Gulf of Maine is also a consequence of the representation of the Gulf Stream position and the Slope Sea conditions, which constrain the regional circulation. Surface fields (SST, SSS, and SSH) are well constrained relative to observations across the domain. Vertical structure validation reveals regional contrasts: the Gulf of Maine shows good

agreement throughout the water column, while the Mid-Atlantic Bight exhibits biases below 50-70 m, particularly during spring and fall. A relevant finding is that the bottom boundary layer efficiency parameter (bbl_effic) affects bottom temperature biases only in waters deeper than 40 m, suggesting that vertical resolution limitations may control errors in shallower regions. Cold SST patches near Nantucket Shoals and Georges Bank, absent in global reanalyses, are realistic and associated with tidally-induced vertical mixing. Surface chlorophyll concentrations and zooplankton representation are on par with remote sensing and observations.

Improving the boundary condition implementation, including time-varying ESPER-derived TA and DIC with an annual adjustment following R23, would reduce the mean state bias but is unlikely to be sufficient for quantitative carbonate chemistry applications in this region without further regional optimization. Validation against in situ carbonate chemistry observations in the Mid-Atlantic Bight and Gulf of Maine will be required before the model can be applied to ocean acidification or carbon budget studies.

MOM6-COBALT-NEUS25 largely benefits from the open community approach of model development established in the MOM6 community and particularly in ~~(MOM6-COBALT-NEUS12 Ross et al., 2023). Based on our findings, future~~ Ross et al. (2023) . Some limitations are clear in the model results. Relevant biases in temperature and salinity persist in vertical profiles below 50 m in summer and fall in the Mid-Atlantic Bight and Georges Bank. In regions shallower than 40 m, bottom temperatures are overestimated in the Mid-Atlantic Bight, which remains unresolved in the current configuration. On the biogeochemical fields, boundary conditions play an important role in the relatively restricted model domain and deserve careful attention in future modeling efforts. Future improvements in the parameterization choices related to vertical mixing in the bottom boundary layer, improved biogeochemical lateral fluxes, and perhaps a more appropriate vertical coordinate on the continental shelf (sigma-coordinates) ~~would~~ may reduce biases in the water column structure~~and bottom temperature~~, bottom temperature, and the representation of surface chlorophyll fields in summer and fall. ~~These improvements will~~ If successful, these improvements would allow future evaluations to be extended to the entire water column ~~in areas outside of~~ outside of the Gulf of Maine and support a more comprehensive description of the biogeochemistry.

Code availability. The source code of MOM6-COBALT-NEUS25 is archived at https://doi.org/10.5281/zenodo.18415604. It was originally obtained from GitHub repositories supported by NOAA https://github.com/NOAA-GFDL/CEFI-regional-MOM6 . Auxiliary tools used to generate preprocessing files are stored in https://doi.org/10.5281/zenodo.18443951. These tools have been updated from the original CEFI repository. Additional preprocessing data are included in a separate zenodo repository (see *Data availability* section).

Data availability. Processed model output used to generate all manuscript figures, along with preprocessing data required to run the model, is available at https://doi.org/10.5281/zenodo.17572586 (Sasaki et al., 2025). Full model output is available upon request to the corresponding author or Cristina Schultz.

DOI or URLS of files used to force the model are listed here: ERA5 - ECMWF Reanalysis v5 - Hourly atmospheric data (https://doi.org/10.24381/cds.adbb2d47), GLORYS12v1: Global Ocean Physics Reanalysis - Daily ocean fields (https://doi.org/10.48670/moi-00021), Glo-

FAS: Global Flood Awareness System - River discharge (https://doi.org/10.24381/cds.a4fdd6b9), GlobalNEWS2: Global river nutrient export model (https://doi.org/10.1016/j.envsoft.2010.01.007, Mayorga et al. (2010)), USGS Water Quality: Chemistry data for US rivers (https://www.ncei.noaa.gov/data/oceans/archive/arc0207/0260455/3.3/), TPXO9: Global ocean tide model (https://www.tpxo.net/tpxo-products-and-registration) WOA23: World Ocean Atlas 2023, temperature (https://doi.org/10.25923/54bh-1613), salinity (https://doi.org/10.25923/70qt-9574), oxygen (https://doi.org/10.25923/rb67-ns53), nutrients (https://doi.org/10.25923/39qw-7j08), ESM4 Historical (https://doi.org/10.22033/ESGF/CMIP6.1407),for estimates of DIC and Alkalinity we used the algorithm of Carter et al. (2021) (https://doi.org/10.5281/zenodo.5512697), CODAP-NA: Coastal Ocean Data Analysis Product in North America - Climatological ocean acidification indicators (https://doi.CODAP-NA: Coastal Ocean Data Analysis Product in North America - Climatological ocean acidification indicators (https://doi.org/10.25921/G8PB-ZY76), NNGv2LDEO: Neural Network Global version 2 LDEO - Climatologies of TCO2 and pCO2 (https://doi.org/10.20350/digitalCSIC/10551), Meinshausen et al. (2017) atmospheric CO2 (https://doi.org/10.22033/ESGF/input4MIPs.1118, Meinshausen and Vogel, 2016; https://doi.org/10.22033/ESGF/input4MIPs.9866, Meinshausen and Nicholls, 2018), while the climatology of (Stock et al., 2014) may be obtained by contacting the authors.

Datasets used for the model validation are: Copernicus Marine Environment Monitoring Service (CMEMS) and the Copernicus Climate Change Service (C3S) Sea level gridded data from satellite observations for the global ocean from 1993 to present (https://doi.org/10.24381/cds.4c328c78), NERACOOS moorings (http://gyre.umeoce.maine.edu/buoyhome.php), Copernicus Global Ocean OSTIA Sea Surface Temperature and Sea Ice Reprocessed (https://doi.org/10.48670/moi-00168), Northwest Atlantic Regional Climatology Version 2 (Seidov et al., 2018) (https://www.ncei.noaa.gov/products/), High resolution bottom temperature product for the northeast U.S. continental shelf (Du Pontavice et al., 2023) may be obtained by request, emolt bottom temperatures (https://comet.nefsc.noaa.gov/erddap/tabledap/eMOLT_historic_non-realtime_bottom_temperatures.html), the World Ocean Database for temperature and salinity profiles (https://www.ncei.noaa.gov/products/world-ocean-database), tide gauges measurements (https://tidesandcurrents.noaa.gov/), NO_3 dataset (Rebuck and Townsend, 2014) originally maintained by University of Maine may be obtained by request, ESA Ocean Colour Climate Change Initiative (Ocean_Colour_cci): Version 6.0, 4km resolution data (https://doi.org/10.5285/5011d22aae5a4671b0cbc7d05c56c4f0), COPEPOD dataset (https://www.st.nmfs.noaa.gov/copepod/).

Author contributions. DKS: Conceptualization, Model compilation/calibration, Formal Analysis, Investigation, Data Curation, Writing – Original Draft, Visualization. CS: Conceptualization, Methodology, Formal Analysis – Review & Editing. EC: Review & Editing.

Competing interests. The contact author has declared that none of the authors has any competing interests.

Acknowledgements. We thank Andrew Ross, Charles Stock for valuable discussions and guidance throughout model calibration and interpretation of the results. We are also grateful to Yi-Cheng Teng, Kate Hedstrom and James Simkins provided helpful advice during the model calibration phase. DKS, CS, and EC acknowledge support from NOAA Grant NA23OAR0170511. The following python packages were used to evaluate the model results: xarray (Hoyer and Hamman, 2017), cartopy (Elson et al., 2024), eofs (Dawson, 2016), gibbs seawater (McDougall and Barker, 2011), geopandas (den Bossche et al., 2025), xesmf (Zhuang et al., 2025), esmpy (Team, 2025).

Appendix A: Appendix A

Table A1. Initial conditions, boundary conditions and surface forcing datasets, variables and references.

Dataset/Algorithm	Type	Key ~~Variables~~ variables	Reference
GLORYS12v1	IC/BC	T, S, currents, SSH	Jean-Michel et al. (2021)
ERA5	SFC	10-m wind, T, humidity, heat fluxes, MSLP, precipitation	Hersbach et al. (2020)
TPXO9	Tides	M2, S2, N2, K2, K1, O1, P1, Q1, MM, MF	Egbert and Erofeeva (2002)
GloFAS	Rivers	Discharge	Harrigan et al. (2021)
WOA23	IC/BC	~~T, S,~~ O_2, NO_3, PO_4, SiO_4	Garcia et al. (2024b)
ESM4	SFC	NO_3, NH_4, lithogenic dust, Fe^a, P^a	Dunne et al. (2020)
RC4US	River BGC	DIC, Alk, NO_3, NH_4, PO_4, O_2, SiO_4, POP^b, PON^b, DOP^b, DON^b	Gomez et al. (2023)
ESPER	IC/BC	DIC^c, $alkalinity^c$	Carter et al. (2021)
CO_2_SSP245	SFC	CO_2 mole fraction	Meinshausen et al. (2020)
global COBALT	IC/BC	other BGC tracers	Stock et al. (2014)

IC = initial conditions; BC = boundary conditions; SFC = surface forcing; MSLP = mean sea level pressure; T = temperature; S = salinity; SSH = sea surface height; O_2 = dissolved oxygen; NO_3 = nitrate; NH_4 = ammonium; PO_4 = phosphate; SiO_4 = silicate; Fe = iron; DIC = dissolved inorganic carbon; Alk = alkalinity; DON = dissolved organic nitrogen;POP = particulate organic phosphorus; PON = particulate organic nitrogen; DOP = dissolved organic phosphorus; DON = dissolved organic nitrogen; P = phosphorus; BGC = biogeochemic. ^{a}Fe is assumed to be 3.5 % of the dust, Phosphorus is assumed to be 564 ppm of the dust. ^{b}50 % of particulate phosphorus is assumed to be buried in estuaries, DON and DOP are fractionated into labile (40 %) semi-labile (30 %), and semi-refractory (30 %). ^{c}Derived from temperature and salinity using ESPER algorithm. All information is detailed in Ross et al. (2023).

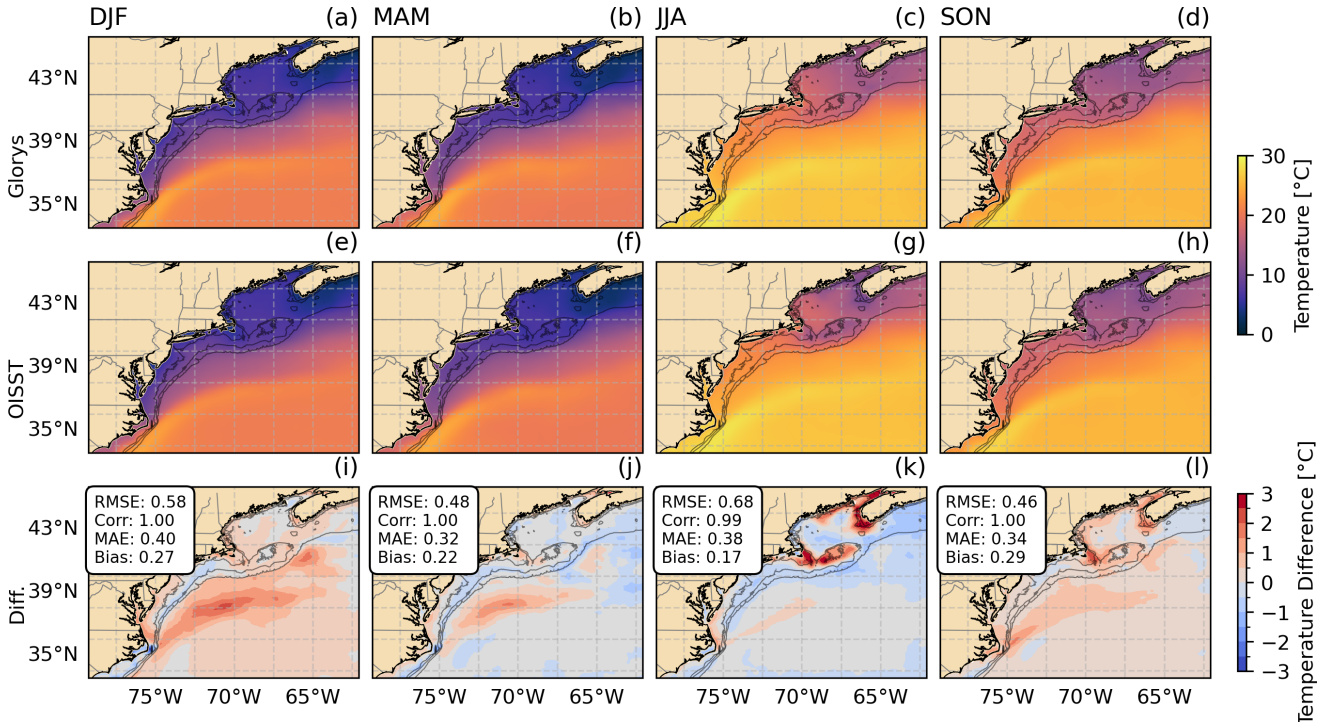

Figure A1. Seasonal averages of sea surface temperature considering Glorys (~~top panels~~a to d), ~~OISST~~ OSTIA SST (~~middle panels~~e to h) and their differences (~~lower panels~~i to l, Glorys - ~~OISST~~OSTIA). Glorys results and OSTIA SST were ~~upscaled to OISST resolution~~ interpolated (~~0.25°~~bilinear) ~~by binning corresponding areas and calculating averages~~to MOM6 resolution. Black contours are the isobath of 40, 80, and 400 m.

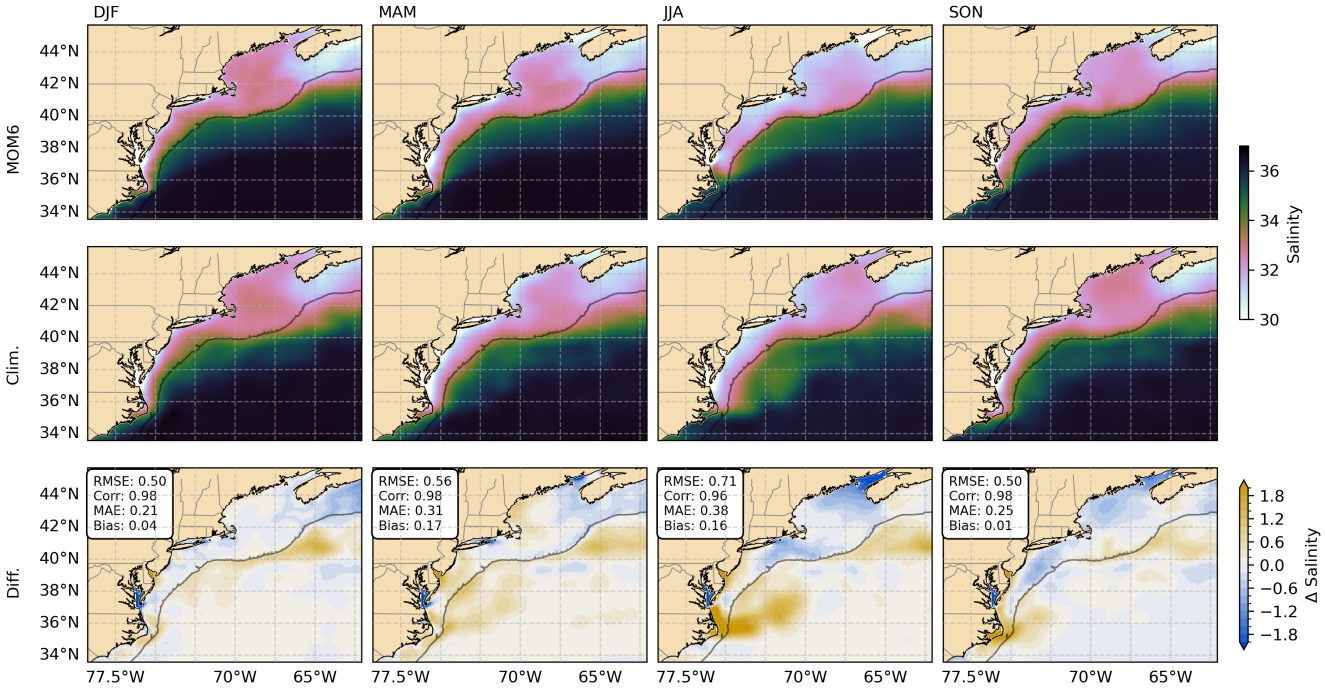

Figure A2. Seasonal averages of sea surface salinity from Glorys (top panels) and NCEI regional climatologies (Clim., middle panels) and seasonal differences (lower panels, Glorys - Clim.). Black contour indicates the 400m isobath, roughly representing the position of the shelf break. Glorys results were upscaled to NCEI climatologies resolution (0.1°) by binning corresponding areas and calculating averages.

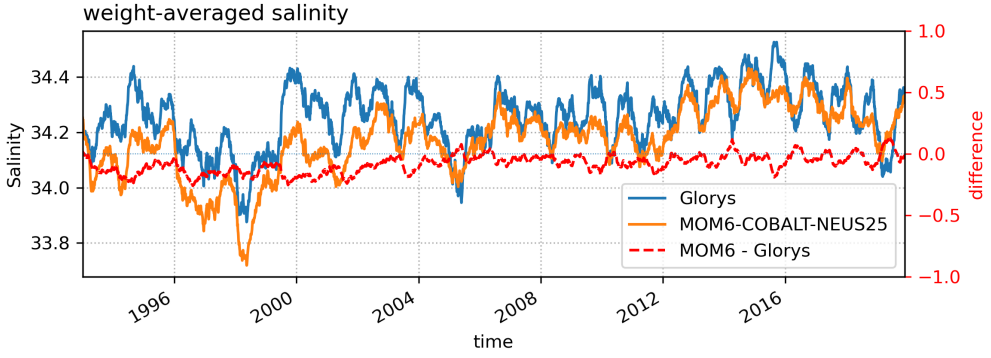

Figure A3. Weight-averaged salinity considering the domain of this study area. The time series show the salinity drift of MOM6-COBALT-NEUS25, Glorys and their differences.

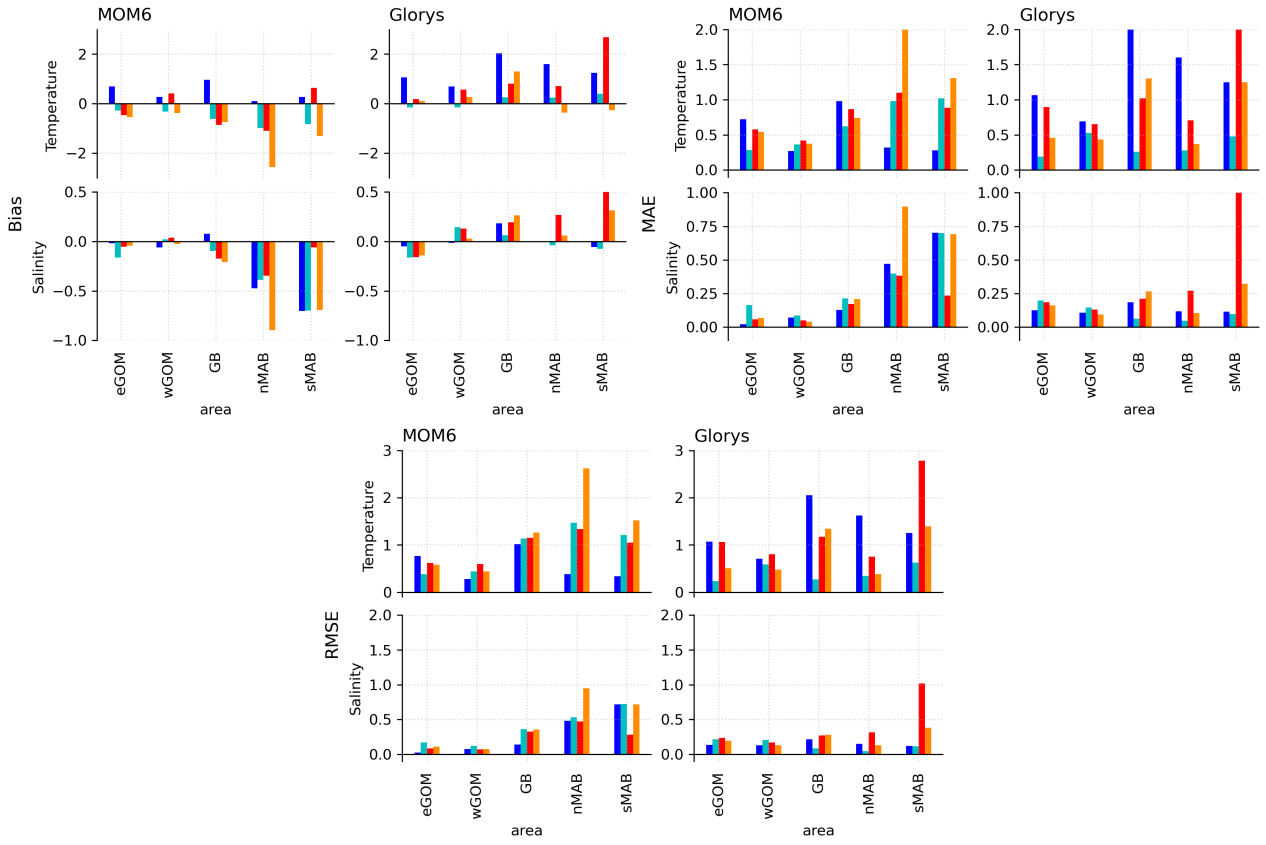

Figure A4. Error statistics of seasonal average profiles at different subdomains of the model. Colors represent winter (blue), spring (cyan), summer (red), and fall (orange)

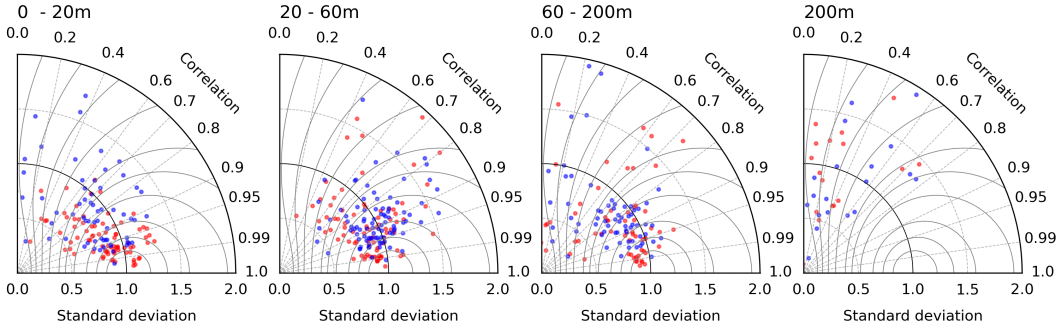

Figure A5. Taylor Diagrams of bottom temperature measurements in lobster thermistors at different bathymetry intervals considering MOM6 (red) and Glorys (blue) results.

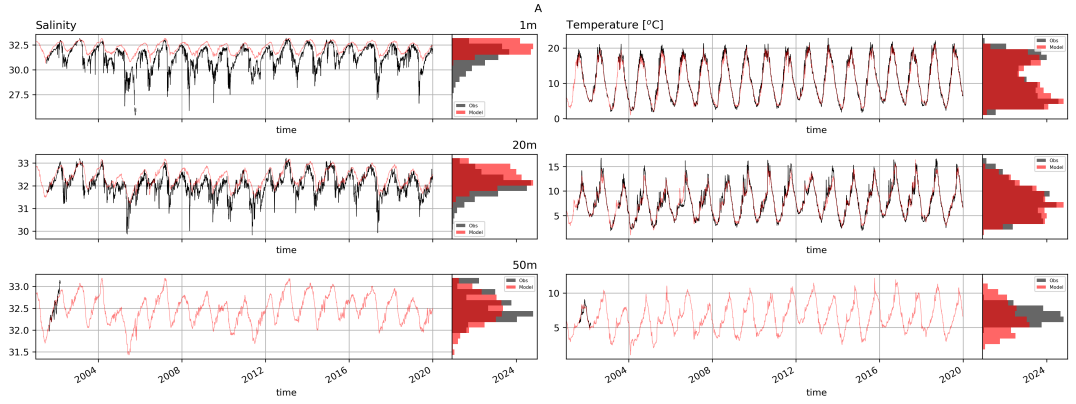

Figure A6. Time series of salinity in temperature of MOM6 (red) and NERACOOS mooring measurements (black) at buoy ~~A01~~A.

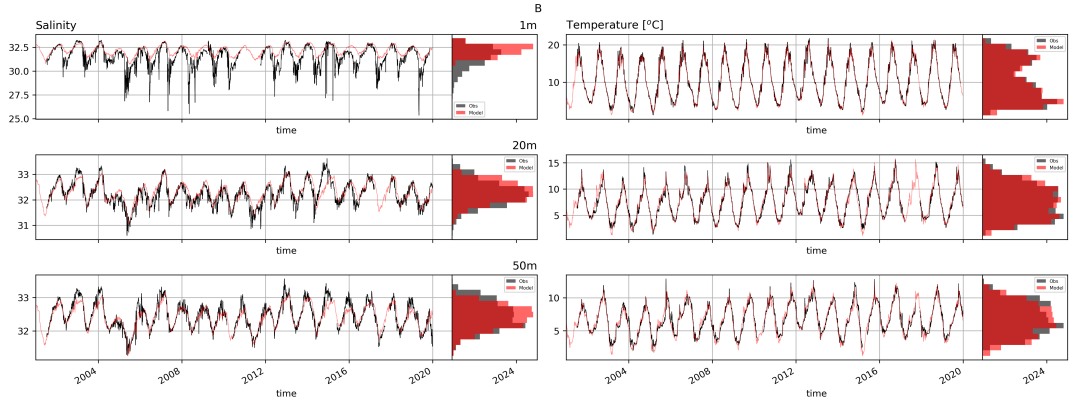

Figure A7. Time series of salinity in temperature of MOM6 (red) and NERACOOS mooring measurements (black) at buoy ~~B01~~B.

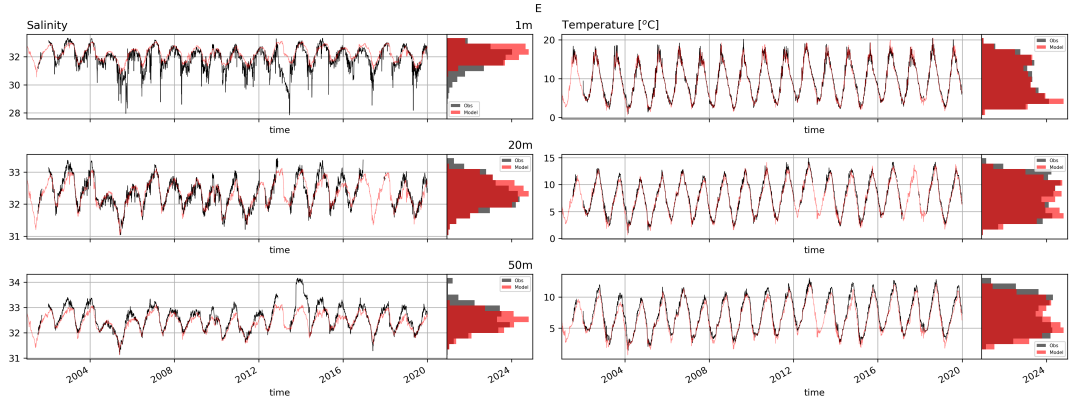

Figure A8. Time series of salinity in temperature of MOM6 (red) and NERACOOS mooring measurements (black) at buoy ~~E01~~E.

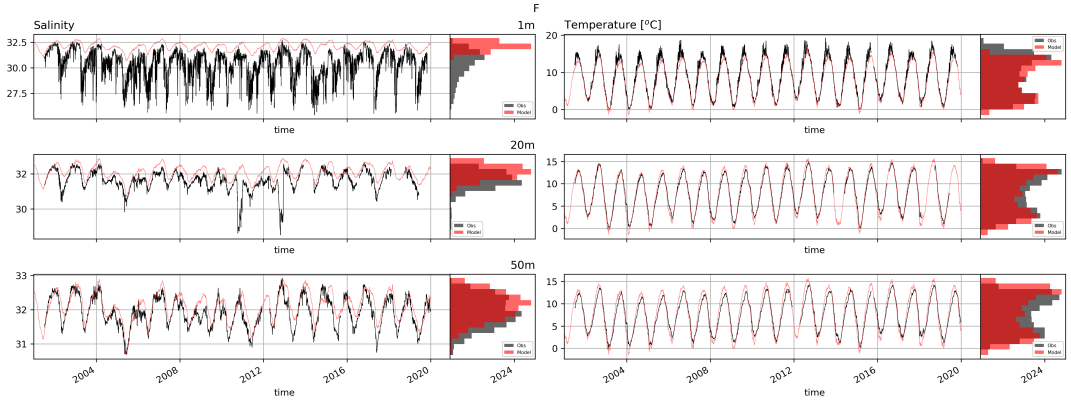

Figure A9. Time series of salinity in temperature of MOM6 (red) and NERACOOS mooring measurements (black) at buoy ~~F01~~F.

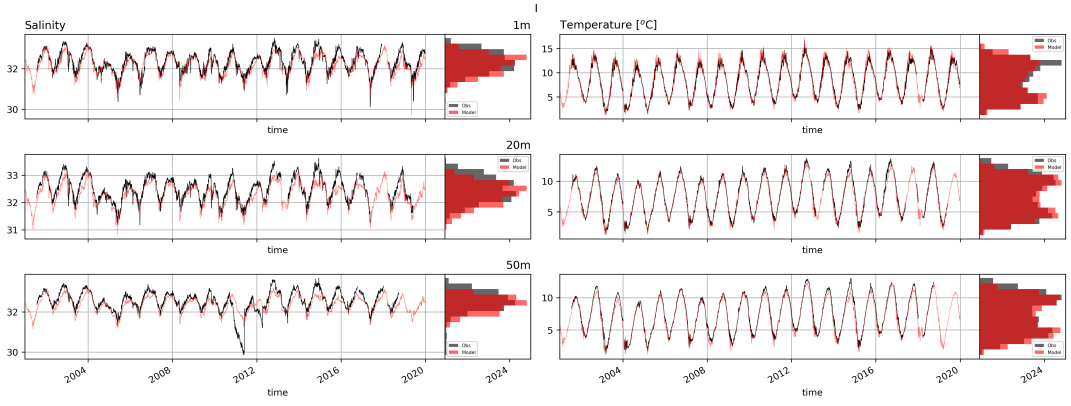

Figure A10. Time series of salinity in temperature of MOM6 (red) and NERACOOS mooring measurements (black) at buoy ~~I01~~I.

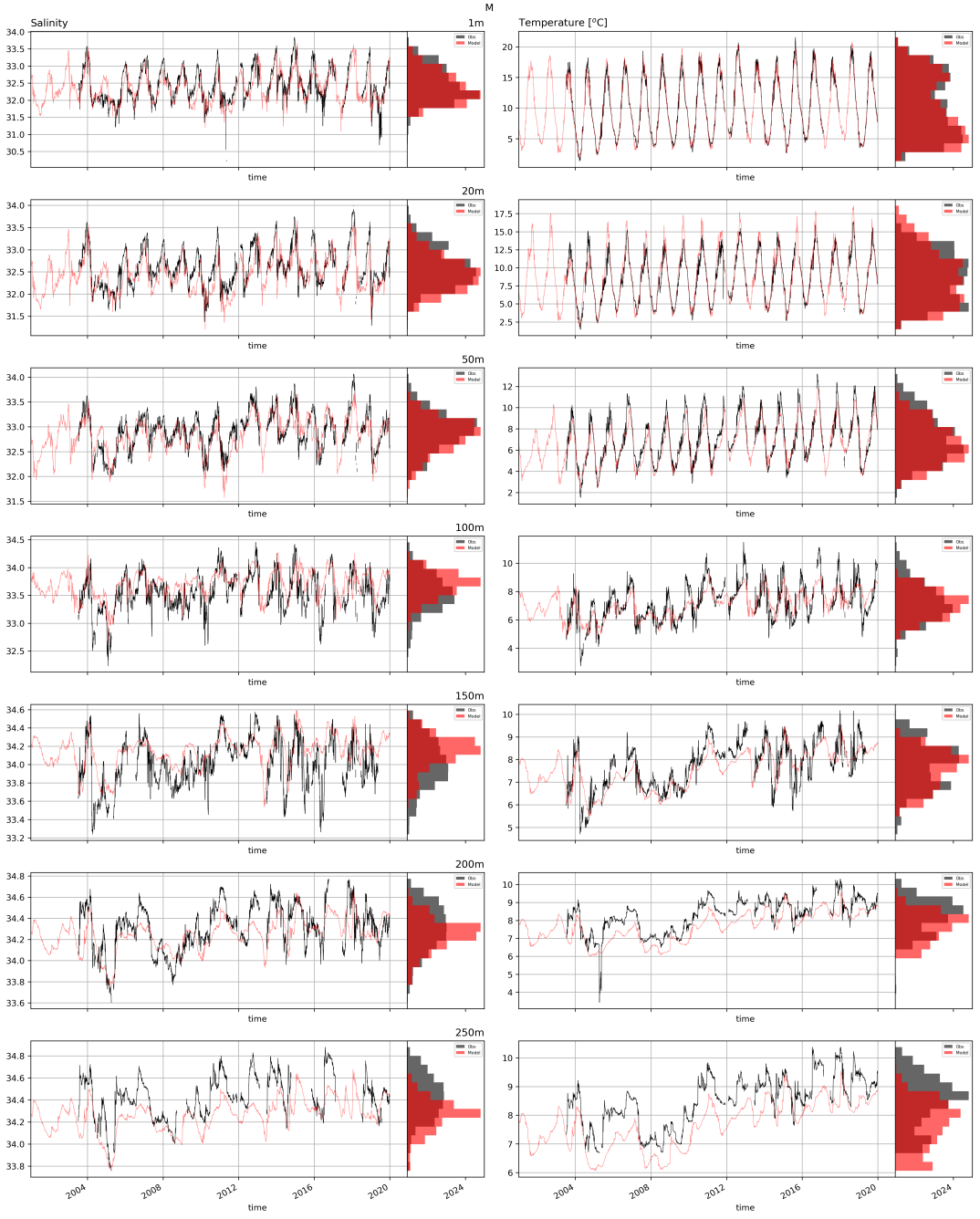

Figure A11. Time series of salinity in temperature of MOM6 (red) and NERACOOS mooring measurements (black) at buoy ~~N01~~N.

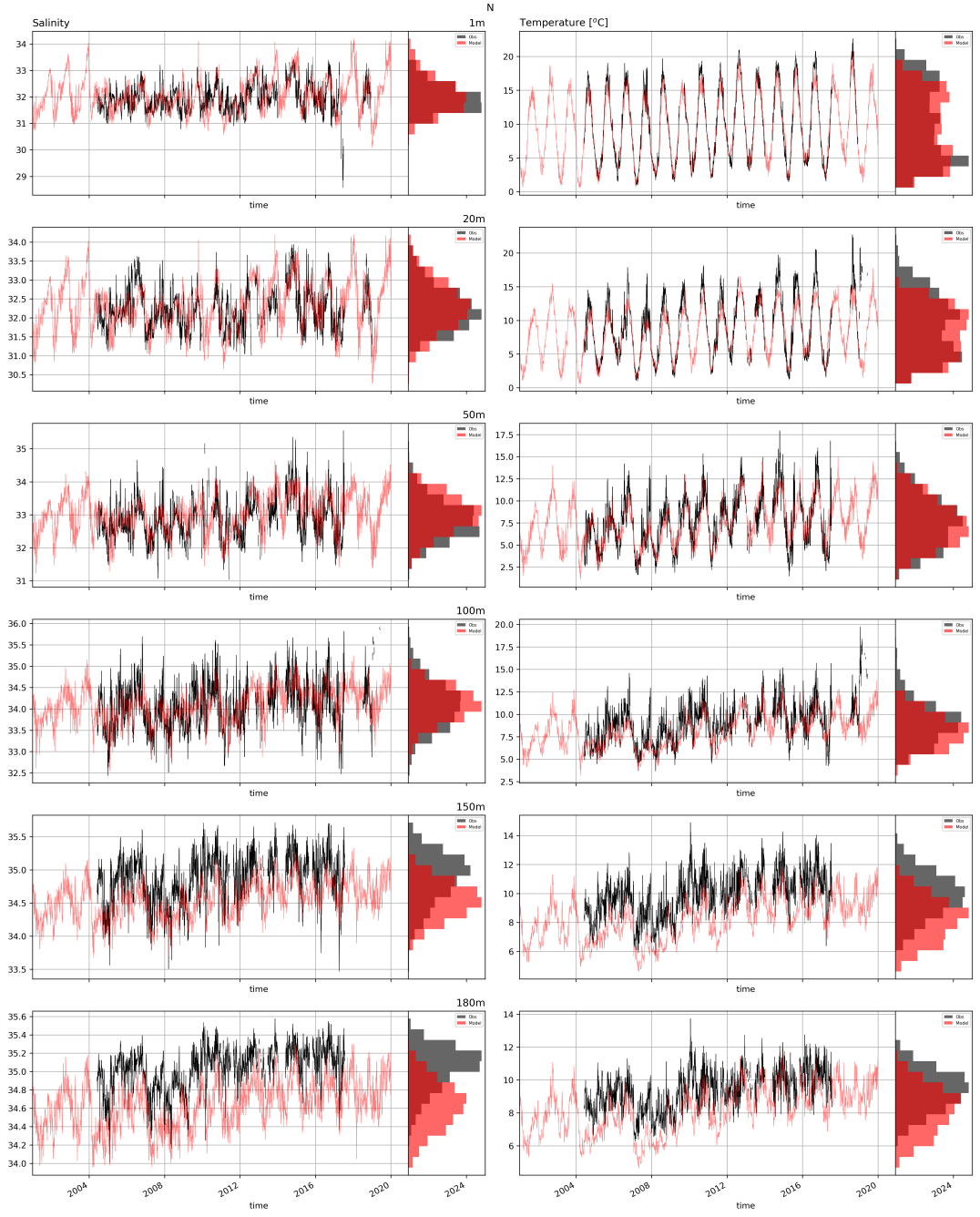

Figure A12. Time series of salinity in temperature of MOM6 (red) and NERACOOS mooring measurements (black) at buoy ~~M01~~M.

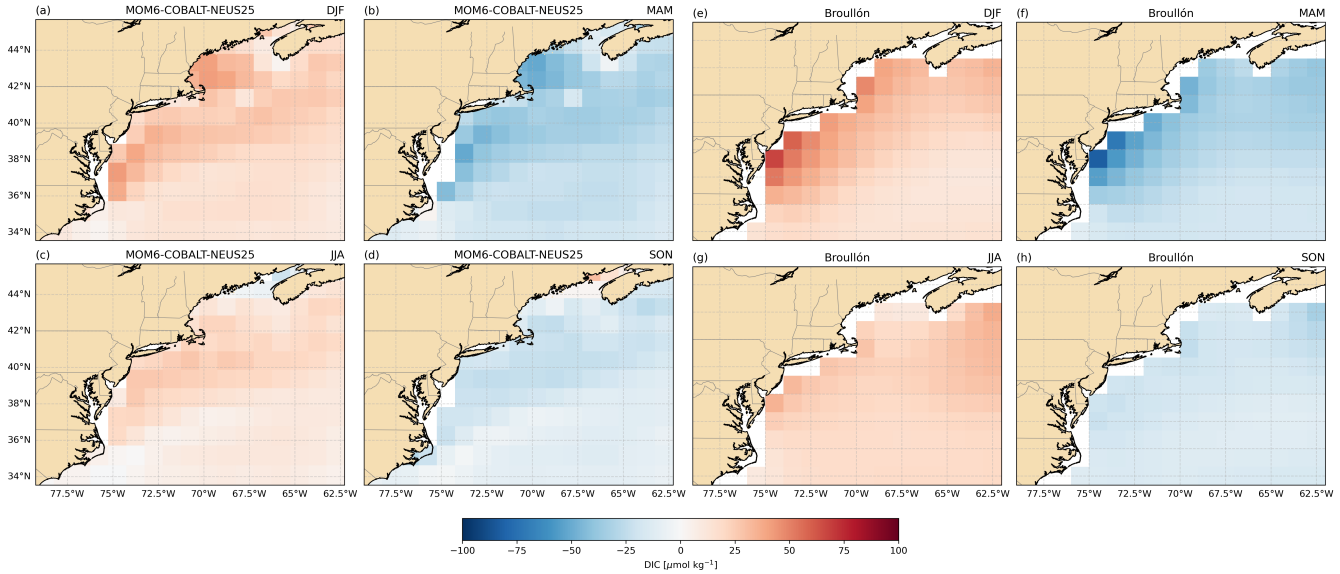

Figure A13. Seasonal climatological anomalies maps of DIC integrated over the upper 10 m considering MOM6-COBALT-NEUS25 and Broullón with respect to the total period. the number of horizontal points is shown in the label. DIC averages for MOM6-COBALT-NEUS25 and Broullòn are 2088 and 2026 μg kg^{-1}.

References

References

Seasonal warming of the Middle Atlantic Bight Cold Pool.

Adcroft, A. and Campin, J.-M.: Rescaled height coordinates for accurate representation of free-surface flows in ocean circulation models, Ocean Modelling, 7, 269–284, https://doi.org/10.1016/j.ocemod.2003.09.003, publisher: Elsevier BV, 2004.

Adcroft, A., Hallberg, R., and Harrison, M.: A finite volume discretization of the pressure gradient force using analytic integration, Ocean Modelling, 22, 106–113, https://doi.org/10.1016/j.ocemod.2008.02.001, 2008.

Adcroft, A., Anderson, W., Balaji, V., Blanton, C., Bushuk, M., Dufour, C. O., Dunne, J. P., Griffies, S. M., Hallberg, R., Harrison, M. J., Held, I. M., Jansen, M. F., John, J. G., Krasting, J. P., Langenhorst, A. R., Legg, S., Liang, Z., McHugh, C., Radhakrishnan, A., Reichl, B. G., Rosati, T., Samuels, B. L., Shao, A., Stouffer, R., Winton, M., Wittenberg, A. T., Xiang, B., Zadeh, N., and Zhang, R.: The GFDL Global Ocean and Sea Ice Model OM4.0: Model Description and Simulation Features, Journal of Advances in Modeling Earth Systems, 11, 3167–3211, https://doi.org/10.1029/2019ms001726, publisher: American Geophysical Union (AGU), 2019.

Andres, M.: On the recent destabilization of the Gulf Stream path downstream of Cape Hatteras, Geophysical Research Letters, 43, 9836–9842, https://doi.org/10.1002/2016GL069966, 2016.

Arakawa, A. and Lamb, V. R.: A Potential Enstrophy and Energy Conserving Scheme for the Shallow Water Equations, Monthly Weather Review, 109, 18–36, https://doi.org/10.1175/1520-0493(1981)109<0018:apeaec>2.0.co;2, publisher: American Meteorological Society, 1981.

Azevedo Correia De Souza, J. M., Suanda, S. H., Couto, P. P., Smith, R. O., Kerry, C., and Roughan, M.: Moana Ocean Hindcast – a > 25-year simulation for New Zealand waters using the Regional Ocean Modeling System (ROMS) v3.9 model, Geoscientific Model Development, 16, 211–231, https://doi.org/10.5194/gmd-16-211-2023, 2023.

Baker, A. and Croot, P.: Atmospheric and marine controls on aerosol iron solubility in seawater, Marine Chemistry, 120, 4–13, https://doi.org/10.1016/j.marchem.2008.09.003, 2010.

Balch, W. M., Drapeau, D. T., Bowler, B. C., Record, N. R., Bates, N. R., Pinkham, S., Garley, R., and Mitchell, C.: Changing Hydrographic, Biogeochemical, and Acidification Properties in the Gulf of Maine as Measured by the Gulf of Maine North Atlantic Time Series, GNATS, Between 1998 and 2018, Journal of Geophysical Research: Biogeosciences, 127, e2022JG006 790, https://doi.org/10.1029/2022JG006790, 2022.

Bittig, H. C., Steinhoff, T., Claustre, H., Fiedler, B., Williams, N. L., Sauzède, R., Körtzinger, A., and Gattuso, J.-P.: An Alternative to Static Climatologies: Robust Estimation of Open Ocean CO2 Variables and Nutrient Concentrations From T, S, and O2 Data Using Bayesian Neural Networks, Frontiers in Marine Science, 5, 328, https://doi.org/10.3389/fmars.2018.00328, 2018.

Bodner, A. S., Fox-Kemper, B., Johnson, L., Van Roekel, L. P., McWilliams, J. C., Sullivan, P. P., Hall, P. S., and Dong, J.: Modifying the Mixed Layer Eddy Parameterization to Include Frontogenesis Arrest by Boundary Layer Turbulence, Journal of Physical Oceanography, 53, 323–339, https://doi.org/10.1175/JPO-D-21-0297.1, 2023.

Brennan, C. E., Bianucci, L., and Fennel, K.: Sensitivity of Northwest North Atlantic Shelf Circulation to Surface and Boundary Forcing: A Regional Model Assessment, Atmosphere-Ocean, 54, 230–247, https://doi.org/10.1080/07055900.2016.1147416, publisher: Informa UK Limited, 2016.

Brooks, D.: A Brief Overview of the Physical Oceanography of the Gulf of Maine, 1992.

Brooks, D. A.: Vernal circulation in the Gulf of Maine, Journal of Geophysical Research: Oceans, 90, 4687–4706, https://doi.org/10.1029/JC090iC03p04687, 1985.

Broullón, D., Pérez, F. F., Velo, A., Hoppema, M., Olsen, A., Takahashi, T., Key, R. M., Tanhua, T., Santana-Casiano, J. M., and Kozyr, A.: A global monthly climatology of oceanic total dissolved inorganic carbon: a neural network approach, Earth System Science Data, 12, 1725–1743, https://doi.org/10.5194/essd-12-1725-2020, 2020.

Brunner, K. and Lwiza, K. M. M.: Tidal velocities on the Mid-Atlantic Bight continental shelf using high-frequency radar, Journal of Oceanography, 76, 289–306, https://doi.org/10.1007/s10872-020-00545-7, 2020.

Carter, B. R., Bittig, H. C., Fassbender, A. J., Sharp, J. D., Takeshita, Y., Xu, Y., Álvarez, M., Wanninkhof, R., Feely, R. A., and Barbero, L.: New and updated global empirical seawater property estimation routines, Limnology and Oceanography: Methods, 19, 785–809, https://doi.org/10.1002/lom3.10461, 2021.

Castillo-Trujillo, A. C., Kwon, Y.-O., Fratantoni, P., Chen, K., Seo, H., Alexander, M. A., and Saba, V. S.: An evaluation of eight global ocean reanalyses for the Northeast U.S. Continental shelf, Progress in Oceanography, 219, 103 126, https://doi.org/10.1016/j.pocean.2023.103126, 2023.

Center for Operational Oceanographic Products and Services: CO-OPS Water Level Data from the Coastal Tide Gauge and Great Lake Water Level Network of the United States and US Territories, https://doi.org/10.25921/DT9G-2P60.

Chapman, D. C. and Beardsley, R. C.: On the Origin of Shelf Water in the Middle Atlantic Bight, Journal of Physical Oceanography, 19, 384–391, https://doi.org/10.1175/1520-0485(1989)019<0384:OTOOSW>2.0.CO;2, 1989.

Chassignet, E. P. and Xu, X.: Impact of Horizontal Resolution (1/12° to 1/50°) on Gulf Stream Separation, Penetration, and Variability, Journal of Physical Oceanography, 47, 1999–2021, https://doi.org/10.1175/JPO-D-17-0031.1, 2017.

Chelton, D. B., deSzoeke, R. A., Schlax, M. G., El Naggar, K., and Siwertz, N.: Geographical Variability of the First Baroclinic Rossby Radius of Deformation, Journal of Physical Oceanography, 28, 433–460, https://doi.org/10.1175/1520-0485(1998)028<0433:GVOTFB>2.0.CO;2, 1998.

Chen, C., Beardsley, R. C., and Limeburner, R.: A Numerical Study of Stratified Tidal Rectification over Finite-Amplitude Banks. Part II: Georges Bank, Journal of Physical Oceanography, 25, 2111–2128, https://doi.org/10.1175/1520-0485(1995)025<2111:ANSOST>2.0.CO;2, 1995.

Chen, C., Huang, H., Beardsley, R. C., Xu, Q., Limeburner, R., Cowles, G. W., Sun, Y., Qi, J., and Lin, H.: Tidal dynamics in the Gulf of Maine and New England Shelf: An application of FVCOM, Journal of Geophysical Research, 116, C12 010, https://doi.org/10.1029/2011JC007054, 2011.

Chen, K. and Yang, J.: What Drives the Mean Along-Shelf Flow in the Northwest Atlantic Coastal Ocean?, Journal of Geophysical Research: Oceans, 129, e2024JC021 079, https://doi.org/10.1029/2024JC021079, 2024.

Chen, Z. and Curchitser, E. N.: Interannual Variability of the Mid-Atlantic Bight Cold Pool, Journal of Geophysical Research: Oceans, 125, e2020JC016 445, https://doi.org/10.1029/2020JC016445, 2020.

Codiga, D. L.: Unified Tidal Analysis and Prediction Using the UTide Matlab Functions, Tech. rep., Graduate School of Oceanography, University of Rhode Island, Narragansett, RI, ftp://www.po.gso.uri.edu/pub/downloads/codiga/pubs/2011Codiga-UTide-Report.pdf, 2011.

Coleman, S., Dewhurst, T., Fredriksson, D. W., St. Gelais, A. T., Cole, K. L., MacNicoll, M., Laufer, E., and Brady, D. C.: Quantifying baseline costs and cataloging potential optimization strategies for kelp aquaculture carbon dioxide removal, Frontiers in Marine Science, 9, 966 304, https://doi.org/10.3389/fmars.2022.966304, 2022.

Dawson, A.: eofs: A Library for EOF Analysis of Meteorological, Oceanographic, and Climate Data, Journal of Open Research Software, 4, 14, https://doi.org/10.5334/jors.122, 2016.

den Bossche, J. V., Jordahl, K., Fleischmann, M., Richards, M., McBride, J., Wasserman, J., Badaracco, A. G., Snow, A. D., Roggemans, P., Ward, B., Tratner, J., Gerard, J., Perry, M., Taves, M., carsonfarmer, Hjelle, G. A., Bell, R., ter Hoeven, E., Cochran, M., Tan, N. Y., rraymondgh, Caria, G., Culbertson, L., Bartos, M., Rey, S., Flavin, J., Eubank, N., sangarshanan, and Gillies, S.: geopandas/geopandas: v1.1.1, https://doi.org/10.5281/ZENODO.2585848, 2025.

Dierssen, H. M.: Perspectives on empirical approaches for ocean color remote sensing of chlorophyll in a changing climate, Proceedings of the National Academy of Sciences, 107, 17 073–17 078, https://doi.org/10.1073/pnas.0913800107, 2010.

Drévillon, M., Fernandez, E., and Lellouche, J. M.: CMEMS-GLO-PUM-001-030 Product User Manual, https://documentation.marine.copernicus.eu/PUM/CMEMS-GLO-PUM-001-030.pdf.

Du, J., Zhang, W. G., and Li, Y.: Variability of Deep Water in Jordan Basin of the Gulf of Maine: Influence of Gulf Stream Warm Core Rings and the Nova Scotia Current, Journal of Geophysical Research: Oceans, 126, https://doi.org/10.1029/2020jc017136, publisher: American Geophysical Union (AGU), 2021.

Du, J., Zhang, W. G., and Li, Y.: Impact of Gulf Stream Warm-Core Rings on Slope Water Intrusion into the Gulf of Maine, Journal of Physical Oceanography, 52, 1797–1815, https://doi.org/10.1175/JPO-D-21-0288.1, 2022.

Du Pontavice, H., Chen, Z., and Saba, V. S.: A high-resolution ocean bottom temperature product for the northeast U.S. continental shelf marine ecosystem, Progress in Oceanography, 210, 102 948, https://doi.org/10.1016/j.pocean.2022.102948, 2023.

Dunne, J. P., John, J. G., Adcroft, A. J., Griffies, S. M., Hallberg, R. W., Shevliakova, E., Stouffer, R. J., Cooke, W., Dunne, K. A., Harrison, M. J., Krasting, J. P., Malyshev, S. L., Milly, P. C. D., Phillipps, P. J., Sentman, L. T., Samuels, B. L., Spelman, M. J., Winton, M., Wittenberg, A. T., and Zadeh, N.: GFDL's ESM2 Global Coupled Climate–Carbon Earth System Models. Part I: Physical Formulation and Baseline Simulation Characteristics, Journal of Climate, 25, 6646–6665, https://doi.org/10.1175/JCLI-D-11-00560.1, 2012.

Dunne, J. P., Horowitz, L. W., Adcroft, A. J., Ginoux, P., Held, I. M., John, J. G., Krasting, J. P., Malyshev, S., Naik, V., Paulot, F., Shevliakova, E., Stock, C. A., Zadeh, N., Balaji, V., Blanton, C., Dunne, K. A., Dupuis, C., Durachta, J., Dussin, R., Gauthier, P. P. G., Griffies, S. M., Guo, H., Hallberg, R. W., Harrison, M., He, J., Hurlin, W., McHugh, C., Menzel, R., Milly, P. C. D., Nikonov, S., Paynter, D. J., Ploshay, J., Radhakrishnan, A., Rand, K., Reichl, B. G., Robinson, T., Schwarzkopf, D. M., Sentman, L. T., Underwood, S., Vahlenkamp, H., Winton, M., Wittenberg, A. T., Wyman, B., Zeng, Y., and Zhao, M.: The GFDL Earth System Model Version 4.1 (GFDL-ESM 4.1): Overall Coupled Model Description and Simulation Characteristics, Journal of Advances in Modeling Earth Systems, 12, e2019MS002 015, https://doi.org/10.1029/2019MS002015, 2020.

Egbert, G. D. and Erofeeva, S. Y.: Efficient Inverse Modeling of Barotropic Ocean Tides, Journal of Atmospheric and Oceanic Technology, 19, 183–204, https://doi.org/10.1175/1520-0426(2002)019<0183:EIMOBO>2.0.CO;2, 2002.

Elson, P., de Andrade, E. S., Lucas, G., May, R., Hattersley, R., Campbell, E., Comer, R., Dawson, A., Little, B., Raynaud, S., scmc72, Snow, A. D., lgolston, Blay, B., Killick, P., lbdreyer, Peglar, P., Wilson, N., Andrew, Szymaniak, J., Berchet, A., Bosley, C., Davis, L., Filipe, Krasting, J., Bradbury, M., stephenworsley, and Kirkham, D.: SciTools/cartopy: REL: v0.24.1, https://doi.org/10.5281/ZENODO.1182735, 2024.

Fairbanks, R. G.: The origin of continental shelf and slope water in the New York Bight and Gulf of Maine: Evidence from $H_2{}^{18}O/H_2{}^{16}O$ ratio measurements, Journal of Geophysical Research: Oceans, 87, 5796–5808, https://doi.org/10.1029/JC087iC08p05796, 1982.

Fennel, K., Mattern, J. P., Doney, S. C., Bopp, L., Moore, A. M., Wang, B., and Yu, L.: Ocean biogeochemical modelling, Nature Reviews Methods Primers, 2, 76, https://doi.org/10.1038/s43586-022-00154-2, 2022.

Filippino, K. C., Mulholland, M. R., and Bernhardt, P. W.: Nitrogen uptake and primary productivity rates in the Mid-Atlantic Bight (MAB), Estuarine, Coastal and Shelf Science, 91, 13–23, https://doi.org/10.1016/j.ecss.2010.10.001, publisher: Elsevier BV, 2011.

Flather, R.: A Tidal Model of the North-West European Continental Shelf, Mem. Soc. R. Sci. Liege., 10, 141–164, 1976.

Fox-Kemper, B. and Ferrari, R.: Parameterization of Mixed Layer Eddies. Part II: Prognosis and Impact, Journal of Physical Oceanography, 38, 1166–1179, https://doi.org/10.1175/2007JPO3788.1, 2008.

Fox-Kemper, B., Ferrari, R., and Hallberg, R.: Parameterization of Mixed Layer Eddies. Part I: Theory and Diagnosis, Journal of Physical Oceanography, 38, 1145–1165, https://doi.org/10.1175/2007JPO3792.1, 2008.

Fox-Kemper, B., Adcroft, A., Böning, C. W., Chassignet, E. P., Curchitser, E., Danabasoglu, G., Eden, C., England, M. H., Gerdes, R., Greatbatch, R. J., Griffies, S. M., Hallberg, R. W., Hanert, E., Heimbach, P., Hewitt, H. T., Hill, C. N., Komuro, Y., Legg, S., Le Sommer, J., Masina, S., Marsland, S. J., Penny, S. G., Qiao, F., Ringler, T. D., Treguier, A. M., Tsujino, H., Uotila, P., and Yeager, S. G.: Challenges and Prospects in Ocean Circulation Models, Frontiers in Marine Science, 6, 65, https://doi.org/10.3389/fmars.2019.00065, 2019.

Garcia, H. E., Bouchard, C., Cross, S. L., Paver, C. R., Reagan, J. R., Boyer, T. P., Locarnini, R. A., Mishonov, A. V., Baranova, O. K., Seidov, D., Wang, Z., and Dukhovskoy, D.: World Ocean Atlas 2023, Volume 4: Dissolved Inorganic Nutrients (phosphate, nitrate and nitrate+nitrite, silicate), https://doi.org/10.25923/39QW-7J08, publisher: NOAA National Centers for Environmental Information, 2024a.

Garcia, H. E., Wang, Z., Bouchard, C., Cross, S. L., Paver, C. R., Reagan, J. R., Boyer, T. P., Locarnini, R. A., Mishonov, A. V., Baranova, O. K., Seidov, D., and Dukhovskoy, D.: World Ocean Atlas 2023, Volume 3: Dissolved Oxygen, Apparent Oxygen Utilization, and Dissolved Oxygen Saturation, https://doi.org/10.25923/RB67-NS53, publisher: NOAA National Centers for Environmental Information, 2024b.

Garrett, C.: Tidal Resonance in the Bay of Fundy and Gulf of Maine, Nature, 238, 441–443, https://doi.org/10.1038/238441a0, 1972.

GEBCO Bathymetric Compilation Group 2023: The GEBCO_2023 Grid - a continuous terrain model of the global oceans and land., https://doi.org/10.5285/F98B053B-0CBC-6C23-E053-6C86ABC0AF7B, 2023.

Gent, P. R. and Mcwilliams, J. C.: Isopycnal Mixing in Ocean Circulation Models, Journal of Physical Oceanography, 20, 150–155, https://doi.org/10.1175/1520-0485(1990)020<0150:IMIOCM>2.0.CO;2, 1990.

Geyer, W., Signell, R., Fong, D., Wang, J., Anderson, D., and Keafer, B.: The freshwater transport and dynamics of the western Maine coastal current, Continental Shelf Research, 24, 1339–1357, https://doi.org/10.1016/j.csr.2004.04.001, publisher: Elsevier BV, 2004.

Gomez, F. A., Lee, S.-K., Stock, C. A., Ross, A. C., Resplandy, L., Siedlecki, S. A., Tagklis, F., and Salisbury, J. E.: RC4USCoast: A river chemistry dataset for regional ocean model application in the U.S. East, Gulf of Mexico, and West Coasts from 1950-01-01 to 2022-12-31 (NCEI Accession 0260455), https://doi.org/10.25921/9JFW-PH50, 2022.

Gomez, F. A., Lee, S.-K., Stock, C. A., Ross, A. C., Resplandy, L., Siedlecki, S. A., Tagklis, F., and Salisbury, J. E.: RC4USCoast: a river chemistry dataset for regional ocean model applications in the US East Coast, Gulf of Mexico, and US West Coast, Earth System Science Data, 15, 2223–2234, https://doi.org/10.5194/essd-15-2223-2023, 2023.

Gonçalves Neto, A., Langan, J. A., and Palter, J. B.: Changes in the Gulf Stream preceded rapid warming of the Northwest Atlantic Shelf, Communications Earth & Environment, 2, 74, https://doi.org/10.1038/s43247-021-00143-5, 2021.

Griffies, S. M., Adcroft, A., and Hallberg, R. W.: A Primer on the Vertical Lagrangian-Remap Method in Ocean Models Based on Finite Volume Generalized Vertical Coordinates, Journal of Advances in Modeling Earth Systems, 12, e2019MS001 954, https://doi.org/10.1029/2019MS001954, 2020.

Hallberg, R.: Using a resolution function to regulate parameterizations of oceanic mesoscale eddy effects, Ocean Modelling, 72, 92–103, https://doi.org/10.1016/j.ocemod.2013.08.007, 2013.

Harrigan, S., Zsoter, E., Barnard, C., Wtterhall, F., Alfieri, L., Salamon, L., and Prudhomme, C.: River discharge historical data from the Global Flood Awareness System, v2.1, https://doi.org/10.24381/CDS.A4FDD6B9, 2021.

He, R. and Wilkin, J. L.: Barotropic tides on the southeast New England shelf: A view from a hybrid data assimilative modeling approach, Journal of Geophysical Research: Oceans, 111, 2005JC003 254, https://doi.org/10.1029/2005JC003254, 2006.

Heiderich, J. and Todd, R. E.: Along-Stream Evolution of Gulf Stream Volume Transport, Journal of Physical Oceanography, 50, 2251–2270, https://doi.org/10.1175/JPO-D-19-0303.1, 2020.

Herbert, R. J., Krom, M. D., Carslaw, K. S., Stockdale, A., Mortimer, R. J. G., Benning, L. G., Pringle, K., and Browse, J.: The Effect of Atmospheric Acid Processing on the Global Deposition of Bioavailable Phosphorus From Dust, Global Biogeochemical Cycles, 32, 1367–1385, https://doi.org/10.1029/2018GB005880, 2018.

Hersbach, H., Bell, B., Berrisford, P., Hirahara, S., Horányi, A., Muñoz-Sabater, J., Nicolas, J., Peubey, C., Radu, R., Schepers, D., Simmons, A., Soci, C., Abdalla, S., Abellan, X., Balsamo, G., Bechtold, P., Biavati, G., Bidlot, J., Bonavita, M., De Chiara, G., Dahlgren, P., Dee, D., Diamantakis, M., Dragani, R., Flemming, J., Forbes, R., Fuentes, M., Geer, A., Haimberger, L., Healy, S., Hogan, R. J., Hólm, E., Janisková, M., Keeley, S., Laloyaux, P., Lopez, P., Lupu, C., Radnoti, G., De Rosnay, P., Rozum, I., Vamborg, F., Villaume, S., and Thépaut, J.: The ERA5 global reanalysis, Quarterly Journal of the Royal Meteorological Society, 146, 1999–2049, https://doi.org/10.1002/qj.3803, 2020.

Hoyer, S. and Hamman, J.: xarray: N-D labeled Arrays and Datasets in Python, Journal of Open Research Software, 5, 10, https://doi.org/10.5334/jors.148, 2017.

Jackson, L., Hallberg, R., and Legg, S.: A Parameterization of Shear-Driven Turbulence for Ocean Climate Models, Journal of Physical Oceanography, 38, 1033–1053, https://doi.org/10.1175/2007JPO3779.1, 2008.

Jean-Michel, L., Eric, G., Romain, B.-B., Gilles, G., Angélique, M., Marie, D., Clément, B., Mathieu, H., Olivier, L. G., Charly, R., Tony, C., Charles-Emmanuel, T., Florent, G., Giovanni, R., Mounir, B., Yann, D., and Pierre-Yves, L. T.: The Copernicus Global 1/12° Oceanic and Sea Ice GLORYS12 Reanalysis, Frontiers in Earth Science, 9, 698 876, https://doi.org/10.3389/feart.2021.698876, 2021.

Jiang, L.-Q., Feely, R. A., Wanninkhof, R., Greeley, D., Barbero, L., Alin, S., Carter, B. R., Pierrot, D., Featherstone, C., Hooper, J., Melrose, C., Monacci, N., Sharp, J. D., Shellito, S., Xu, Y.-Y., Kozyr, A., Byrne, R. H., Cai, W.-J., Cross, J., Johnson, G. C., Hales, B., Langdon, C., Mathis, J., Salisbury, J., and Townsend, D. W.: Coastal Ocean Data Analysis Product in North America (CODAP-NA) – an internally consistent data product for discrete inorganic carbon, oxygen, and nutrients on the North American ocean margins, Earth System Science Data, 13, 2777–2799, https://doi.org/10.5194/essd-13-2777-2021, 2021.

Jiang, L.-Q., Boyer, T. P., Paver, C. R., Reagan, J. R., Alin, S. R., Barbero, L., Carter, B. R., Feely, R. A., and Wanninkhof, R.: Climatological distribution of ocean acidification indicators from surface to 500 meters water depth on the North American ocean margins from 2003-12-06 to 2018-11-22 (NCEI Accession 0270962), https://doi.org/10.25921/G8PB-ZY76, 2022.

Kelly, S. M. and Lermusiaux, P. F. J.: Internal-tide interactions with the Gulf Stream and Middle Atlantic Bight shelfbreak front, Journal of Geophysical Research: Oceans, 121, 6271–6294, https://doi.org/10.1002/2016JC011639, 2016.

Large, W. G., McWilliams, J. C., and Doney, S. C.: Oceanic vertical mixing: A review and a model with a nonlocal boundary layer parameterization, Reviews of Geophysics, 32, 363–403, https://doi.org/10.1029/94rg01872, publisher: American Geophysical Union (AGU), 1994.

Laurent, A., Fennel, K., and Kuhn, A.: An observation-based evaluation and ranking of historical Earth system model simulations in the northwest North Atlantic Ocean, Biogeosciences, 18, 1803–1822, https://doi.org/10.5194/bg-18-1803-2021, 2021.

Lehmann, M. K., Fennel, K., and He, R.: Statistical validation of a 3-D bio-physical model of the western North Atlantic, 2009.

Lentz, S. J.: A climatology of salty intrusions over the continental shelf from Georges Bank to Cape Hatteras, Journal of Geophysical Research: Oceans, 108, 2003JC001 859, https://doi.org/10.1029/2003JC001859, 2003.

Lentz, S. J.: The Mean Along-Isobath Heat and Salt Balances over the Middle Atlantic Bight Continental Shelf, Journal of Physical Oceanography, 40, 934–948, https://doi.org/10.1175/2009JPO4214.1, 2010.

Li, D., Wang, Z., Xue, H., Thomas, A. C., and Etter, R. J.: Wind-Modulated Western Maine Coastal Current and Its Connectivity With the Eastern Maine Coastal Current, Journal of Geophysical Research: Oceans, 127, e2022JC018 469, https://doi.org/10.1029/2022JC018469, 2022.

Li, X., Wu, Z., Ouyang, Z., and Cai, W.-J.: The source and accumulation of anthropogenic carbon in the U.S. East Coast, Science Advances, 10, eadl3169, https://doi.org/10.1126/sciadv.adl3169, 2024.

Li, Y. and He, R.: Spatial and temporal variability of SST and ocean color in the Gulf of Maine based on cloud-free SST and chlorophyll reconstructions in 2003–2012, Remote Sensing of Environment, 144, 98–108, https://doi.org/10.1016/j.rse.2014.01.019, 2014.

Linder, C. A. and Gawarkiewicz, G.: A climatology of the shelfbreak front in the Middle Atlantic Bight, Journal of Geophysical Research: Oceans, 103, 18 405–18 423, https://doi.org/10.1029/98JC01438, 1998.

Loder, J. W.: Topographic Rectification of Tidal Currents on the Sides of Georges Bank, Journal of Physical Oceanography, 10, 1399–1416, https://doi.org/10.1175/1520-0485(1980)010<1399:TROTCO>2.0.CO;2, 1980.

Lopez, A.: Sea level daily gridded data from satellite observations for the global ocean from 1993 to present, https://doi.org/10.24381/CDS.4C328C78, 2018.

Lovato, T., Peano, D., Butenschön, M., Materia, S., Iovino, D., Scoccimarro, E., Fogli, P. G., Cherchi, A., Bellucci, A., Gualdi, S., Masina, S., and Navarra, A.: CMIP6 Simulations With the CMCC Earth System Model (CMCC-ESM2), Journal of Advances in Modeling Earth Systems, 14, e2021MS002 814, https://doi.org/10.1029/2021MS002814, 2022.

López, A. G., Wilkin, J. L., and Levin, J. C.: Doppio – a ROMS (v3.6)-based circulation model for the Mid-Atlantic Bight and Gulf of Maine: configuration and comparison to integrated coastal observing network observations, Geoscientific Model Development, 13, 3709–3729, https://doi.org/10.5194/gmd-13-3709-2020, 2020.

Manning, J.: Middle Atlantic Bight salinity: interannual variability, Continental Shelf Research, 11, 123–137, https://doi.org/10.1016/0278-4343(91)90058-e, publisher: Elsevier BV, 1991.

Manning, J. and Pelletier, E.: Environmental monitors on lobster traps (eMOLT): long-term observations of New England's bottom-water temperatures, Journal of Operational Oceanography, 2, 25–33, https://doi.org/10.1080/1755876x.2009.11020106, publisher: Informa UK Limited, 2009.

Marchesiello, P., McWilliams, J. C., and Shchepetkin, A.: Open boundary conditions for long-term integration of regional oceanic models, Ocean Modelling, 3, 1–20, https://doi.org/10.1016/s1463-5003(00)00013-5, publisher: Elsevier BV, 2001.

Mayorga, E., Seitzinger, S. P., Harrison, J. A., Dumont, E., Beusen, A. H., Bouwman, A., Fekete, B. M., Kroeze, C., and Van Drecht, G.: Global Nutrient Export from WaterSheds 2 (NEWS 2): Model development and implementation, Environmental Modelling & Software, 25, 837–853, https://doi.org/10.1016/j.envsoft.2010.01.007, 2010.

McDougall, T. J. and Barker, P. M.: Getting started with TEOS-10 and the Gibbs Seawater (GSW) Oceanographic Toolbox, Trevor J McDougall, Battery Point, Tas., ISBN 978-0-646-55621-5, oCLC: 724024071, 2011.

Meinshausen, M., Nicholls, Z. R. J., Lewis, J., Gidden, M. J., Vogel, E., Freund, M., Beyerle, U., Gessner, C., Nauels, A., Bauer, N., Canadell, J. G., Daniel, J. S., John, A., Krummel, P. B., Luderer, G., Meinshausen, N., Montzka, S. A., Rayner, P. J., Reimann, S., Smith, S. J., Van Den Berg, M., Velders, G. J. M., Vollmer, M. K., and Wang, R. H. J.: The shared socio-economic pathway (SSP) greenhouse

gas concentrations and their extensions to 2500, Geoscientific Model Development, 13, 3571–3605, https://doi.org/10.5194/gmd-13-3571-2020, 2020.

Mishonov, A. V.: World Ocean Database 2023, https://doi.org/10.25923/Z885-H264, publisher: NOAA National Centers for Environmental Information, 2024.

Moriarty, R. and O'Brien, T. D.: Distribution of mesozooplankton biomass in the global ocean, 2013.

Mountain, D. G.: Variability in the properties of Shelf Water in the Middle Atlantic Bight, 1977–1999, Journal of Geophysical Research: Oceans, 108, 2001JC001 044, https://doi.org/10.1029/2001JC001044, 2003.

Mountain, D. G.: Labrador slope water entering the Gulf of Maine—response to the North Atlantic Oscillation, Continental Shelf Research, 47, 150–155, https://doi.org/10.1016/j.csr.2012.07.008, 2012.

Mountain, D. G., Strout, G. A., and Beardsley, R. C.: Surface heat flux in the Gulf of Maine, Deep Sea Research Part II: Topical Studies in Oceanography, 43, 1533–1546, https://doi.org/10.1016/S0967-0645(96)00057-4, 1996.

Mupparapu, P. and Brown, W. S.: Role of convection in winter mixed layer formation in the Gulf of Maine, February 1987, Journal of Geophysical Research: Oceans, 107, https://doi.org/10.1029/1999JC000116, 2002.

Murphy, S. C., Nazzaro, L. J., Simkins, J., Oliver, M. J., Kohut, J., Crowley, M., and Miles, T. N.: Persistent upwelling in the Mid-Atlantic Bight detected using gap-filled, high-resolution satellite SST, Remote Sensing of Environment, 262, 112 487, https://doi.org/10.1016/j.rse.2021.112487, 2021.

Olsen, A., Lange, N., Key, R. M., Tanhua, T., Álvarez, M., Becker, S., Bittig, H. C., Carter, B. R., Cotrim Da Cunha, L., Feely, R. A., Van Heuven, S., Hoppema, M., Ishii, M., Jeansson, E., Jones, S. D., Jutterström, S., Karlsen, M. K., Kozyr, A., Lauvset, S. K., Lo Monaco, C., Murata, A., Pérez, F. F., Pfeil, B., Schirnick, C., Steinfeldt, R., Suzuki, T., Telszewski, M., Tilbrook, B., Velo, A., and Wanninkhof, R.: GLODAPv2.2019 – an update of GLODAPv2, Earth System Science Data, 11, 1437–1461, https://doi.org/10.5194/essd-11-1437-2019, 2019.

O'Reilly, J. E. and Zetlin, C. A.: Seasonal, horizontal, and vertical distribution of phytoplankton chlorophyll a in the northeast U.S. continental shelf ecosystem, Technical Report 139, NMFS (National Marine Fisheries Service), Atlantic Coast (U.S.), https://repository.library.noaa.gov/view/noaa/31157, 1998.

Orlanski, I.: A simple boundary condition for unbounded hyperbolic flows, Journal of Computational Physics, 21, 251–269, https://doi.org/10.1016/0021-9991(76)90023-1, publisher: Elsevier BV, 1976.

Pereira, F., Bouali, M., Polito, P. S., Da Silveira, I. C. A., and Candella, R. N.: Discrepancies between satellite-derived and in situ SST data in the Cape Frio Upwelling System, Southeastern Brazil (23˚S), Remote Sensing Letters, 11, 555–562, https://doi.org/10.1080/2150704X.2020.1742941, 2020.

Pershing, A. J., Alexander, M. A., Hernandez, C. M., Kerr, L. A., Le Bris, A., Mills, K. E., Nye, J. A., Record, N. R., Scannell, H. A., Scott, J. D., Sherwood, G. D., and Thomas, A. C.: Slow adaptation in the face of rapid warming leads to collapse of the Gulf of Maine cod fishery, Science, 350, 809–812, https://doi.org/10.1126/science.aac9819, 2015.

Petrie, B. and Drinkwater, K.: Temperature and salinity variability on the Scotian Shelf and in the Gulf of Maine 1945–1990, Journal of Geophysical Research: Oceans, 98, 20 079–20 089, https://doi.org/10.1029/93JC02191, 1993.

Pettigrew, N. R., Churchill, J. H., Janzen, C. D., Mangum, L. J., Signell, R. P., Thomas, A. C., Townsend, D. W., Wallinga, J. P., and Xue, H.: The kinematic and hydrographic structure of the Gulf of Maine Coastal Current, Deep Sea Research Part II: Topical Studies in Oceanography, 52, 2369–2391, https://doi.org/10.1016/j.dsr2.2005.06.033, 2005.

Pettigrew, N. R., Fikes, C. P., and Beard, M. K.: Advances in the Ocean Observing System in the Gulf of Maine: Technical Capabilities and Scientific Results, Marine Technology Society Journal, 45, 85–97, https://doi.org/10.4031/mtsj.45.1.11, publisher: Marine Technology Society, 2011.

Pujol, M.-I., Faugère, Y., Taburet, G., Dupuy, S., Pelloquin, C., Ablain, M., and Picot, N.: DUACS DT2014: the new multi-mission altimeter data set reprocessed over 20years, Ocean Science, 12, 1067–1090, https://doi.org/10.5194/os-12-1067-2016, 2016.

Rakshit, S., Luo, J. Y., and Stock, C. A.: Mechanistic evaluation of benthic carbon sequestration as a marine carbon dioxide removal strategy, https://doi.org/10.22541/essoar.176087318.87558880/v1, submitted.

Rasmussen, L. L., Gawarkiewicz, G., Owens, W. B., and Lozier, M. S.: Slope water, Gulf Stream, and seasonal influences on southern Mid-Atlantic Bight circulation during the fall-winter transition, Journal of Geophysical Research: Oceans, 110, https://doi.org/10.1029/2004jc002311, publisher: American Geophysical Union (AGU), 2005.

Rebuck, N. and Townsend, D.: A climatology and time series for dissolved nitrate in the Gulf of Maine region, Deep Sea Research Part II: Topical Studies in Oceanography, 103, 223–237, https://doi.org/10.1016/j.dsr2.2013.09.006, publisher: Elsevier BV, 2014.

Reichl, B. G. and Hallberg, R.: A simplified energetics based planetary boundary layer (ePBL) approach for ocean climate simulations., Ocean Modelling, 132, 112–129, https://doi.org/10.1016/j.ocemod.2018.10.004, publisher: Elsevier BV, 2018.

Reynolds, R. W., Banzon, V. F., and Program, N. C.: NOAA Optimum Interpolation 1/4 Degree Daily Sea Surface Temperature (OISST) Analysis, Version 2, https://doi.org/10.7289/V5SQ8XB5, 2008.

Ross, A. C., Stock, C. A., Adcroft, A., Curchitser, E., Hallberg, R., Harrison, M. J., Hedstrom, K., Zadeh, N., Alexander, M., Chen, W., Drenkard, E. J., Du Pontavice, H., Dussin, R., Gomez, F., John, J. G., Kang, D., Lavoie, D., Resplandy, L., Roobaert, A., Saba, V., Shin, S.-I., Siedlecki, S., and Simkins, J.: A high-resolution physical–biogeochemical model for marine resource applications in the northwest Atlantic (MOM6-COBALT-NWA12 v1.0), Geoscientific Model Development, 16, 6943–6985, https://doi.org/10.5194/gmd-16-6943-2023, 2023.

Rutherford, K. and Fennel, K.: Diagnosing transit times on the northwestern North Atlantic continental shelf, Ocean Science, 14, 1207–1221, https://doi.org/10.5194/os-14-1207-2018, 2018.

Saba, V. S., Griffies, S. M., Anderson, W. G., Winton, M., Alexander, M. A., Delworth, T. L., Hare, J. A., Harrison, M. J., Rosati, A., Vecchi, G. A., and Zhang, R.: Enhanced Warming of the N Orthwest A Tlantic O Cean under Climate Change, 121, 118–132, https://doi.org/10.1002/2015JC011346, 2016.

Sadourny, R.: The Dynamics of Finite-Difference Models of the Shallow-Water Equations, 32, 680–689, https://doi.org/10.1175/1520-0469(1975)032<0680:TDOFDM>2.0.CO;2, 1975.

Sasaki, D. K., Silva, D., Del Giovannino Júnior, S. R., Almeida Da Silveira, I. C., Belo, W. C., Martins, R. P., and Dottori, M.: Hydrographic climatology of the South Brazil Bight continental shelf and slope, Theoretical and Applied Climatology, 155, 9407–9425, https://doi.org/10.1007/s00704-024-05144-w, 2024.

Sasaki, D. K., Schultz, C., and Curchitser, E.: "A High-Resolution Coupled Physical-Biogeochemical Model of the Northeastern US Continental Shelf: MOM6-COBALT-NEUS25v1.0" - auxiliary datasets, https://doi.org/10.5281/ZENODO.17572585, 2025.

Sathyendranath, S., Brewin, R., Brockmann, C., Brotas, V., Calton, B., Chuprin, A., Cipollini, P., Couto, A., Dingle, J., Doerffer, R., Donlon, C., Dowell, M., Farman, A., Grant, M., Groom, S., Horseman, A., Jackson, T., Krasemann, H., Lavender, S., Martinez-Vicente, V., Mazeran, C., Mélin, F., Moore, T., Müller, D., Regner, P., Roy, S., Steele, C., Steinmetz, F., Swinton, J., Taberner, M., Thompson, A., Valente, A., Zühlke, M., Brando, V., Feng, H., Feldman, G., Franz, B., Frouin, R., Gould, R., Hooker, S., Kahru, M., Kratzer, S., Mitchell, B., Muller-Karger, F., Sosik, H., Voss, K., Werdell, J., and Platt, T.: An Ocean-Colour Time Series for Use in Climate Stud-

ies: The Experience of the Ocean-Colour Climate Change Initiative (OC-CCI), Sensors, 19, 4285, https://doi.org/10.3390/s19194285, publisher: MDPI AG, 2019.

Scully, M. E., Geyer, W. R., Borkman, D., Pugh, T. L., Costa, A., and Nichols, O. C.: Unprecedented summer hypoxia in southern Cape Cod Bay: an ecological response to regional climate change?, Biogeosciences, 19, 3523–3536, https://doi.org/10.5194/bg-19-3523-2022, 2022.

Seidov, D., Mishonov, A., Reagan, J., Baranova, O., Cross, S., and Parsons, R.: Regional Climatology of the Northwest Atlantic Ocean: High-Resolution Mapping of Ocean Structure and Change, Bulletin of the American Meteorological Society, 99, 2129–2138, https://doi.org/10.1175/bams-d-17-0205.1, publisher: American Meteorological Society, 2018.

Seidov, D., Mishonov, A., Reagan, J., and Parsons, R.: Eddy-Resolving In Situ Ocean Climatologies of Temperature and Salinity in the Northwest Atlantic Ocean, Journal of Geophysical Research: Oceans, 124, 41–58, https://doi.org/10.1029/2018jc014548, publisher: American Geophysical Union (AGU), 2019.

Siedlecki, S., Salisbury, J., Gledhill, D., Bastidas, C., Meseck, S., McGarry, K., Hunt, C., Alexander, M., Lavoie, D., Wang, Z., Scott, J., Brady, D., Mlsna, I., Azetsu-Scott, K., Liberti, C., Melrose, D., White, M., Pershing, A., Vandemark, D., Townsend, D., Chen, C., Mook, W., and Morrison, R.: Projecting ocean acidification impacts for the Gulf of Maine to 2050, Elementa: Science of the Anthropocene, 9, 00 062, https://doi.org/10.1525/elementa.2020.00062, 2021.

Stock, C. A., Dunne, J. P., and John, J. G.: Global-scale carbon and energy flows through the marine planktonic food web: An analysis with a coupled physical–biological model, Progress in Oceanography, 120, 1–28, https://doi.org/10.1016/j.pocean.2013.07.001, 2014.

Stock, C. A., Dunne, J. P., Fan, S., Ginoux, P., John, J., Krasting, J. P., Laufkötter, C., Paulot, F., and Zadeh, N.: Ocean Biogeochemistry in GFDL's Earth System Model 4.1 and Its Response to Increasing Atmospheric CO_2, Journal of Advances in Modeling Earth Systems, 12, e2019MS002 043, https://doi.org/10.1029/2019MS002043, 2020.

Stommel, H.: Varieties of Oceanographic Experience: The ocean can be investigated as a hydrodynamical phenomenon as well as explored geographically., Science, 139, 572–576, https://doi.org/10.1126/science.139.3555.572, 1963.

Sánchez-Román, A., Pujol, M. I., Faugère, Y., and Pascual, A.: DUACS DT2021 reprocessed altimetry improves sea level retrieval in the coastal band of the European seas, Ocean Science, 19, 793–809, https://doi.org/10.5194/os-19-793-2023, 2023.

Takahashi, T., Sutherland, S. C., and Kozyr, A.: LDEO Database (Version 2019): Global Ocean Surface Water Partial Pressure of CO2 Database: Measurements Performed During 1957-2019 (NCEI Accession 0160492), https://doi.org/10.3334/CDIAC/OTG.NDP088(V2015), 2017.

Team, E. C.: esmf-org/esmf: ESMF 8.9.0, https://doi.org/10.5281/ZENODO.11205526, 2025.

Thomas, A. C., Townsend, D. W., and Weatherbee, R.: Satellite-measured phytoplankton variability in the Gulf of Maine, Continental Shelf Research, 23, 971–989, https://doi.org/10.1016/s0278-4343(03)00086-4, publisher: Elsevier BV, 2003.

Tian, R., Chen, C., Qi, J., Ji, R., Beardsley, R. C., and Davis, C.: Model study of nutrient and phytoplankton dynamics in the Gulf of Maine: patterns and drivers for seasonal and interannual variability, ICES Journal of Marine Science, 72, 388–402, https://doi.org/10.1093/icesjms/fsu090, 2015.

Townsend, D. W.: Sources and cycling of nitrogen in the Gulf of Maine, Journal of Marine Systems, 16, 283–295, https://doi.org/10.1016/s0924-7963(97)00024-9, publisher: Elsevier BV, 1998.

Townsend, D. W. and Pettigrew, N. R.: The role of frontal currents in larval fish transport on Georges Bank, Deep Sea Research Part II: Topical Studies in Oceanography, 43, 1773–1792, https://doi.org/10.1016/S0967-0645(96)00040-9, 1996.

Townsend, D. W., Rebuck, N. D., Thomas, M. A., Karp-Boss, L., and Gettings, R. M.: A changing nutrient regime in the Gulf of Maine, Continental Shelf Research, 30, 820–832, https://doi.org/10.1016/j.csr.2010.01.019, 2010.

Townsend, D. W., Pettigrew, N. R., Thomas, M. A., and Moore, S.: Warming waters of the Gulf of Maine: The role of Shelf, Slope and Gulf Stream Water masses, Progress in Oceanography, 215, 103 030, https://doi.org/10.1016/j.pocean.2023.103030, 2023.

Wang, Z., Li, D., Xue, H., Thomas, A. C., Zhang, Y. J., and Chai, F.: Freshwater Transport in the Scotian Shelf and Its Impacts on the Gulf of Maine Salinity, Journal of Geophysical Research: Oceans, 127, e2021JC017 663, https://doi.org/10.1029/2021JC017663, 2022.

Willmott, C. J.: ON THE VALIDATION OF MODELS, Physical Geography, 2, 184–194, https://doi.org/10.1080/02723646.1981.10642213, publisher: Informa UK Limited, 1981.

Worsfold, M., Good, S., Atkinson, C., and Embury, O.: Presenting a Long-Term, Reprocessed Dataset of Global Sea Surface Temperature Produced Using the OSTIA System, 16, 3358, https://doi.org/10.3390/rs16183358, 2024.

Xu, Y., Chant, R., Gong, D., Castelao, R., Glenn, S., and Schofield, O.: Seasonal variability of chlorophyll a in the Mid-Atlantic Bight, Continental Shelf Research, 31, 1640–1650, https://doi.org/10.1016/j.csr.2011.05.019, publisher: Elsevier BV, 2011.

Xue, H., Chai, F., and Pettigrew, N. R.: A Model Study of the Seasonal Circulation in the Gulf of Maine, Journal of Physical Oceanography, 30, 1111–1135, https://doi.org/10.1175/1520-0485(2000)030<1111:AMSOTS>2.0.CO;2, 2000.

Yoder, J. A., Schollaert, S. E., and O'Reilly, J. E.: Climatological phytoplankton chlorophyll and sea surface temperature patterns in continental shelf and slope waters off the northeast U.S. coast, Limnology and Oceanography, 47, 672–682, https://doi.org/10.4319/lo.2002.47.3.0672, publisher: Wiley, 2002.

Zang, Z., Ji, R., Feng, Z., Chen, C., Li, S., and Davis, C. S.: Spatially varying phytoplankton seasonality on the Northwest Atlantic Shelf: a model-based assessment of patterns, drivers, and implications, ICES Journal of Marine Science, 78, 1920–1934, https://doi.org/10.1093/icesjms/fsab102, publisher: Oxford University Press (OUP), 2021.

Zhuang, J., Dussin, R., Huard, D., Bourgault, P., Banihirwe, A., Raynaud, S., Malevich, B., Schupfner, M., Filipe, Gauthier, C., Levang, S., Jüling, A., Almansi, M., RichardScottOZ, RondeauG, Rasp, S., Smith, T. J., Mares, B., Stachelek, J., Plough, M., Pierre, Bell, R., Caneill, R., and Li, X.: pangeo-data/xESMF: v0.8.10, https://doi.org/10.5281/ZENODO.4294774, 2025.